10-22-2012 12:00 AM

Evaluation of Jarosite as a Biosignature: A Comparison of Biogenic and Synthetic Jarosites

Liane Loiselle
The University of Western Ontario

Supervisor
Dr. Gordon Southam
The University of Western Ontario

Graduate Program in Geology
A thesis submitted in partial fulfillment of the requirements for the degree in Master of Science

EVALUATION OF JAROSITE AS A BIOSIGNATURE: A COMPARISON OF BIOGENIC AND SYNTHETIC JAROSITES

(Spine title: Jarosite as a biosignature)

(Thesis format: Integrated Article)

by

Liane M. Loiselle

Graduate Program in Geology and Planetary Science

A thesis submitted in partial fulfillment
of the requirements for the degree of
Master of Science

The School of Graduate and Postdoctoral Studies
The University of Western Ontario
London, Ontario, Canada

THE UNIVERSITY OF WESTERN ONTARIO
School of Graduate and Postdoctoral Studies

CERTIFICATE OF EXAMINATION

Supervisor	Examiners
_____	_____
Dr. Gordon Southam	Dr. Brian Branfireun
	_____
Supervisory Committee	Dr. Norm Duke
_____	_____
Dr. Gordon Southam	Dr. Susan Koval
_____	
Dr. Neil Banerjee	

The thesis by

Liane M. Loiselle

entitled:

Evaluation of jarosite as a biosignature: A comparison of biogenic and synthetic jarosites

is accepted in partial fulfilment of the
requirements for the degree of
Master of Science

Date: _____ _____
Chair of the Thesis Examination Board

Abstract

The detection of jarosite $(K)Fe_3(SO_4)_2OH_6$ on Mars has been interpreted as mineralogical evidence of acid-sulfate aqueous processes, including putative evidence of biological activity. Terrestrial environments where such acidic conditions occur are inhabited by microbiota and generate biological signatures. A biotic and synthetic jarosite were produced to evaluate the ability and effectiveness of existing analytical methods to identify biosignatures in targeted geological materials. Using a comprehensive suite of microscopic (light microscopy, SEM and TEM), mineralogical (XRD), spectroscopic (IR, LIBS, Mössbauer, VNIR, and Raman) and mass spectrometry (ToF SIMS) techniques, the two jarosites were found to be morphologically distinct. The identification of organic signatures in biogenic samples was masked by the iron-hydroxyl-sulfate matrix, but biogenicity was detectable using SEM and TEM, techniques which are not practical on Mars. Jarosite produced in 2-year-old abiotic control medium was similar to biogenic samples indicating that the presence of jarosite is not evidence of life.

Keywords: jarosite, biogenic jarosite, synthetic jarosite, Mars, Rio Tinto, biosignatures, biomarker, analogue environment, Acidithiobacillus ferrooxidans (syn. Thiobacillus ferrooxidans), biomarkers, biogenicity, scanning electron microscopy (SEM), transmission electron microscopy (TEM), X-ray diffraction (XRD), Raman spectroscopy, infrared spectroscopy (IR), Mössbauer spectroscopy, time of flight secondary ion mass spectrometry (ToF SIMS), visible-near infrared spectroscopy (VNIR), laser induced breakdown spectroscopy (LIBS).

Co-authorship Statements

The work presented here is a result of my scientific efforts in conjunction with discussions with my supervisor, Dr. Gordon Southam.

Chapter 2 entitled "Jarosite as a biosignature: A structural characterization of biogenic and synthetic jarosites" was written by L.M. Loiselle and has been prepared as a manuscript for submission and publication in the journal Earth and Planetary Science Letters. Loiselle performed all the microscopy and analyses, prepared the figures and drafted the manuscript. Southam provided study funding, collected the iron oxides from the Rio Tinto River, and advised on all aspects of this research.

Chapter 3 entitled "Detecting biogenicity: A comparison of biogenic and synthetic jarosite samples using mass spectrometry and spectral analyses" was written by L.M. Loiselle and was prepared as a manuscript for publication in Earth and Planetary Science Letters. Loiselle conducted the microscopy, mass spectrometry, along with Raman, IR, and LIBS analyses, prepared the tables and figures as well as drafted the manuscript. Dr. Darby Dyar provided her expertise and carried out the Mössbauer spectroscopy data collection at Mount Holyoke College. Dr. Penny King provided access to her IR laboratory facilities at the University of New Mexico as well as her guidance and expertise during IR data collection and interpretation. Dr. Sean Shieh provided access to his laboratory facilities at the University of Western Ontario and offered his expertise and guidance during the collection and interpretation of Raman spectral data. Dr. Ed Cloutis permitted access to his equipment at the University of Winnipeg where Michael Craig

conducted VNIR analyses on my behalf. Both Cloutis and Craig provided guidance during the interpretation of the VNIR spectral data sets. Drs Richard Léveillé and Alexander Koujelev provided access to the LIBS instrument set up at the Canadian Space Agency (CSA), while Dr. Siu-Lung Lui carried out the analysis and provided significant input and guidance during LIBS data interpretation. Dr. Heng-Yong Nie provided access and assistance to the ToF SIMS instrument at the Surface Science Western research facility at the University of Western Ontario. Dr. Southam aided in the development and design of the study, and he offered guidance throughout the research and manuscript preparation. This study was funded by grants bestowed to Southam and Loiselle.

To my family,

who were there all along,

with unconditional love, support, and unselfish giving.

Acknowledgements

First, I would like to thank my supervisor Gordon Southam whose mentorship throughout my graduate career has been invaluable. Gord, I am grateful and appreciative of all the opportunities you made available to me during my time in your research group including travel to various conferences and research facilities; all have been invaluable experiences and have greatly helped my research endeavours as well as enriched my graduate experience. I am thankful that you welcomed me into your research group, that you always encouraged my passion for science, and that you ardently believed in me and my abilities, even when I did not. I enjoyed my time as a student under your guidance, I learned a great deal about all aspects of scientific research, and am a better scientist as a result because of your mentorship. Thank you.

Second, I would like to thank my Mum and Dad (Margaret and Michel) as well as my siblings (Jacqueline and Joel) and to acknowledge their support in my academic pursuits. I am grateful to each of them for their own encouragements, reassurances, confidence, understanding, thoughtfulness, curiosity, and guidance throughout the years. I began exploring my passion for scientific inquiry during high school where I participated in regional and national science fairs. There steadfast encouragement, assistance, pride, and unwavering support have always been constants in my life and during my pursuits of scientific inquiry; so have proudly displayed and uniquely handcrafted Christmas tree ornaments documenting my accomplishments and milestones over the years. I would not have developed the courage, assertiveness, perseverance, or the abilities to be able wildly pursue my ambitions or passions without all of their assistance, love, and support. Thank you.

Additionally, I would like to recognize my fellow lab mates with whom I've had the distinct pleasure of working with over the past few years. Each provided support, guidance and inspiration along the way and I am excited to see where their journeys take them: Gordon Campbell, Andrea Fernandes, Nahed Mahrous, Jenine McCutcheon, Alexandra Pontefract, Maija Raudepp, Jie Ren, Jeremiah Shuster, Jessica Stromberg and Dusa Vukosavljevic as well as Drs Christopher Omelon, Ian Power, and Louisa Preston.

Finally, I would like to recognize the assistance and contributions while extending a big thank you to: Todd Simpson and Tim Goldhawk at the Nanofabrication Facility for all their help with SEM analyses; to Brian Hart and Heng-Yong Nie at Surface Science Western for their assistance with ToF SIMS; to Roberta Flemming for the use of her hot plate during synthesis experiments as well as access to her EVA software ; to Kimberly Law and Grace Yau for their assistance with powder XRD; to Sean Shieh for his guidance with Raman spectroscopy; to Karen Nygard and Nicole Bechard as well as Richard Gardiner at the Biotron Institute for Experimental Climate Change Research for assistance with confocal, light, and transmission electron microscopy respectively; to Penny King for inviting me into her laboratory at the University of New Mexico for IR spectral analyses and for her mentorship, candid guidance as well as advice during the past few years; to Richard Léveillé for hosting me for a term at the Canadian Space Agency and to Alex Koujelev and Siu-Lung Lui for access and assistance with LIBS analyses; to David Fernandez-Remolar for the invitation to join the CAB and the IPBSL team for drilling operations in 2011; to Ed Cloutis and Michael Craig for NIR analyses; and to Darby Dyar at Mount Holyoke College for providing Mössbauer analyses.

This research was financially supported by funds provided by the Canadian Space Agency (CSA) and the Centro de Astrobiología (CAB) / Instituto National de Técnica Aeroespacial (INTA); as well as additional grants by the Natural Science and Engineering Research Council (NSERC), Graduate Thesis Research Fund (GTRF) at the University of Western Ontario, and a Canadian Astrobiology Training Program CREATE graduate research fellowship.

Table of Contents

Certificate of Examination ii

Abstract iii

Keywords iii

Co-Authorship Statements iv

Dedication vi

Acknowledgements vii

Table of Contents x

List of Tables xiv

List of Figures xv

List of Appendices xvii

List of Abbreviations and Symbols xviii

Chapter 1. Introduction 1

1.1. Jarosite Mineralogy 1

1.2. Mars Exploration 3

1.2.1. Viking mission and biological experiments 4

1.2.2. Evidence of biogenic processes in Martian meteorite ALH84001? 5

1.2.3. In situ detection of jarosite on the Martian surface by MER Opportunity 7

1.2.4. Jarosite as a mineralogical biosignature and analogue sites 8

1.3. Biomineralization and biosignatures 9

1.4. Study goals 11

References 13

Chapter 2. Jarosite as a biosignature: A structural characterization of biogenic and synthetic jarosites 21

2.1. Introduction 21

2.1.1. Background 21

2.1.2. Site description 23

2.1.3. Study goals 26

2.2. Methods 27

2.2.1. Sample collection 27

2.2.2. Microbial culturing 27

2.2.3. Synthetic jarosite preparations 31

2.2.4. Powder X-ray Diffraction (XRD) 32

2.2.5. Light microscopy and microbial viability 33

2.2.6. Scanning electron microscopy (SEM) 34

2.2.7. Transmission electron microscopy (TEM) 35

2.3. Results and Discussion 35

2.3.1. Microbial culturing 36

2.3.2. Mineralogical characterization of precipitates 38

2.3.3. Light, epifluorescence, and confocal microscopy 42

2.3.4. High resolution microscopy (SEM and TEM) of jarosite precipitates 46

2.4. Conclusions 56

References 58

Chapter 3. Detecting biogenicity: A comparison of biogenic and synthetic jarosite samples using mass spectrometry and spectral analyses 64

3.1. Introduction 64

3.1.1. Background 64

3.1.2. Study context and aims 66

3.2. Material and Methods 67

3.2.1. Biogenic and synthetic jarosite samples 67

3.2.2. Raman spectroscopy (Raman) 68

3.2.3. Infrared spectroscopy (IR) 70

3.2.4. Visible-near infrared reflectance spectroscopy (VNIR) 70

3.2.5. Mössbauer spectroscopy (Mössbauer) 71

3.2.6. Laser induced breakdown spectroscopy (LIBS) 72
3.2.7. Time of flight secondary ion mass spectrometry (ToF SIMS) 74
3.3. Results 74
3.3.1. Raman spectroscopy (Raman) 74
3.3.2. Infrared spectroscopy (IR) 78
3.3.3. Visible-near infrared reflectance spectroscopy (VNIR) 81
3.3.4. Mössbauer spectroscopy (Mössbauer) 84
3.3.5. Laser induced breakdown spectroscopy (LIBS) 87
3.3.6. Time of flight secondary ion mass spectrometry (ToF SIMS) 93
3.4. Discussion 102
3.4.1. Missing organic responses in ToF SIMS, Raman and reflectance spectroscopy 102
3.4.2. Elemental detection of organics in LIBS spectra? 105
3.4.3. Mössbauer spectroscopy- potential biosignature or false biosignature 108
3.5. Conclusions 110
References 112

Chapter 4. Conclusions **120**
References 126

Appendix A. Experimental synthesis of alkali jarosite minerals **128**
Introduction 128
Methods 130
Jarosite 130
Natrojarosite 131
Ammoniojarosite 132
Hydronium jarosite 132
Results and Discussion 133
Conclusion 140

References 141

Curriculum vitae **142**

List of Tables

Chapter 3. Detecting biogenicity: A comparison of biogenic and synthetic jarosite samples using mass spectrometry and spectral analyses

3.1.	Raman peaks assignments for synthetic and biogenic jarosite spectra in Figure 3.2.	75
3.2.	IR peak positions and assignments for spectra of biogenic and synthetic jarosites from Figure 3.3.	79
3.3.	Reflectance spectra band positions and assignments of biogenic and synthetic jarosite of spectra in Figure 3.4.	82
3.4.	Mössbauer parameters for biogenic and synthetic jarosites corresponding to spectra in Figure 3.5.	85
3.5.	LIBS emission lines used in this study to evaluate the jarosite spectra in Figure 3.6.	88

List of Figures

Chapter 2. Jarosite as a biosignature: A structural characterization of biogenic and synthetic jarosites

2.1. Geographic map of the Tinto River Basin region 29

2.2. Field photographs of Rio Tinto sampling site 30

2.3. Powder XRD pattern of microbial culture (biogenic) and synthesized jarosite (synthetic) material 39

2.4. Comparison of powder X-ray diffraction patterns of biogenic precipitates collected at different culture ages 40

2.5. Powder XRD diffraction pattern of material generated from abiotic oxidation of culture media 43

2.6. Confocal micrograph of biogenic jarosite stained with fluorescent probes 45

2.7. SEM micrographs of biogenic and synthetic jarosites 48

2.8. SEM micrographs of organic material in biogenic sample 50

2.9. TEM micrographs of biogenic jarosite 52

2.10. SEM micrographs of precipitates generated by chemical oxidation of abiotic culture media 55

Chapter 3. Detecting biogenicity: A comparison of biogenic and synthetic jarosite samples using mass spectrometry and spectral analyses

3.1. SEM and TEM micrographs of biogenic and synthetic jarosite 69

3.2. Raman spectra of biogenic and synthetic jarosite ((A) 200 to 800 cm^{-1} (B) 850 to 1550 cm^{-1} (C) 3150 to 3650 cm^{-1}) 76

3.3. IR spectra of biogenic and synthetic jarosite from 400 to 4000 cm^{-1} 80

3.4. VNIR reflectance spectra of synthetic and biogenic jarosite 83

3.5. Mössbauer spectra of synthetic and biogenic jarosite 86

3.6. LIBS spectra of synthetic, biogenic, dry and wet samples 90

3.7. ToF SIMS spectra of positive ions for biogenic and synthetic jarosite samples at (A) 0 to 250 amu and (B) 250 to 450 amu 95

3.8. ToF SIMS spectra of positive ions for biogenic and synthetic jarosite samples at (C)450 to 650 amu and (D) 650 to 900 amu 97
3.9. TOF SIMS spectra of negative ions for biogenic and synthetic jarosite samples at (E) 0 to 250 amu and (F) 250 to 450 amu 99
3.10. TOF SIMS spectra of negative ions for biogenic and synthetic jarosite samples at (G)450 to 650 amu and (H) 650 to 900 amu 101

Appendix A. Experimental synthesis of alkali jarosite minerals

A.1. Photograph of synthesized alkali-jarosite mineralogical powders 129
A.2. XRD patterns of synthesized alkali-jarosite precipitates 135
A.3. SEM micrographs of synthetic jarosite minerals 139

List of Appendices

Appendix A. Experimental synthesis of alkali jarosite minerals 128

List of Abbreviation and Symbols

AMD	acid mine drainage
amu	atomic mass unit (s)
APXS	alpha particle X-ray spectrometer
atm	atmosphere(s)
BCM	biologically controlled mineralization
BF	bright field microscopy
BIM	biologically induced mineralization
cm^{-1}	wavenumber
CRISM	Compact Reconnaissance Imaging Spectrometer for Mars
CSA	Canadian Space Agency
DF	dark field microscopy
DIC	differential interference contrast microscopy
DRIFTS	diffuse reflectance infrared Fourier transform spectroscopy
EPS	extracellular polymeric substances / exopolysaccharides
eV	electron volt
Fe^{2+}	ferrous iron
Fe^{3+}	ferric iron
FWHM	full width half maximum
g	gram(s)
GCMS	gas chromatography-mass spectrometry
h	hour(s)
ICDD	International Centre for Diffraction Data
IR	infrared spectroscopy

km	kilometer(s)
kV	kilovolt
L	liter(s)
lb	pound(s)
LIBS	laser induced breakdown spectroscopy
M	molarity
mA	milli-amps
MER	Mars Exploration Rover
min	minute(s)
mL	milliliter(s)
mm	millimeter(s)
mol	mole(s)
MRO	Mars Reconnaissance Orbiter
MSL	Mars Science Laboratory
OMEGA	Observatoire pour la Minéralogie, l'Eau, les Glaces et l'Activité
NAI	NASA Astrobiology Institute
NASA	National Aeronautics and Space Administration
nm	nanometer(s)
PAH	polycyclic aromatic hydrocarbon
PC	phase contrast microscopy
pH	$-\log[H^+]$
RT	room temperature
SEM	scanning electron microscope
TEM	transmission electron microscope
ToF SIMS	time of flight secondary ion mass spectrometry

VNIR	visible-near infrared spectroscopy
XRD	X-ray diffraction
XRF	X-ray fluorescence
µL	microliter(s)
µm	micrometer(s)
°C	(degrees) Celsius
δ	isomer shift
ΔE_Q	quadrupole splitting
%	percent
θ	theta

Chapter 1.

Introduction

For clarity, jarosite, *sensu stricto*, will be used as the mineralogical name of the potassium jarosite mineral throughout this thesis. All other minerals in the jarosite subgroup will also be referred to using their mineral names as outlined in Jambor (1999) and Dutrizac and Jambor (2000).

1.1. Jarosite Mineralogy

The jarosite group of minerals is part of the alunite supergroup, which comprises more than 40 mineral species, all of which have the general formula $AB_3(TO_4)_2(OH)_6$. The supergroup is subdivided based on the trivalent metal cation present in the tetrahedral coordination site which forms the spine of the mineral. Minerals with formulae where Fe^{3+} exceeds Al^{3+} are assigned to the jarosite family, and those minerals with less Fe^{3+} to Al^{3+} allotted to the alunite family (i.e., $Fe^{3+} > Al^{3+}$ = jarosite family mineral; $Al^{3+} > Fe^{3+}$ = alunite family mineral) (Dutrizac and Jambor, 2000). There is extensive solid solution within the jarosite subgroup, where the A site is a monovalent cation (i.e., H_3O^+, Na^+, K^+, Rb^+, Ag^+, Tl^+, NH_4^+, ½ Ca^{2+}, or ½ Pb^{2+}) and characterized by site B = Fe^{3+} and site T = S. The chemistry of the depositional environment exhibits significant control over the monovalent cation that ends up in site A of the jarosite subgroup mineral, and thus the name of the mineral.

Jarosite (A = K) and natrojarosite (A = Na) are the most prevalent species of the subgroup found in nature, as alkali-rich jarosites precipitate favorably from solution. Although naturally occurring, hydronium jarosite (A = H_3O^+) is very rare since it will only form in solutions which are entirely depleted of alkali cations (Basciano and Peterson, 2008, 2007b). Partial substitution of hydronium for potassium, sodium, or ammonium in A-sites is common and observed for both synthetic and natural samples of the jarosite subgroup. Iron (or aluminum) deficiencies in the B-site are also well documented for natural and synthetic alunite group minerals (Basciano and Peterson, 2008, 2007a, 2007b; Drouet and Navrotsky, 2003; Drouet et al., 2004; Grohol et al., 2003; Hendricks, 1937; Kubisz, 1970; Lager et al., 2001; Majzlan et al., 2004; Parker, 1962). These nonstoichiometric arrangements maintain charge neutrality by the protonation of hydroxyl groups within their crystal configurations, which lead to the inclusion of weakly bound structural water molecules within their crystal structure (Brophy and Sheridan, 1965; Drouet and Navrotsky, 2003; Ripmeester et al., 1986). Iron deficiencies in the B site of alkali jarosites lead to a decrease in unit-cell parameter *c* and any subsequent hydronium substitution will result in an increase in unit-cell parameter *a* (Basciano and Peterson, 2008). The solid-solution series among the alkali jarosite endmembers is well-established having been previously studied by Alpers et al. (1992), Basciano and Peterson (2008, 2007a, 2007b), Brophy and Sheridan (1965), Brown (1970), Drouet and Navrotsky (2003), Dutrizac (1983), Kubisz (1970, 1971, 1972), Long et al. (1992), and Stoffregen et al., (2000).

The jarosite group of minerals have been extensively studied as a result of its importance as a by-product of metallurgy practices as well as being extremely common in

supergene systems and acid mine drainage (AMD) environments. Jarosites also play an important role in the metallurgy industry, since their precipitation helps eliminate alkalis, iron, and sulfates from hydrometallurgical process solutions; advantages include excellent settling and filtration properties as well as decrease in the loss of "sought-after" divalent base metals (i.e., Zn^{2+}, Cu^{2+}, and Ni^{2+}; Dutrizac, 1983). Naturally occurring jarosite mineral deposits can be used as environmental indicators of sulfide mineralization processes and, in specific instances (e.g., upwelling of subsurface groundwater), can be used in mineral exploration to indicate the subsurface occurrence of sulfide deposits. Some jarosite mineral species include economically desirable metals (e.g. lead (Pb) or silver (Ag)) in the monovalent cation site and some deposits are rich enough to constitute ore minerals and are mined (Schempp, 1923).

Jarosite subgroup minerals are common and form in a series of diverse environments. Natural varieties have been found in many localities and settings on Earth. Jarosite has also been identified at several locales on Mars, but most notably at Meridiani Planum, strongly indicating that liquid water once existed on the surface of Mars (Christensen et al., 2004b; Klingelhofer et al., 2004; Squyres et al., 2004a, 2004b, 2004c).

1.2. Mars Exploration

Our knowledge of the occurrence of minerals on Mars is limited to data obtained from remote sensing of the planet's surface using Earth based telescopes and data obtained from orbital and *in situ* robotic missions at Mars (i.e., flybys and orbiters, landers and rovers). Unlike exploration of the Moon, there have been no human or

sample return missions to Mars. Our sample suite of Martian materials is limited to these data sets as well as laboratory analyses of the few Martian meteorites (63 as of July 7th, 2012) discovered on Earth (e.g., Allan Hills 84001, Chassigny, Nakhla, and Shergotty), representing a natural mechanism for sample return. Currently, there are five active missions exploring the Martian planetary surface: three orbiters returning remote sensing data (Mars Odyssey, Mars Express, and Mars Reconnaissance Orbiter) and two rovers conducting active *in situ* analyses (MER-B *Opportunity* and MSL *Curiosity*).

1.2.1. Viking mission and biological experiments

The detection of amorphous iron oxides as well as the presence of water-bearing phases was postulated by many in the 1970s based on Earth based telescopic measurements (Clark and McCord, 1982; Houck et al., 1973). Images and visible multispectral data collected by instruments aboard the Mariner 9 and Viking orbiters led to the supposition that Mars experienced aqueous alteration and thus may have been a habitable at one point during its geological history (Pollack et al., 1987). In 1975, Viking 1 and Viking 2 were the first spacecraft to successfully land on the Martian surface and return *in situ* analyses including geochemical information about the Martian surface using X-ray fluorescence (XRF; Clark et al., 1982, 1977). The objective of these lander missions was to determine if there was any measureable evidence of life on Mars by conducting a series of biological experiments. Results from these experiments yield contradictory information about the presence of organics in the Martian regolith and are considered insufficient to adequately resolve the existence of life on Mars. Since the discovery of indigenous perchlorates in Martian soils at the Phoenix Mars Lander landing

site (Chevrier et al., 2009; Hecht et al., 2009) some have suggested that they may account for the lack of organics observed during the Viking mission experiments. Recently, Navarro-Gonzalez et al. (2010) conducted experiments using soil samples containing organic carbon and magnesium perchlorate from the Atacama Desert, which they considered to be analogous to the samples analyzed by Viking. They demonstrated that upon heating (~500°C), perchlorate rapidly broke down the organics to generate chloromethane and dichloromethane, compounds identical to those detected *in situ* by the thermal analyses of the Viking biological experiments. Navarro-Gonzalez et al. (2010) further argued that the generation of the chlorohydrocarbons detected at the Martian surface during by Viking (which were initially considered to be terrestrial contaminants, although not observed in *in situ* blanks) were the result of interactions of Martian organic material with indigenous perchlorate ions during *in situ* sample analysis preparation. Additionally, suggestions have been made that the instrumentation aboard the Viking payload lacked the sensitivity to be able to detect trace amounts of organic compounds (Navarro-Gonzalez et al., 2006). Even with additional *in situ* data obtained from additional lander and rover missions (e.g., Phoenix) the initial Viking results are considered inconclusive to the majority of the scientific community (Biemann, 2006).

1.2.2. Evidence of biogenic processes in Martian meteorite ALH84001?

Currently, no sample return missions have flown to Mars, the only samples of the planet available are in the form of meteorites which have been discovered here on Earth. Analyses of these 63 Martian meteorites have greatly improved our geochemical and

mineralogical knowledge and understanding about Mars and have also been useful in ascertaining chronological characteristics of the Martian crust (McSween, 2008; 2007).

In 1996, the scientific community was roused with the declaration of evidence of possible remnant life within the Martian meteorite ALH84001. McKay et al. (1996) assert in their seminal paper that the presence of carbonate globules, magnetite, indigenous reduced carbon (e.g., PAHs), and bacteria-like morphological structures within the carbonate globules, along with their observed proximity and propinquity to know terrestrial biogenic traits, were strong evidence for ancient microbial life within the meteorite. This biogenic theory, albeit extremely controversial, has been vigorously disputed and intensively studied with advocates endorsing both sides of the argument (Becker et al., 1998; Bradley et al., 1998; Scott et al., 1997; Thomas-Keprta et al., 2009, 2002).

The publication of this seminal paper by McKay et al. (1996) and the ensuing debate have highlighted the difficulty in positively identifying and establishing proof of life. This debate has not only inspired numerous studies which have attempted to refute or support the biogenic theory, but it has also stirred new debates about life on Earth (e.g., maximum temperature life can remain viable at, theoretical minimum size of life) as well as exposed new ways to search for life beyond our planet. Along with other technological and scientific innovations, this debate led to the foundation of the NASA Astrobiology Institute (NAI) as well as renewed interest in the exploration of Mars, which had practically been forgotten since the Viking missions in the 1970s.

1.2.3. In situ detection of jarosite on the Martian surface by MER Opportunity

The more recent Martian Exploration Rovers (MER) Spirit and Opportunity have provided a wealth of *in situ* mineralogical and geochemical information, in part due to their extended mission lives, and have particularly provided new insights into the aqueous processes at their respective landing sites [Spirit at Guvev Crater (Christensen et al., 2004a) and Opportunity at Meridiani Planum (Squyres et al., 2004a; 2004b)]. The layered and etched, sulfate- and hematite-bearing deposits at Meridiani Planum have been intensively studied with orbital investigations (Arvidson et al., 2005; Christensen et al., 2001, 2000; Griffes et al., 2007; Wiseman et al., 2007) and *in situ* by the Opportunity rover (Squyres et al., 2006, 2004b, 2004c). The occurrence of sulfates (e.g., Ca-and Mg-sulfates), jarosite, and hematite, along with siliclastic constituents in outcrops of sedimentary material at Meridiani Planum have been interpreted as mineralogical indicators of aqueous paleo-environmental conditions in the region (Christensen et al., 2004b; Clark et al., 2005; Klingelhofer et al., 2004; Morris et al., 2006; Squyres et al., 2004a, 2004b, 2004c).

Jarosite was identified in the Eagle Crater outcrop at Meridiani Planum *in situ* Mössbauer analyses and confirmed by subsequent analyses with the Alpha Particle X-Ray Spectrometer (APXS) and the mini-TES instruments (Christensen et al., 2004b; Klingelhofer et al., 2004). Navrotsky et al. (2005) calculated the equilibrium decomposition curve of jarosite on Mars using thermochemical data and demonstrated that the mineral is thermodynamically stable under most present-day Martian surface pressures and temperatures. They further implied that this attribute (i.e., minimal alteration of the mineral since its initial deposition) makes jarosite an intriguing target for

Martian paleo-environmental investigations as it would retain minimally altered textural, chemical, and isotopic evidence of its depositional environment, including any possible biological activity. On Earth, jarosites form in acidic, oxidizing, and wet environments (e.g. AMD sites) known to harbour bacterial life. Jarosites are suggested as mineralogical biosignatures which retain evidence of the biological influence exerted in these systems (e.g., texture, crystallinity, isotopic signature, trace element composition. Due to this suggested exobiological potential, jarosite deposits at Meridiani Planum have been championed as good target materials for future sample return missions.

1.2.4. Jarosite as a mineralogical biosignature and analogue sites

Several studies have set out to characterize and study terrestrially analogous environments to the "wetter" Meridiani Planum condition in order to investigate the possibility of biosignatures and the detection of biomarkers (Amils et al., 2007; Battler et al., 2011; Lacelle and Léveillé, 2010; Parro et al., 2011, 2005; Stoker et al., 2008). Jarosite group minerals are paleo-environmental indicators of aqueous process at very acidic and oxidizing conditions (Bigham and Nordstrom, 2000). Terrestrial jarosite is formed through the oxidation of iron sulfides in acidic environments or via the interaction (and addition) of sulfur to basaltic precursor minerals (e.g. H_2SO_4 derived from SO_2 rich volcanic emissions). The presence of jarosite at the Meridiani Planum region indicates that previously the local Martian environment was acidic, oxidizing and had liquid water. Terrestrial analogue sites can be used to investigate these processes, akin to studying a modern environment in order to understand ancient deposits and signatures in the

geological record. Several natural acidic environments on Earth are currently used as analogues environments to study, characterize and evaluate the aqueous processes that generate the Mg-Fe-Ca sulfates and iron oxides observed in the environments suggested by these aforementioned theories. These include copper and zinc mines at Iron Mountain, California (Jamieson et al., 2005; Nordstrom and Alpers, 1999), basaltic tephra on Mauna Kea in Hawaii (Morris et al., 2005); acidic saline lakes in Western Australia (Benison and Bowen, 2006; Bowen and Benison, 2009); and the acidic Rio Tinto River in Spain (Fernandez-Remolar and Knoll, 2008; Fernandez-Remolar et al., 2008, 2005; Preston et al., 2011).

The Rio Tinto River system in Spain provides a good analogue of the hypothesized conditions at Meridiani Planum which are thought to generate biogenic jarosite deposits. Efflorescent minerals (including jarosite) precipitate along the river which is colonized by acidophilic microbial communities. The local climate generates annual wet and dry periods which provide an opportunity to conduct natural (i.e., real time) geological studies examining the generation, preservation and detectability of any biosignatures and/or fossils.

1.3. Biomineralization and biosignatures

Microbial biomineralization describes the formation and deposition of minerals directly mediated or indirectly influenced by microorganisms. Microbial biominerals may differ distinctly from their inorganically formed equivalents in crystallinity, isotopic signature, shape, size, and trace element composition (Konhauser, 2007). In terms of

astrobiological investigations (a subfield of geomicrobiology), it is extremely important that we understand and can confidently recognize these interactions in terrestrial environments prior to searching for them in other planetary materials.

Nucleation and growth of biominerals are extracellular processes generated by the metabolic activity of microorganisms; biomineralization takes place because of changes in the chemical equilibrium of the surrounding environment which in turn may be linked to specific metabolic products. Minerals generated as a result of biological activities typically possess poor crystallinities, are chemically heterogeneous, and are closely associated with the cell wall. Active biomineralization processes involve the direct redox conversion of metal ions bound to the microbial cell surface or the excretion of metabolically produced ions, in so forming minerals. Passive mineralization processes can be mediated by dead cells and involves non-specific binding of cations and the involvement of surrounding anions causes nucleation and growth of minerals. It is possible to differentiate active and passive mineralization processes from one another.

There are two modes of microbial biomineralization, biologically controlled mineralization (BCM) and biologically induced mineralization (BIM). BCM implies that the organisms actively control the nucleation site, growth, morphology, and location of the biomineralized product; BCM commonly occurs in closed or isolated environments. A well-known example of this form of mineralization is the production of magnetite or greigite (Fe_3S_4) crystals by magnetotactic bacteria within their cells, which is comprehensively reviewed by Bazylinski and Frankel (2003) and the references therein; when preserved in sediments these crystals are called magnetofossils. BIM processes are generally more a passive mineralization type where exopolysaccharides (EPS, also

referred to as extracellular polymeric substances) are particularly involved in the mineralization process. Mineral nucleation and growth can be mediated by the non-specific binding of cations and/or the attachment of surrounding anions to dead cells. BIM is comprehensively reviewed by Frankel and Bazylinski (2003) and the reference therein.

In terms of astrobiological investigations, it is extremely important that we understand and can confidently recognize these biological interactions, characteristics and indications in terrestrial environments (versus their abiotic counterparts) prior to searching for evidence of life in extraterrestrial materials. This can be achieved by studying microbe-mineral interactions actively occurring in contemporary planetary science analogues of extraterrestrial environments, materials, and systems.

1.4. Study goals

In this study, biosignatures in jarosites have been investigated as well as their detection using analytical techniques currently used to characterize and examine geological materials *in situ* on the Martian surface. Precipitates produced by enrichment cultures derived from Rio Tinto River sediments are compared to synthetic and abiotic media precipitates in Chapter 2. The aim was to determine the most useful microscopic methods in the search for morphological indications of biogenic activity as well as to assess the suggestion that jarosite represents a mineralogical biosignature. Light, confocal, epifluorescence, and electron microscopy analyses were employed to investigate the microbe-mineral interactions of mineralized products from enrichment

cultures in addition to assessing the differences of jarosite mineral morphologies. The detection of biogenicity within jarosites is investigated in Chapter 3 by comparing biogenic and synthetic jarosite. Mineral samples were analyzed using instrumentation which is currently used on active Martian missions (IR, VNIR, Mössbauer and LIBS spectroscopy), as well as those currently receiving considerable attention for future missions (Raman spectroscopy and ToF SIMS).

References

Alpers, C.N., Rye, R.., Nordstrom, D.K., White, L.D., King, B.S., 1992. Chemical, crystallographic and stable isotopic properties of alunite and jarosite from acid-hypersaline Australian lakes. Chem. Geol. 96, 203–226.

Amils, R., Gonzalez-Toril, E., Fernandez-Remolar, D., Gomez, F., Aguilera, A., Rodriguez, N., Malki, M., Garcia-Moyano, A., Fairen, A.G., de la Fuente, V., Sanz, J.L., 2007. Extreme environments as Mars terrestrial analogs : The Rio Tinto case. Planet. Space Sci. 55, 370–381.

Arvidson, R.E., Poulet, F., Bibring, J.P., Wolff, M., Gendrin, A., Morris, R.V., Freeman, J.J., Langevin, Y., Mangold, N., Bellucci, G., 2005. Spectral reflectance and morphologic correlations in eastern Terra Meridiani, Mars. Science 307, 1591–1594.

Basciano, L.C., Peterson, R.C., 2008. Crystal chemistry of the natrojarosite-jarosite and natrojarosite-hydronium jarosite solid-solution series: A synthetic study with full Fe site occupancy. Am. Mineral. 93, 853–862.

Basciano, L.C., Peterson, R.C., 2007a. The crystal structure of ammoniojarosite, $(NH_4)Fe_3(SO_4)_2(OH)_6$ and the crystal chemistry of the ammoniojarosite-hydronium jarosite solid-solution series. Mineral. Mag. 71, 427–441.

Basciano, L.C., Peterson, R.C., 2007b. Jarosite-hydronium jarosite solid-solution series with full iron site occupancy: Mineralogy and crystal chemistry. Am. Mineral. 92, 1464– 1473.

Battler, M.M., Osinski, G.R., Lim, D.S.S., Davila, A.F., Michel, F.A., Craig, M.A., Izawa, M.R.M., Leoni, L., Slater, G.F., Fairen, A.G., Preston, L.J., Banerjee, N.R., 2012. Characterization of the acidic cold seep emplace jarosite Golden Deposit, NWT, Canada, as an analogue for jarosite deposition on Mars. Icarus (in press) http://dx.doi.org/10.1016/j.icarus.2012.05.015

Bazylinski, D.A., Frankel, R.B., 2004. Magnetosome formation in prokaryotes. Nature Rev. Microbiol. 2, 217–230.

Bazylinski, D.A., Frankel, R.B., 2003. Biologically controlled mineralization in prokaryotes. Rev. Mineral. Geochem. 54, 217–247.

Becker, L., Popp, B., Rust, T., Bada, J.L., 1999. The origin of organic matter in the Martian meteorite ALH84001. Earth Planet. Sci. Lett. 167, 71–79.

Benison, K.C., Bowen, B.B., 2006. Acid saline lake systems give clues about past environments and the search for life on Mars. Icarus 183, 225–229.

Biemann, K., 2006. On the ability of the Viking gas-chromatograph-mass spectrometer to detect organic matter. PNAS 104, 10310–10313.

Bigham, J.M., Nordstrom, D.K., 2000. Iron and aluminium hydroxysulfates from acid sulfate waters. *In*: Alpers, C.N., Jambor, J.L., Nordstrom, D.K., Sulfate minerals:

Crystallography, geochemistry, and environmental significance. Rev. Mineral. Geochem. 40, 351–403.

Bradley, J.P., Harvey, R.P., McSween, H.Y., 1998. Epitaxial growth of nanophase magnetite in Martian meteorite Allan Hills 84001: implications for biogenic mineralization. Meteor. Planet. Sci. 33, 765–773.

Brophy, G.P., and Sheridan, M.F., 1965. Sulfate studies IV: The jarosite-natrojarosite-hydronium jarosite solid solution series. Am. Mineral. 50, 1595–1607.

Bowen, B.B., Benison, K.C., 2009. Geochemical characteristics of naturally acid and alkaline saline lakes in southern Western Australia. Appl. Geochem. 24, 268–284.

Brown, J.B., 1970. A chemical study of some synthetic potassium-hydronium jarosites. Can. Mineral. 10, 696–703.

Chevrier, V.F., Hanley, J., Atheide, T.S., 2009. Stability of perchlorate hydrates and their liquid solutions at the Phoenix landing site, Mars. Geophys. Res. Lett. 36, L10202, doi: 10.1029/2009GL037497.

Christensen, P.R., Ruff, S.W., Fergason, R.L., Knudson, A.T., Arvidson, R.E., Bandfield, J.L., Blaney, D.L., Budney, C., Calvin, W.M., Glotch, T.D., Golombek, M.P., Graff, T.G., Hamilton, V.E., Hayes, A., Johnson, J.R., McSween, H.Y., Mehall, G.L., Mehall, G.L., Moersch, J.E., Morris, R.V., Rogers, A.D., Smith, M.D., Squyres, S.W., Wolff, M.J., Wyatt, M.B., 2004a. Initial results from the Mini-TES experiment in Gusev crater from the Spirit Rover, Science 305, 837–842.

Christensen, P.R., Wyatt, M.B., Glotch, T.D., Rogers, A.D., Anwar, S., Arvidson, R.E., BAndfield, J.L., Blaney, D.L., Budney, C., Calvin, W.M., Fallacaro, A., Fergason, R.L., Gorelick, N., Graff, T.G., Hamilton, V.E., Hayes, A.G., Johnson, J.R., Knudson, A.T., McSween, H.Y., Mehall, G.L., Mehall, L.K., Moersch, J.E., Morris, R.V., Smith, M.D., Squyres, S.W., Ruff, S.W., Wolf, M.J., 2004b. Mineralogy at Meridiani Planum from the Mini-TES experiment on the Opportunity rover. Science 306, 1733–1739.

Christensen, P.R., Bandfield, J.L., Hamilton, V.E., Ruff, S.W., Kieffer, H.H., Titus, T.N., Malin, M.C., Morris, R.V., Lane, M.D., Clark, R.L., Jakosky, B.M., Mellon, M.T., Pearl, J.C., Conrath, B.J., Smith, M.D., Clancy, R.T., Kuzmin, R.O., Roush, T., Mehall, G.L., Gorelick, N., Bender, K., Murray, K., Dason, S., Greene, E., Silverman, S., Greenfield, M., 2001. Mars Global Surveyor Thermal Emission Spectrometer experiment: Investigation description and surface science results. J. Geophys. Res. 106, E10, 23823–23871.

Christensen, P.R., Bandfield, J.L., Smith, M.D., Hamilton, V.E., Clark, R.N., 2000. Identification of a basaltic component on the Martian surface from Thermal Emission Spectrometer data. J. Geophys. Res. 105, 9609–9622.

Clark, R.N, McCord, T.B.,1982. Mars residual north polar cap: Earth-based spectroscopic confirmation of water ice as a major constituent and evidence for hydrated minerals. J. Geophys. Res. 87, 367–370.

Clark, B.C., Morris, R.V., McLennan, S.M, Gellert, R., Jolliff, B., Knoll, A.H., Squyres, S.W., Lowenstein, T.K., Ming, D.W., Tosca, N.J., Yen, A., Christensen, P.R, Gorevan, S., Bruckner, J., Clavin, W., Dreibus, G., FArrand, W., Klingelhofer, G., Waenke, H., Zipfel, J., Bell III, J.F., Grotzinger, J., McSween, H.Y., Rieder, R., 2005.Chemistry and mineralogy of outcrops at Meridiani Planum. Earth Planet. Sci. Lett. 240, 73–94.

Clark, B.C., Baird, A.K. , Weldon, R.J., Tsusaki, D.M., Schnabel, L., Candelaria,M.P., 1982. Chemical composition of Martian fines, J. Geophys. Res. 87, 10059–10067.

Clark, B.C., Baird, A.K., Rose, Jr., H.J., Toulmin, III, P., Christian, R.P., Kelliher, W.C., Castro, A.J., Rowe, C.D., Keil, K.,Huss, G.R., 1977. The Viking X-ray fluorescence experiment: Analytical methods and early results. J. Geophys., Res. 82, 4577–4594.

Drouet, C., Navrotsky, A., 2003. Synthesis, characterization, and thermochemistry of K-Na-H_3O jarosites. Geochim. Cosmochim Ac. 67, 2063–2076.

Drouet, C., Pass, K.L., Baron, D., Draucker, S., Navrotsky, A., 2004. Thermochemistry of jarosite-alunite and natrojarosite-natroalunite solid solutions. Geochim. Cosmochim Ac.68, 2197–2205

Dutrizac, J.E., 1983. Factors affecting alkali jarosite precipitation. Metallurgical Transactions 14B, 531–539.

Dutrizac, J.E., Jambor, J.L., 2000. Jarosites and their application in hydrometallurgy. In C.N., Alpers, J.L., Jambor, D.K., Nordstrom, Eds., Sulfate Minerals – Crystallography, Geochemistry, and Environmental Significance, vol. 40, p. 405–452. Reviews in Mineralogy and Geochemistry, Mineralogical Society of America, Chantilly, Virginia.

Fernandez-Remolar, D.C., Knoll, A.H., 2008. Fossilization potential of iron-bearing minerals in acidic environments of Rio Tinto, Spain: Implications for Mars exploration. Icarus 194, 72–85.

Fernandez-Remolar, D.C., Prieto-Ballesteros, Olga, Rodriguez, N., Gomez, F., Amils, R., Gomez-Elvira, Stoker, C.R., 2008. Underground habitats in the Rio Tinto Basin: A model for subsurface life habitats on Mars. Astrobiology 8, 1023–1047.

Fernández-Remolar, D.C., Morris, R.V., Gruener, J.E., Amils R., Knoll, A., 2005. The Rio Tinto Basin Spain, Mineralogy, sedimentary geobiology, and implications for interpretation of outcrop rocks at Meridiani Planum, Mars. Earth Planet. Sci. Lett. 240, 149–167.

Griffes, J. L., Arvidson, R.E., Poulet, F., Gendrin, A., 2007. Geologic and spectral mapping of etched terrain deposits in northern Meridiani Planum. J. Geophys. Res. 112, E08S09, doi:10.1029/2006JE002811.

Grohol, D., Nocera, D.G., and Papoutsakis, D., 2003. Magnetism of pure iron jarosites. Physical Review B: Condens. Matt. Mater. Phys. 67, 1–13.

Hecht, M.H., Kounaves, S.P., Quinn, R.C., West, S.J., Young, S.M.M., Ming, D.W., Catling, D.C., Clark, B.C., Boynton, W.V., Hoffman, J., DeFlores, L.P., Gospodinova, K., Kapit, J., Smith, P.H., 2009. Detection of perchlorate and the solubility chemistry of Martian soil at the Phoenix Lander site. Science 325, 64–67.

Hendricks, S.B., 1937. The crystal structure of alunite and the jarosites. Am. Mineral. 22, 773–784.

Houck, J.R., Pollack, J.B., Sagan, C., Schaack, D., Decker, J., 1973. High altitude infrared spectroscopic evidence for bound water on Mars. Icarus 18, 470–480.

Jambor, J.L., 1999. Nomenclature of the alunite supergroup. Can. Mineral. 37, 1323–1341.

Jamieson, H.E., Robinson, C., Alpers, C.N., Nordstrom, D.K., Poustovetov, A., Lowers, H.A., 2005. The composition of coexisting jarosite-group minerals and water from the Richmond Mine, Iron Mountain, California. Can. Mineral. 43, 1225–1242.

Konhauser, K.O., 2007. Introduction to Geomicrobiology. Blackwell Publishing, Oxford, UK, p. 145.

Klingelhofer, G., Morris, R.V., Bernhardt, B., Schroder, C., Rodionov, D., de Souza, P.A.J., Yen, A.S., Gellert, R., Evlanov, E.N., Zubkov, B., Foh, J., Bonnes, U., Kankeleit, E., Gulich, P., Ming, D.W., Renz, F., Wdowiak, T.J., Squyres, S.W., Arvidson, R.E., 2004. Jarosite and hematite at Meridiani Planum from Opportunity's Mössbauer spectrometer. Science 306, 1740–1745.

Kubisz, J., 1972. Studies on synthetic alkali-hydronium jarosites. III. Infrared absorption study. Mineralogica Polonica 3, 23–36.

Kubisz, J., 1971. Studies on synthetic alkali-hydronium jarosites. II. Thermal investigations. Mineralogica Polonica 2, 51–59.

Kubisz, J., 1970. Studies on synthetic alkali-hydronium jarosites. I. Synthesis of jarosite and natrojarosite. Mineralogica Polonica 1, 47–57.

Lacelle, D., Léveillé, R., 2010. Acid drainage generation and associated Ca-Fe-SO_4 minerals in a periglacial environment, Eagle Plains, Northern Yukon, Canada: A potential analogue for low-temperature sulfate formations on Mars. Planet. Space Sci. 58, 509–521.

Lager, G.A., Swayze, G.A., Loong, C.H., Rotella, F.J., Richardson, J.W., Stoffregan, R.E., 2001. Neutron spectroscopic study of synthetic alunite and oxonium-substituted alunite. Can. Mineral. 39, 1131–1138.

Long, D.T., Fegan, N.E., McKee, J.D., Lyons, W.B., Hines, M.E., Macumber, P.G., 1992. Formation of alunite, jarosite and hydrous iron oxides in a hypersaline system: Lake Tyrrell, Victoria, Australia. Chem. Geol. 96, 183–202.

McKay, D.S., Gibson Jr., E.K., Thomas-Keptra, K.L., Vali, H., Romanek, C.S., Clemett, S.J., Chillier, X.D.F., Maechling, C.R., Zare, R.N., 1996. Search for past life on

Mars : possible relic biogenic activity in Martian meteorite ALH 84001. Science 273, 924–930.

Majzlan, J., Stevens, R., Boerio-Goates, J., Woodfield, B.F., Navrotsky, A., Burns, P.C., Crawford, M.K., Amos, T.G., 2004. Thermodynamic properties, low-temperature heat-capacity anomalies, and single-crystal X-ray refinement of hydronium jarosite, $(H_3O)Fe_3(SO_4)_2(OH)_6$. Phys. Chem. Mineral. 31, 518–531.

McSween, H.Y., 2008. Martian meteorites as crustal samples. *In*: Bell III, J.F., ed. The Martian Surface: Composition, Mineralogy and Physical Properties, Cambridge University Press, Cambridge, pp. 383–396.

McSween H.Y., 2007. Mars. *In*: Holland, H.D., Turekian, K.K., eds. Treatise on Geochemistry, Elsevier Science, Oxford, 1.22, pp. 1–27.

Morris, R. V., Klingelhöfer, G., Schröder, C., Rodionov, D.S., Yen, A., Ming, D.W., de Souza Jr., P.A., Wdowiak, T., Fleischer, I., Gellert, R., Bernhardt, B., Bonnes, U., Cohen, B.A., Evlanov, E.N., Foh, J., Gütlich, P., Kankeleit, E., McCoy, T., Mittlefehldt, D.W., Renz, F., Schmidt, M.E., Zubkov, B., Squyres, S.W., Arvidson, R.E., 2006. Mössbauer mineralogy of rock, soil, and dust at Meridiani Planum, Mars: Opportunity's journey across sulfate-rich outcrop, basaltic sand and dust, and hematite lag deposits. J. Geophys. Res. 111, E12S15, doi:10.1029/2006JE002791.

Morris, R.V., Ming, M.W., Graff, T.G., Arvidson, R.E., Bell III, J.F., Squyres, S.W., Mertzman, S.A., Gruener, J.E., Golden, D.C., Le, L., Robinson, G.A., 2005. Hematite spherules in basaltic tephra altered under aqueous, acid-sulfate conditions on Mauna Kea volcano, Hawaii: Possible clues for the occurrence of hematite-rich spherules in the Burns formation at Meridiani Planum, Mars. Earth Planet. Sci. Lett. 240, 168–178.

Morris, R.., Ming, D.W., Golden, D.C., Bell III, J.F., 1996. An occurrence of jarositic tephra on Mauna Kea, Hawaii: Implications for the ferric mineralogy of the Martian surface. In *Mineral Spectroscopy: A Tribute to Roger G. Burns*. Eds. Dyar, M.D., McCammon, C., Schaefer, M.W.. Huston: *The Geochemical Society*, Special Publication No. 5, pp. 327–336.

Navarro-Gonzalez, R., Vargas, E., de la Rosa, J., Raga, A.C., McKay, C.P., 2010. Reanalysis of the Viking results suggests perchlorate and organics at midlatitudes on Mars. J. Geophys. Res. 115, E12010, doi: 10.1029/2010JE003599.

Navarro-Gonzalez, R., Navarro, K.F., de la Rosa, J., Iniguez, E., Molina, P., Miranda, L.D., Morales, P., Cienfuegos, E., Coll, P., Raulin, F., Amils, R., McKay, C.P., 2006. The limitations on organic detection in Mars-like soils by thermal volatilization-gas chromatography-MS and their implications for the Viking results. PNAS (Proceedings of the National Academy of Sciences of the United States of America) 103, 16089–16094.

Navrotsky, A., Forray, F.L., Drouet, C., 2005. Jarosite stability on Mars. Icarus 176, 250–253.

Nordstrom, D.K., Alpers, C.N., 1999. Negative pH, efflorescent mineralogy, and consequences for environmental restoration at the Iron Mountain Superfund site, California. P. Natl. Acad. Sci. USA 96, 3455–3462.

Parker, R.L., 1962. Isomorphous substitution in natural and synthetic alunite. Am. Mineral. 47, 127–136.

Parro, V., Fernández-Remolar, D., Rodríguez-Manfredi, J.A., Cruz-Gil, P., Rivas, L.A., Ruiz- Bermejo, M., Moreno-Paz, M., García-Villadangos, M., Gómez-Ortiz, D., Blanco-López, Y., Menor-Salván, C., Prieto-Ballesteros, O., Gómez-Elvira, J., 2011. Classification of modern and old Rio Tinto sedimentary deposits through the biomolecular record using a life marker biochip : Implications for detecting life on Mars. Astrobiology 11, 29–44.

Parro, V., Rodriguez-Manifredi, J.A., Briones, C., Compositizo, C., Herrero, P.L., Vez, E., Sebastianm E., Moreno-Paz, M., Garcia-Villadangos, M., Fernandez-Calvo, P., Gonzalez-Toril, E., Perez-Mercader, J., Fernandez-Remolar, D., Gomez-Elvira, J., 2005. Instrument development to search for biomarkers on Mars: terrestrial acidophile, iron-powered chemolithoautotrophic communities as model systems. Planet. Space Sci. 53, 729–737.

Pollack, J.B., Kasting, J.F., Richardson, S.M., Poliakoff, K., 1987. The case for a wet, warm climate on early Mars. Icarus 71, 203–224.

Preston, L.J., Shuster, J., Fernández-Remolar, D., Banerjee, N.R., Osinski, G.R., Southam, G., 2011. The preservation and degradation of filamentous bacteria and biomolecules within iron oxide deposits at Rio Tinto, Spain. Geobiology 9, 233–249.

Ripmeester, J.A., Ratcliffe, C.I., Dutrizac, J.E., Jambor, J.L., 1986. Hydronium ion in the alunite-jarosite group. Can. Mineral. 24, 435–447.

Schempp, C.A., 1923. Argento-jarosite; a new silver mineral. Amer. J.Sci. 206, 73–75.

Scott, W.R., Yamaguchi, A., Krot, A.N., 1997. Petrological evidence for shock melting of carbonates in the Martian meteorite ALH84001. Nature 22, 377–379.

Stoffregen, R.E., Alpers, C.N., Jambor, J.L., 2000. Alunite-jarosite crystallography, thermodynamics and geochronology. In C.N. Alpers, J.L., Jambor, D.K., Nordstrom, Eds., Sulfate Minerals – Crystallography, Geochemistry, and Environmental Significance, vol. 40, p. 453–479. Reviews in Mineralogy and Geochemistry, Mineralogical Society of America, Chantilly, Virginia.

Stoker, C.R, Cannon, H.N., Dunagan, S.E., Lemke, L.G., Glass, B.J., Miller, D., Gomez-Elvira, J., Davis, K., Zavaleta, J., Winterholler, A., Roman, M., Rodrigue-Manifredi, J.A., Bonaccorsi, R., Bell, M.S., Brown, A., Battler, M., Chen, B., Cooper, G., Davidson, M., Fernandez-Remolar, D., Gonzales-Pastor, E., Heldmann, J.L., Martinez-Frias, J., Parro, V., Prieto-Ballesteros, O., Sutter, B., Schuerger, A.C., Schutt, J., Rull, F., 2008. The 2005 MARTE Robotic Drilling

Experiment in Rio Tinto, Spain: Objectives, approach, and results of a simulated mission to search for life in the Martian subsurface. Astrobiology 8, 921–945.

Squyres, S.W., Knoll, A.H., Arvidson, R.E., Clark, B.C., Grotzingter, J.P., Jolliff, B.L., McLennan, S.M., Tosca, N., Bell III, J.R., Calvin, W.M., Farrand, W.H., Glotch, T.D., Golombek, M.P., Herkenhoff, K.E., Johnson, J.R., Klingelhöfer, G., McSween, H.Y., Yen, A.S., 2006. Two years at Meridiani Planum: Results from the Opportunity rover. Science 313, 1403–1407.

Squyres, S.W., Arvidson, R., Bell III, J.F., Bruckner, J., Cabrol, N.A., Calvin, W., Carr, M.H., Christensen, P.R., Clark, B.C., Crumpler, L., Des Marais, D.J., d'Uston, C., Economou, T., Farmer, J., Farrand, W., Folkner, W., Golombek, M., Gorevan, S., Grant, A., Greeley, R., Grotzinger, J., Haskin, L., Herekenhoff, K.E., Hviid, S., Johnson, J., Klingelhofer, G., Knoll, A., Landis, G., Lemmon, M., Li, R., Madsen, M.B., Malin, M.C., McLennan, S., McSween, H.Y., Ming, D.W., Moersch, J., Morris, R.V., Parker, T., Rice, J.W., Richter, L., Rieder, R., Sims, M., Smith, M., Smith, P., Soderblom, L.A., Sullivan, R., Wanke, H., Wdowiak, T., Wolff, M., Yen, A., 2004a. The Opportunity Rover's Athena Science Investigationat Meridiani Planum, Mars. Science 306, 1698–1703.

Squyres, S.W., Arvidson, R., Bell III, J.F., Bruckner, J., Cabrol, N.A., Calvin, W., Carr, M.H., Christensen, P.R., Clark, B.C., Crumpler, L., Des Marais, D.J., d'Uston, C., Farmer, J., Farrand, W., Folkner, W., Golombek, M., Gorevan, S., Grant, A., Greeley, R., Grotzinger, J., Haskin, L., Herekenhoff, K.E., Hviid, S., Johnson, J., Knoll, A., Landis, G., Lemmon, M., Li, R., Madsen, M.B., Malin, M.C., McLennan, S., McSween, H.Y., Ming, D.W., Moersch, J., Morris, R.V., Parker, T., Rice, J.W., Richter, L., Rieder, R., Sims, M., Smith, M., Smith, P., Soderblom, L.A., Sullivan, R., Wanke, H., Wdowiak, T., Wolff, M., Yen, A., 2004b. Initial results from the Athena Science Investigation at Gusev crater, Mars. Science 305, 794–799.

Squyres, S.W., Grotzinger, J.P., Arvidson, R.E., Bell III, J.F., Calvin, W., Christensen, P.R., Clark, B.C., Crisp, J.A., Farrand, W.H., Herkenhoff, K.E., Johnson, J.R., Klingelhofer, G., Knoll, A.H., McLennan, S.M., McSween, H.Y., Morris, R.V., Rice, J.W., Rieder, R., Soderblom, L.A., 2004c. In situ evidence for an ancient aqueous environment at Meridiani Planum, Mars. Science 306, 1709–1714.

Thomas-Keprta, K.L., Clemett, S.J., McKay, D.S., Gibson, Jr., E.K., Wentworth, S.J., 2009. Origins of magnetite nanocrystals in Martian meteorite ALH84001. Geochim. Cosmochim. Act. 73, 6631–6677.

Thomas-Keprta, K.L., Clemett, S.J., Bazylinski, D.A., Kirschvink, J.L., McKay, D.S., Wentworth, S.J., Vali, H., Gibson, Jr., E.K., Romanek, C.S., 2002. Magnetofossils from ancient Mars: A robust biosignature in the Martian meteorite ALH84001. App. Envir. Microbiol. 68, 3663–3672.

Wiseman, S. M., Griffes, J.L., Arvidson, R.E., Murchie, S., Poulet, F., Knudson, A.T., Seelos, F.P., Tosca, N., CRISM Science Team, 2007. New analyses of MRO

CRISM, HiRISE, and CTX data over layered sedimentary deposits in Meridiani. LPI Contrib., 7th International Conference on Mars, July 9 –13, 2007, Pasadena CA, Abs. #3111.

Chapter 2.

Jarosite as a biosignature: A structural characterization of biogenic and synthetic jarosites

2.1. Introduction

2.1.1. Background

Jarosites are of considerable interest in environmental, geological, astrobiological, geomicrobiological, and metallurgical fields. Environmental interests lay with the capacity of jarosite to sorb and co-precipitate with many elements, some which are particularly toxic (e.g., As), removing them from acid mine drainage (Dutrizac and Jambor, 2000). Some jarosites co-precipitate with metals of economic interest (e.g., Ag, Pb) and in some historical instances, have generated deposits large enough to be economically viable, such as the argentiferous plumbojarosite pockets at the Matagente mine in Peru, which was mined by the Incas (Allen, 1973). Two million tonnes of silver bearing jarosite was also mined in the Rio Tinto region (Spain) during the Roman era, which contributed to the expansive wealth of the region (Dutrizac and Jambor, 2000; Dutrizac et al., 1983; Roca et al., 1999). Jarosite deposits are also important for mineral exploration, as they are indicators of unexposed sulfide deposits, akin to gossans, through the exposure of sulfides to surficial weathering processes (e.g., Golden Deposit, Canada; Rio Tinto, Spain). The jarosite accumulation at Golden Deposit is the result of the upwelling of concentrated mineralized groundwater, which has encountered a sulfide-bearing horizon during its subsurface flow (Battler et al., 2012; Lacalle and Léveillé, 2010; Michel and van Everdingen, 1987).

Astrobiological interest in jarosite lies with the *in situ* detection of jarosite on the Martian planetary surface at Meridiani Planum by the MER Opportunity rover (Christensen et al., 2004; Klingelhofer et al., 2004; Squyres et al., 2004). It has assumed potential as a mineralogical biomarker resulting from presumed capability of retaining and preserving signatures of *in situ* biological influence, if it was formed via biogenic processes (Navrotsky et al, 2005). Astrobiology investigates the potential of life, extant or extinct, on other planetary bodies, and receives a great deal of attention from both the scientific and public communities (e.g., McKay et al., 1996). Exobiological investigations require a detailed understanding of life's interactions with terrestrial environments here on Earth before we can be sure that we can confidently recognize any clues, indicators, or signals of biogenic interactions on other planetary bodies (e.g., Mars, Enceladus, Europa, and Titan) or in extraterrestrial materials (e.g. Martian meteorites ALH84001 and Nakhla). That is to say, our capacity to detect and assign biogenicity in any geological material is only as good as our ability to do so with terrestrial materials, which in turn is a reflection of our understanding of the terrestrial biosphere.

One particularly notable area of inquiry in this field is our capacity to detect and assign biogenicity to any signature observed in extraterrestrial material, as abiological processes can easily create these signatures as well, and that they may be misinterpreted as biological, or signs of life (i.e., a false signature). However, this difficulty is not limited to extraterrestrial materials (Walsh and Westall, 2009). It is often difficult to discern microbial versus abiological processes and respective contributions to mineral precipitation. Confusion arises as it is easily forgotten that simply because a microbe is found in association with a mineralogical phase on Earth does not signify that the

mineralization was influenced by biological processes; or that it will contain or preserve any indication of this biological association (Westall, 2008). Emerson and Revsbech (1994a, 1994b) demonstrated this using ferrihydrite and passive iron mineralization.

Analogue environments are locations on Earth where contemporary environmental and geological conditions are similar to those found on another planetary body. These analogue environments are commonly used to test methodologies, protocols, technologies, and instrumentation in development for use on future planetary exploration missions (Bonaccorsi and Stoker, 2008; Edwards et al. 2007; Parro et al., 2005; Pullan et al., 2008; Roach et al., 2006; Sobron et al., 2009; Stoker et al., 2008; Sutter et al., 2008). Additionally, these environments are used to develop our understanding of biosignatures in geological materials (Foster et al., 2010; Gleeson et al., 2010; Preston et al., 2011). Martian jarosites have been taken as an environmental indicator of oxidizing, acidic aqueous conditions at the planetary surface. Terrestrial jarosites are known to precipitate in acidic, oxidizing, environments (e.g., AMD) and these environments are commonly associated with acidophilic microbial communities and the precipitation of efflorescent minerals. Rio Tinto has been suggested as a modern terrestrial analogue environment of the paleo-environmental conditions that may have persisted at Meridiani Planum when the region was exposed to aqueous conditions (Fernandez-Remolar et al., 2008, 2005, 2004).

2.1.2. Site description

Located in southwestern Spain, the Rio Tinto River originates in the Sierra Morena Mountains of Andalusia in the core of the Iberian Pyrite Belt, one of the largest iron and copper sulfide districts known globally, and flows southward to the Atlantic

Ocean at Huelva. The Rio Tinto watershed covers 1,696 km^2, the river itself is 92 km long and has a gentle slope (average 0.59%). Gentle flow facilitates the growth of microbial communities which settle and coat the riverbed, particularly in the headwater regions (Gonzalez-Toril et al., 2003b). As a result of the Mediterranean-type climate regime, seasonal variations of geochemical conditions occur in the area with the alternating wet and dry seasons. There is little to no precipitation in the summer months (July-September) and heavy rainfalls (in excess of 120 mm) are common during the wet season (Aguilers et al, 2007; Lopez-Archilla et al., 2001).

The pH of the system remains low, fluctuating within a narrow range (between 1.5 to 3.1, annual mean ~2.2) irrespective of the temperature or flow of the river. This narrow pH range is thought to be the result of the buffering effect of high ferric iron concentrations (Lopez-Archilla et al., 1993) in the waters. Ferric iron is produced in this system as a result of the metabolism of iron oxidizing microorganisms which are active in the aerobic portion of the river system. Ferric oxide is responsible for the notable deep reddish hue of the waters of this river (Aguilers et al., 2006). Sulfur oxidizing microbial communities are also present in this system and generate sulfuric acid as a by-product of the chemolithic oxidation of sulfides along the river. H_2SO_4 can also be generated in the river by the chemical oxidation of certain sulfide mineral substrates (Gonzalez-Toril et al., 2003a). The effect of the ferric iron and sulfuric acid generation is a highly acidic system that promotes the dissolution of other heavy metal bearing minerals, particularly in comparison to more alkaline flows (e.g., springs and streams) nearby that traverse the same bedrock (Fernandez-Remolar et al., 2003).

The river's extremely low pH and high concentration of sulfate, ferric iron, and other heavy metals make the system a prime example of an AMD environment. There is

disagreement whether these conditions are naturally occurring or the result of anthropogenic AMD as a result of intensive mining activity carried out in the region for over 5000 years (Davis et al., 2000; Leblanc et al., 2000; van Geen et al., 1997). Support for a natural development and evolution of the system is provided by evidence in the form of massive laminated iron "bioformations" within ancient river terraces that predate the earliest known mining activity in the area. Fernandez-Remolar et al (2003) and Gonzalez-Toril et al. (2003b) suggest that deposition these laminated sedimentary facies, (morphologically similar to banded iron formation) constitute evidence supporting the development and evolution of the Tinto system via naturally occurring processes which have not changed significantly over time. Intuitively, both perspectives are correct. Both natural and anthropogenic AMD contribute to the current chemistry and mineralogy of this system. Regardless, the extreme conditions observed in the Rio Tinto system are the result of metabolic activity of chemolithotrophic microorganisms dwelling in the waters. Eukaryotic diversity is relatively low in this system, and microbial species like *Acidithiobacillus ferrooxidans* are considered to be primarily responsible for the extreme conditions of this acidic environment (Colmer et al., 1950, 1947; Edwards et al., 2007, 2000). Acidic habitats, like Rio Tinto, are especially interesting in term of geomicrobiological investigations because the acidic pH of the environment is a direct consequence of microbial metabolism and not a condition imposed by the system, as is the case in many other extreme environments (i.e., temperature, ionic strength, high pH, radiation, and pressure) (Gonzalez-Toril et al., 2003b).

2.1.3. Study goals

The purpose of this chapter is to gain insight into the interaction between acidophilic iron oxidizing bacteria and jarosite derived from an enrichment culture obtained from the Rio Tinto River. The aim is to characterize this 'biogenic' product and compare it to a synthetic and abiogenic jarosite in order to evaluate if jarosite can be utilized as a mineralogical biomarker. Biogenically derived jarosite precipitates are also compared to an 'abiogenic' jarosite derived from an identical control environment (i.e., same low temperature and aqueous geochemical conditions; omission of cells to culture). This is the first time that such a comparison has been documented. Most studies seek to appraise biosignatures without examining the abiotic process associated with the same thermodynamic reactions (i.e., identical starting reactions and experimental conditions) which are taken advantage of by bacterial populations. In all cases of mineralization the thermodynamic principles guiding the process are the same, for a mineral to precipitate "a certain threshold of energy must be invested" and overcome (Konhauser, 2007).

This study aims to investigate if the geomicrobiological interactions of the biota in these acidic, aqueous, sulfate rich systems produce biological structures or signatures which are captured and/or persist within the mineralogical matrix. If so, this may represent a mineralogical signature of biogenicity, as bacteria can serve as templates for iron deposition. The organic remains are frequently incorporated into mineral precipitates during crystal nucleation and growth, resulting in iron-organic composites that may or may not retain their microbial origin. Furthermore, is it important to assess the exobiological potential of jarosites; by assessing our ability, in controlled laboratory experiments, to observe and detect mineralogical biosignatures in terrestrial jarosite

samples we can gain insight into the preservation potential of signatures within similar materials on Mars.

2.2. Methods

2.2.1. Sample collection

The Rio Tinto River is located in southwestern Spain and represents an extraordinary ecosystem. The river flows over the Iberian Pyrite Belt (IPB), a region rich in massive sulphite deposits, has a constant acidic pH (~2.2), and a high concentration of heavy metals. Grab samples of iron oxides from the Rio Tinto River riverbed were collected near Berrocal, Spain (Figure 2.1. and Figure 2.2.A-C) using a sterile, disposable plastic pipette and sealed in sterile 50 ml Falcon tubes with no headspace. Samples were stored at room temperature (~22°C) and transported to the Geomicrobiology Laboratory at the University of Western Ontario for analysis.

2.2.2. Microbial culturing

Iron oxides from the Rio Tinto River were processed through limiting dilutions in 9K buffer (per L dH_2O): 0.1 g K_2HPO_4, 0.4 g $MgSO_4 \cdot 7H_2O$, 0.4 g $(NH_4)_2SO_4$, to isolate individual bacteria. Iron oxidizing bacteria were cultured and maintained in 9K buffer containing 33.3 g/L $FeSO_4 \cdot 7H_2O$. Buffer and the iron stock solutions were adjusted to pH 2.2 prior to filter sterilization (0.45 µm pore size, Millipore). The culture medium was dispensed into autoclaved 13 x 100 mm test tubes, inoculated, and covered with plastic push caps to allow free gas diffusion. Cultures were incubated and left to grow at

Figure 2.1. Geographic map of the Tinto River Basin region. Detailed geographic map of the Tinto River adapted from Preston et al. (2011); originally from Fernández-Remolar et al., (2003). Inset (A) in upper right hand corner shows the region of the Tinto River Basin (box) in relation to the Iberian Peninsula and the Atlantic Ocean. On the detailed map, towns and cities are noted in black text (i.e., Huelva, Niebla, Berrocal, Minas de Riotinto, and Nerva) and notable sites from previous studies are indicated by a small black dot and annotated with grey text (i.e., Peña de Hierro, Alto de la Mesa, and Minas de Tharsis). The sampling location where the initial samples of iron oxides were collected from the riverbed, near the town of Berrocal (Figure 2.2A), is marked by a grey star.

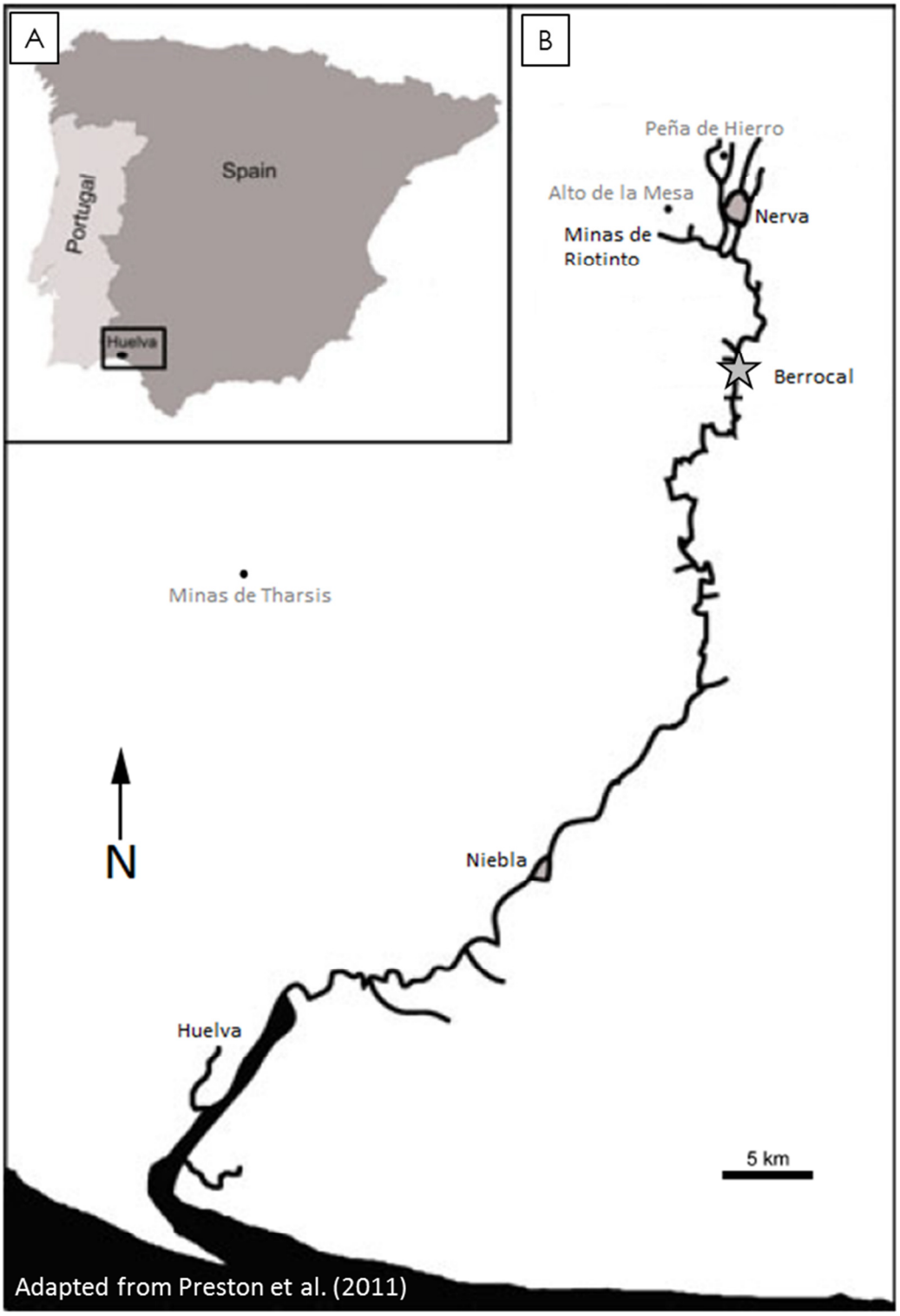

Adapted from Preston et al. (2011)

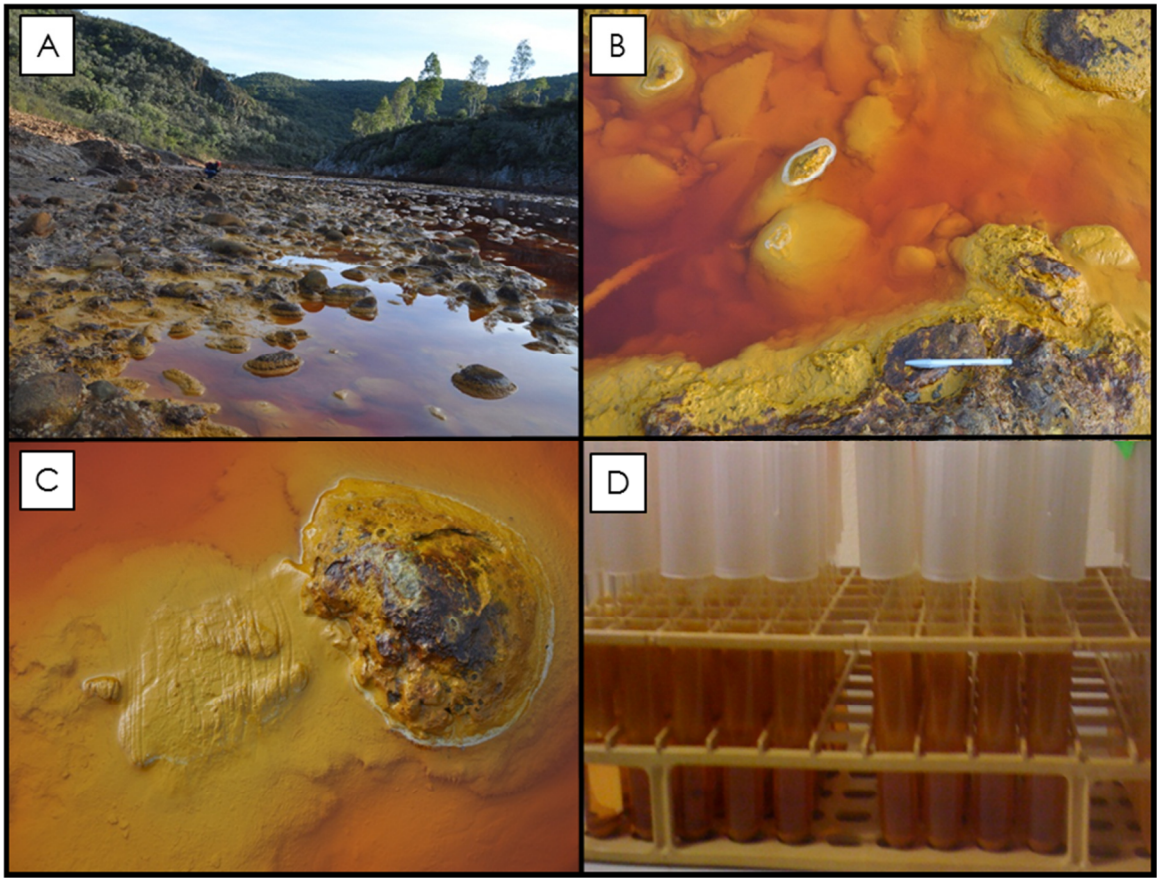

Figure 2.2. Photographs of the Rio Tinto sampling site. (A) Photograph of the sampling locality near Berrocal where samples were taken. (B) The flowing waters of the Tinto River are red and transparent and the riverbed below can be seen clearly from the surface. (C) The riverbed is lined with cobbles, which when submerged are covered with an accumulation of lighter yellow flocculent material (a highly hydrated iron oxide material), and as the cobbles are exposed to more arid or evaporation conditions this material becomes less hydrated and become darker in color and forms crusts. (D) Grab samples were collected from the river (see groves in C) and enrichment cultures were maintained in a laboratory. After 7 weeks culture solutions were orange and had precipitated along the side of tubes.

room temperature (~22°C), stationary on the laboratory bench for seven weeks. Culture growth was based on the phenotypic colour change of the initial medium solution from clear to a bright orange solution and the development of a crust at the water air interface of the test tube (Figure 2.2.D). Microbial culture precipitate powders were generated by harvesting microbial cultures from test tubes (minimum n = 25) using 0.45 μm pore size filters (Millipore), rinsed with 500 mL ultra-pure water (18 MΩ cm, Milli-Q) and dried in an oven at 60°C for 24 – 72 h to remove any water molecules adsorbed to the mineral precipitates.

A long term abiotic culture medium control (abiogenic) sample was derived from sterile (i.e. no bacteria inoculation) enrichment media control samples which were prepared in parallel to the enrichment cultures. Solutions were prepared by following the enrichment culture protocol above and omitting the addition of a bacterial inoculum to the solution. These abiotic culture samples were permitted to chemically oxidize stationary on a laboratory bench alongside the cultures so that all test tube samples experienced identical environmental conditions (e.g., temperature, humidity, sunlight). The abiogenic control represents an identical replica of the biogenic system with identical thermodynamic, temperature, and geochemical condition parameters.

2.2.3. Synthetic jarosite preparations

A suite of synthetic jarosites were prepared in an effort to try and find material that was comparable to the biological material harvested from the above cultures. A representative synthetic jarosite was selected for further analysis in this study; the details of the experimental synthesis investigations can be found in Appendix A (page 128).

Briefly, potassium jarosite (herein referred to by its mineral name, jarosite) was synthesized using a method adapted from a protocol described in Dutrizac and Kaiman (1976). A 1 L solution containing 30 g of KNO_3, 8 g of $Fe_2(SO_4)_3$, and 0.01 M H_2SO_4 was heated in open air and continuously stirred for 3 h at 85°C. Sulfuric acid was used to prevent iron hydrolysis and precipitation. Potassium nitrate was used as an alternative to potassium sulfate as previous studies (Dutrizac and Kaiman, 1976) have demonstrated that the resulting precipitates yield richer potassic products. The precipitate was scraped from the beaker, filtered, and rinsed using copious amounts of deionized water to remove any soluble ions. The rinsed precipitate was then dried for 24 – 72 h in an oven at 60°C to remove any loosely bound water from the mineral precipitate. Powder X-ray diffraction analysis of the precipitate was used to verify the composition and mineralogy of the synthesized material.

2.2.4. X-ray diffraction (XRD)

Mineralogical phase identifications were completed on both microbial culture precipitates and the synthetic material using powder X-ray diffraction analyses. Data were collected from 2-82°2θ (CoKα radiation) using a Rigaku Rotaflex 180 mm diffractometer with a rotating-anode diffractometer as well as a graphite-diffracted beam monochromator for all mineralogical samples. Before each experiment, the diffractometer was calibrated using a quartz standard. X-rays were collimated using 1° divergent and scatter slits, and a 0.15 mm receiving slit. Powder mounts of dried culture precipitates and synthetic jarosite were prepared by pressing fine-grained powder samples (ground with a mortar and pestle) into the window of a frosted glass slide and preparing smooth, flat mounts. In all cases, Co X-ray tube was operated at 45 kV and 160

mA. Profiles were taken with a step interval of 0.5°2θ, with a counting time per step of 30 s. The Bruker AXS EVA software package (BrukerAXS, 2005) was used to integrate the profiles as well as match identified peaks with the International Centre for Diffraction Data (ICDD) database.

2.2.5. Light microscopy and microbial viability

Microbial viability of the liquid phase of the cultures was assessed following the epifluorescence two stain protocol using the LIVE/DEAD® *BacLight*™ Bacterial Viability Kit (Invitrogen molecular probes (Eugene, Oregon, USA, Invitrogen.com); live bacteria with intact membranes fluoresce green (SYTO®9), while dead bacteria appear red (propidium iodide) when imaged with epifluorescence microscopy conditions. One millilitre of the aqueous phase of a microbial test tube culture was partitioned into a micro centrifuge tube. The sample was centrifuged for 1 min at 14,000 x g, generating an aggregate of solid material in the bottom of the tube, the supernatant discarded, then 1 mL of ultrapure water was added to the micro centrifuge tube and the sample was vortexed for several minutes in order to re-suspend the cells and mineral into solution. Tubes were covered with aluminum foil ensuring that the prepared sample remained in the dark, minimizing the loss of fluorescence before microscopic analysis. 500 µL each of SYTO®9 and propidium dye were added to the re-suspended solution in the micro centrifuge tube and briefly agitated, then left stationary in a dark drawer for 10 min. Prior to microscope analysis 150 µL of the stained solution was spotted onto a glass slide.

Light and confocal microscopy analyses of the biological and synthetic jarosite samples were completed at the Biotron Experimental Climate Change Research Centre at

the University of Western Ontario. Both samples were imaged using a Zeiss Imager.Z1 microscope equipped with an AxioCam digital camera to complete bright field microscopy (BF), dark field microscopy (DF), differential interference contrast microscopy (DIC), and phase contrast microscopy (PC). Epifluorescence microscope analysis was conducted on only the biological sample using a Zeiss LSM 5 Duo in order to image the microbial cells and their context within the mineralogical matrix framework.

2.2.6. Scanning electron microscopy (SEM)

Microbial cultures were fixed using glutaraldehyde (2% v/v) in preparation for scanning electron microscope (SEM) analyses, immobilized onto 0.45 μm filters (Whatman-type) and dehydrated using a graded ethanol series (25%, 50%, 75%, and 100% × 3) for 30 min at each interval. Samples were then critical point dried to 37^{o}C in a SamDri® Critical Point Drier (Tousimis Research Corp., Rockville, MD, USA) in order to preserve the structure of the cells present in the samples. Samples were mounted onto aluminum stubs with 12 mm carbon adhesive tabs (EM Science). The same synthetic jarosite powders that were used for powder XRD analysis (above) were utilized in the preparation of samples for SEM analysis. Synthetic powders were pressed onto carbon adhesive tabs attached to aluminum stubs. All samples for SEM analyses were platinum coated using a Denton Vacuum Desk II sputter coater to reduce charging artifacts. Analyses were conducted and high resolution images obtained using a LEO 1530 Field Emission SEM (CarlZeiss SMT AG, Oberkochem, Germany) at the Nanofabrication Facility at the University of Western Ontario.

2.2.7. Transmission electron microscopy (TEM)

Synthetic jarosites and microbial culture precipitates were prepared for transmission electron microscopy (TEM) analysis by being embedded into plastic and cut into ultrathin sections. For both samples, small amounts of dried mineralogical powder precipitates were enrobed in noble agar (2% w/v), processed through a graded acetone series (25%, 50%, 75%, and 100% × 3) for 15 min at each interval and then embedded in Epon resin (EM Science). Samples were transferred into fresh Epon resin and cured at 60°C for 48 h. The embedded samples were ultrathin sectioned (70 nm thickness) using a diamond knife on a Reichert-Jung Ultracut E ultra-microtome (Reichert Microscope Services, Depeco, NY, USA) and collected on Formvar carbon-coated 200 mesh copper grids. Unstained ultrathin sections were examined at 80 kV with a Phillips CM-10TEM (Philips, Amsterdam, Netherlands) at the Biotron Experimental Climate Change Research Centre at the University of Western Ontario.

2.3. Results and Discussion

For the sake of clarity, microbial culture precipitated jarosite, sensu stricto, will be referred to as biogenic jarosite; precipitates created from synthetic protocols will be denoted as synthetic jarosite; and jarosite material produced from the long term abiotic chemical oxidation of sterile media (i.e. ‘control system’) will be designated as abiogenic jarosite. Additionally, biogenic jarosite samples analysed in this study were cultured after 7 weeks, unless stated otherwise.

2.3.1. Microbial culturing

Microbial culture growth was determined by an observed colour change of inoculated samples from a clear, transparent solution (i.e., initial medium) to a bright orange solution approximately seven weeks after inoculation (Figure 2.2). This lag period is common with in vitro systems and is consistent with previous studies using similar enrichment cultures (Bingham et al., 1996; Liu et al., 2007). Furthermore, microbes using Fe^{2+} as a source of energy must oxidize large quantities of ferrous iron to grow in solution as the oxidation reaction has low energy yields (ΔG_r = 6.5 kcal/mol with O_2 as the electron acceptor at pH 2.5; Lees et al., 1969). To generate the color change observed in the cultures, bacterial populations must multiply and increase in size to a reach critical level of metabolic activity within the new environment (growth medium) for the oxidation of ferrous iron to proceed rapidly. In addition, cemented iron oxide precipitates, based on the color change, were produced at the solution air interface as a thin lens (or rind/coating) in all biogenic samples and some particulate material also formed and precipitated out of solution in older samples. Over time, i.e., in older microbial culture samples, the color of the solutions became a deeper orange ochre, the precipitate crustal rinds at the interface became thicker (macroscopic observation) and the system lost water (evaporation) and the crust grew down the test tube walls. While this represents an artifact of the experimental system, it is analogous to the dehydration of natural iron oxides with changing hydrologic regimes including the potential formation of efflorescent minerals associated with these analogues (Fernadez-Remolar et al., 2005; Frost et al., 2007b).

Enrichment cultures were dominated by aerobic, Fe oxidizing, acid tolerant, rod shaped bacteria, similar to *Acidithiobacillus ferrooxidans* (*A. ferrooxidans*). Samples collected from older enrichment cultures yielded more mineralogical material per test tube harvested, which is consistent with other studies using similar microbial cultures. For example, Liu et al. (2007) observed that the precipitation of jarosite in their experimental batch cultures corresponded to the logarithmic growth phase of *A. ferrooxidans* and that as the community population size increased, so did the production rate of ferric iron and the subsequent precipitation of jarosite within their system.

Abiotic chemical controls (i.e., no bacterial cells) prepared in parallel to the biotic cultures, remained clear and free of any precipitates. Furthermore, the control system first showed evidence of ferrous iron oxidation (i.e., color change) and production of precipitates only after ~8 months and significant (approx. 50%) drying of the culture tubes. In comparison to the progression of the biogenic and synthetic mineralogical precipitates, the precipitation of the abiogenic chemical oxidation product required a significantly longer period of time to develop and precipitate from solution. This study represents the first investigation, to our knowledge, which directly compares biogenic and abiogenic jarosite materials generated from identical low temperature, thermodynamic processes, and environmental systems. The abiotic chemical oxidation of the ferrous iron in the control system, noted by the distinctive colour change of the clear medium solution to an deep orange-ochre hue (albeit more dilute in appearance than the microbial enrichment cultures), took a significantly longer period of time (e.g. 2 yrs) on a stationary laboratory bench to generate evidence of mineral precipitation in the system. Abiogenic precipitates generated were the same deep ochre orange as the biogenic material.

The pH of both the abiotic and enrichment culture experimental systems remained constant, at 2.2, regardless of the age of the culture, the hue of culture solution, the presence of precipitates, or the amount of water lost from the system (i.e., evaporation) which had occurred in the system.

2.3.2. Mineralogical characterization of precipitates

The powder X-ray diffraction (XRD) patterns obtained of all jarosite minerals in this study matched very well to the known and well-established patterns of other natural and synthetic jarosite materials which have previously been documented (Baron and Palmer, 1996; Bigham et al., 2010; Drouet and Navrotsky, 2003; Dutrizac and Kaiman, 1976; Frost et al., 2007a; Smith et al., 2006) including studies characterizing other microbial mediated jarosite precipitates (Giaveno et al., 2008; Grishin et al., 1988; Wang et al., 2006). XRD patterns generated from the analysis of biogenic precipitates (t = 7 wks) were mineralogically identified as jarosite (Figure 2.3.). No additional mineral phases were observed and no impurities were detected as all of the peaks generated during XRD analysis of the biogenic material corresponded to those of pure phase jarosite (ICDD card no. 00-036-0427).

The XRD patterns of biogenic material indicate that no other mineralogical phases were generated or produced at detectable levels in any of the microbial culture precipitate samples over the 8-month sampling and analysis period (i.e., no additional peaks were generated). Figure 2.4. demonstrates the gradual progression of the diffraction patterns of the biological precipitates as the enrichment culture is permitted to grow for increasing

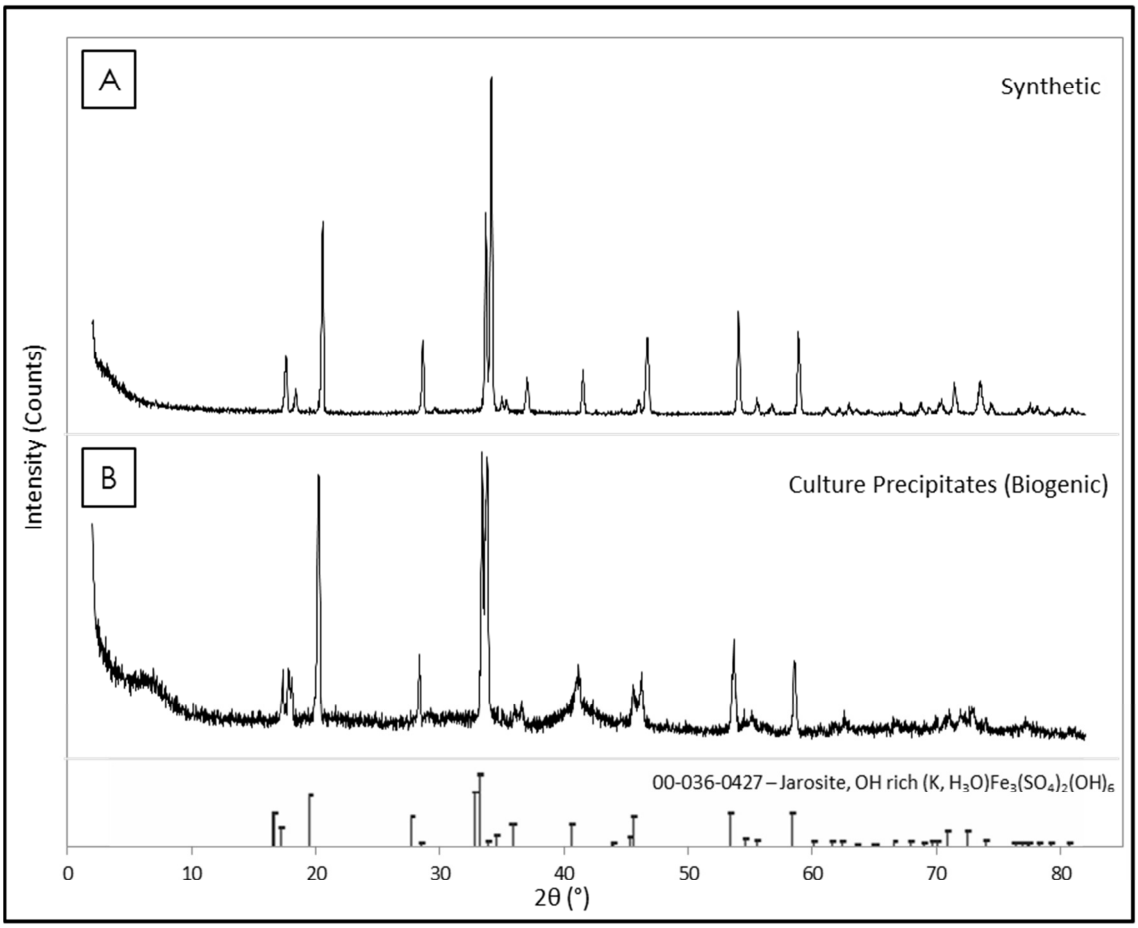

Figure 2.3. Powder X-ray diffraction (XRD) pattern of synthesized jarosite mineral (A) and microbial culture precipitates (B). The matching mineral phase from the ICDD database, jarosite (card no. 00-036-0427) $KFe_3(SO_4)_2(OH)_6$, is indicated by stick pattern.

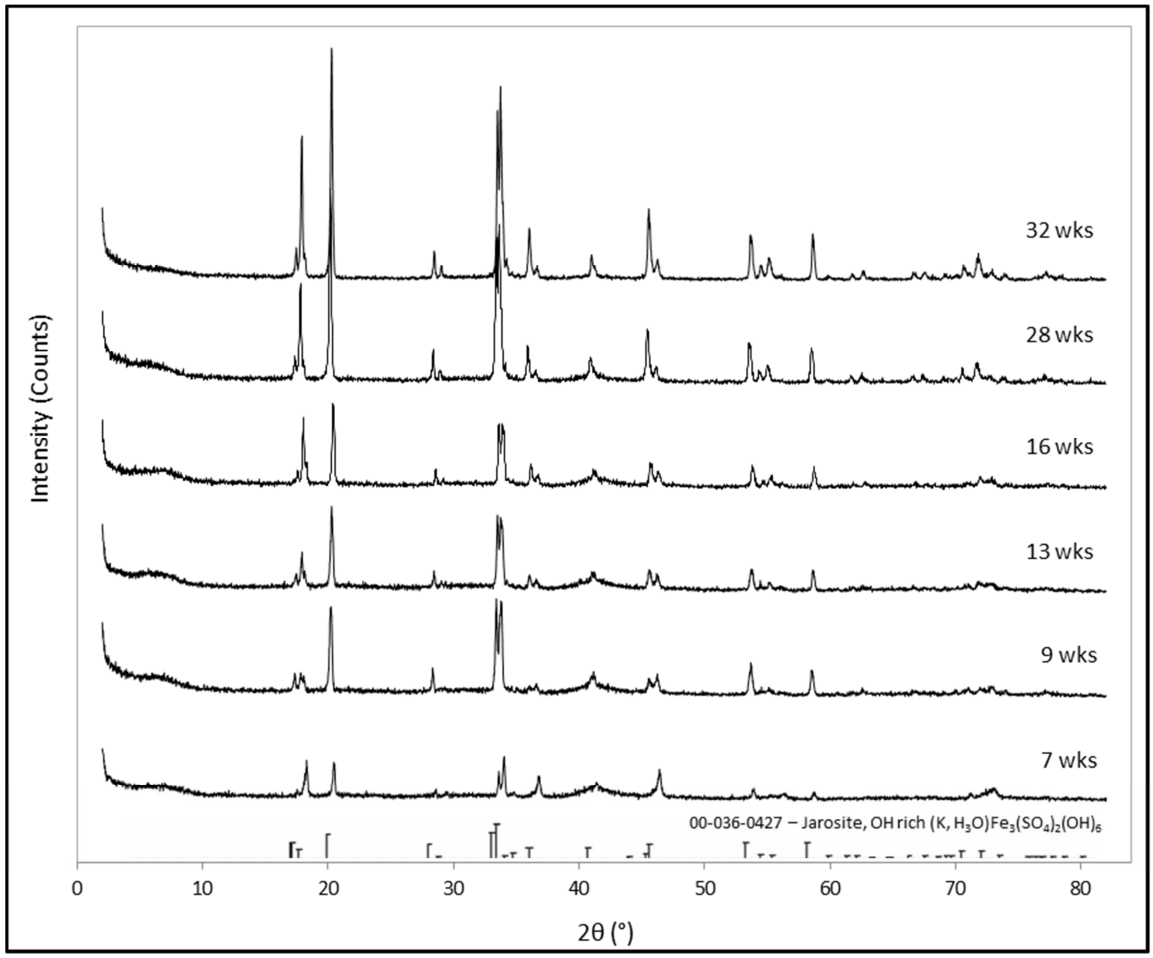

Figure 2.4. Powder X-ray diffraction patterns of microbial culture precipitates collected at various culture ages. Analyses of these patterns indicate that mineral precipitates generated for all sampling intervals (7 wks, 9 wks, 13 wks, 16 wks, 28 wks, and 32 wks) were identified as jarosite. No additional mineral phases appeared as the cultures increased in age. Peaks became more intense, narrower (FWHM) and better resolved (particularly above 60-80°) with increases in culture age.

periods of time prior to collection; all samples have the same general pattern. The initial pattern (t = 7wks) corresponds well to a jarosite mineral which is rich in hydroxyl (OH). Diffraction pattern peaks become more intense and narrow as samples increase in age (i.e., 9 wks, 13 wks, 16 wks, 28 wks, and 32 wks), resulting in an overall higher signal to noise ratio in the oldest sample. Most noticeably, the broad peaks observed in the youngest sample at approximately 41° and 73°2θ narrow significantly over time becoming well defined peaks in the oldest sample. This peak narrowing is indicative of a transition from a poorly organized amorphous material with adsorbed hydroxyl molecules to a mineralogical material that is better organized, with no adsorbed OH, and an overall increased crystallinity. Peaks observed around 37 and 46°2θ in the youngest precipitates shifted to slightly lower 2θ values in older precipitates.

These peak shifts are not representative of any new mineralogical phases or the presence of any additional peaks in the diffraction pattern. These minor peak shifts are representative of the mineralogical material becoming more crystalline with increasing culture age and is documentation of the removal of non-structural OH groups which were incorporated into the mineral layers of the precipitates. Likewise, all of these well resolved patterns exhibit a mineralogical composition which no longer corresponds best to a mineralogical composition of pure single phase jarosite (Figure 2.4.; Kato and Miura, 1977) and no longer the OH-rich variety. The consistency of the diffraction patterns and the absence of additional peaks over time demonstrates that the biogenic jarosite materials did not transform into and secondary minerals or contain any impurities (i.e., goethite, gypsum, schwertmannite, hematite) when cultures were left to grow for extended periods

of time as some previous studies have noted (Barron et al., 2006; Gramp et al., 2009; Smith et al., 2006).

Abiotic chemical oxidation products (t = 2 yrs) were also identified as the mineral jarosite (ICDD card no. 00-036-0427; Figure 2.5.) with very well defined sharp peaks, indicative of a very well defined crystalline mineralogical phase. In comparison to the oldest biogenic jarosite material, the abiogenic jarosite sample pattern indicated that this abiogenic material was more crystalline than the biogenic jarosite material, but less so that the synthetic jarosite material.

The XRD pattern of the synthetic material (Figure 2.3.), which was synthesized to match the XRD pattern of the microbial culture material, was identified as single-phase jarosite and correlated well with the biogenic pattern (t = 7 wks) (see Appendix A for more details). Unlike the biogenic samples, the synthetic material generated peaks with higher intensities and narrower widths, which was expected and common of synthetic and biological or natural jarosite mineralogical diffraction pattern comparisons (Basciano and Peterson, 2008; 2007) Unlike the biogenic material which required a lag period (~ several weeks) to produce precipitates, generation of the synthetic, fine-grained, canary yellow precipitate required only a few hours (Dutrizac and Kaiman, 1976) (see Appendix A for details).

2.3.3. Light, epifluorescence, and confocal microscopy

Note: due to equipment limitations at the time of study, a confocal microscope was used to image samples prepared with epifluorescence techniques. Light microscopes, when properly equipped, are appropriate instruments to conduct similar analyses, and

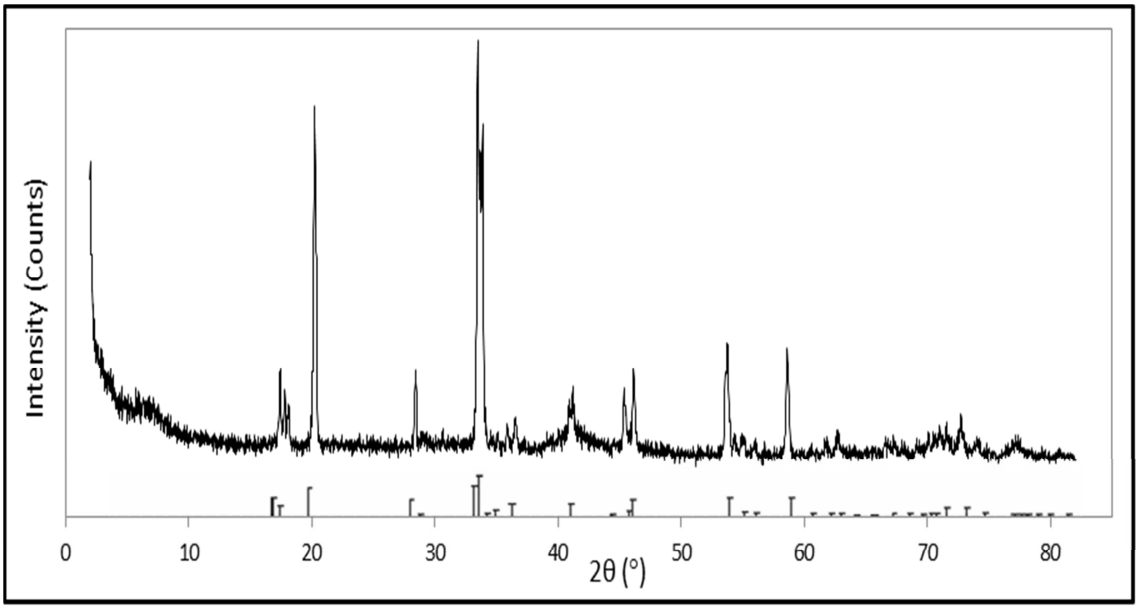

Figure 2.5. Powder X-ray diffraction pattern of mineral precipitates generated from abiotic, sterile media that was left to chemically oxidize for two years. The plot is of X-ray intensity versus 2θ and the stick pattern shown is the ICDD database card, which matches with the observed peaks and identifies the a sole mineral phase, jarosite (card no. 00-036-0427, Jarosite, OH rich (K, H_3O)$Fe_3(SO_4)_2(OH)_6$.

confocal microscopes are not required to observe fluorescence in stained samples.)

Bacterial cells were difficult to observe in relation to the mineralogical matrix when biogenic mineralogical samples were examined using bright field, phase contrast and differential interference contrast light microscopy techniques (data not shown). However, cells were easily distinguished from the mineral matrix when stained with nucleic acid molecular probes and imaged using epifluorescence microscopy techniques on a confocal microscope (Figure 2.6.). In this system, bacterial cells were clearly identified and easily differentiated from the geological matrix where viable bacteria (i.e., cells with intact membranes) fluoresce green (SYTO ® 9) and dead cells appear red (propidium iodide), ultimately making it possible to differentiate the biogenic and synthetic samples.

In order to successfully differentiate biogenic and synthetic materials using epifluorescence analyses, biological cells must be present and targeted in pursued materials. Furthermore, any cells contained within samples must contain molecules which are capable of being chemically targeted and labelled with a fluorescent stain (resulting in observed fluorescence during microscopy, e.g. Figure 2.6.), as molecular probes are specifically designed so that they only bind to certain biological fragments (e.g., DNA, RNA, nuclei). Since epifluorescence analyses target cellular materials and constituents, it represents a poor technique to use in ascertaining the biogenicity of a mineralogical product. Any signature that is used to ascertain the biogenicity of a material, especially from its synthetic counterpart, must remain and/or impart itself into the mineralogical matrix or environment and must not vanish or become destroyed as the

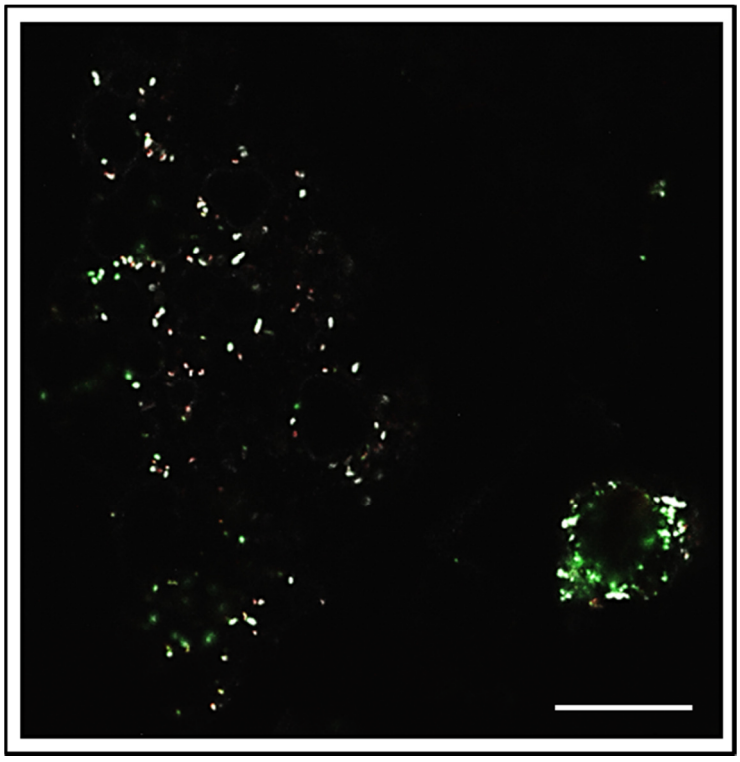

Figure 2.6. Confocal micrograph of microbial culture precipitates stained with fluorescent probes (scale bar = 2μm). Cells were easily distinguished from the mineral matrix when stained with nucleic acid molecular probes. In this micrograph, live bacterial cells fluoresce green, while dead cells appear red, and the mineralogical aggregates are visible as the dark, rounded shadows associated with the fluorescing cells.

result of cells dying and/or lysing (Farmer and Des Marais, 1999; Summons et al., 2011). While biological cells make a strong biosignature, they are unlikely to be preserved over geologic time, and life detection instruments that target highly specific biomarkers (e.g. immunisensors) are highly limited in their abilities to detect the biogenicity of geological materials (Parro et al., 2005; Summons et al., 2008). Thus, in order to ascertain if there were any other biological signatures beyond the presence of biological cells, higher resolution electron microscope techniques (i.e., SEM and TEM) were utilised to better differentiate between these two mineral precipitates, i.e., to investigate the microbe-mineral interactions of the biogenic sample, and to search for any possible 'biological' mineralogical markers.

2.3.4. High resolution microscopy (SEM and TEM) of jarosite precipitates

Although light micrographs of the synthetic jarosites were comparable to the biogenic precipitates (data not shown), these synthetic and biogenic precipitates were easily distinguishable from one another using high-resolution microscopy analyses; particularly scanning electron microscopy (SEM). Synthetic (Figure 2.7.C and 2.7.E) and biogenic (Figure 2.7.D and 2.7F) jarosite samples possess clearly different and distinct morphologies when examined under high magnification, but at lower resolutions the jarosite minerals were morphologically similar and could be easily mistaken for one another (Figure 2.7.A and 2.7.B).

The images of synthetic and biogenic jarosites presented herein are of a much higher quality than previously published images for any jarosite samples, mainly in terms of demonstrating the fine scale morphological textures of these materials (particularly Figure 2.7.E and 2.7.F). Synthetic jarosite materials exhibited uniform and homogenous

Figure 2.7. Comparative high resolution scanning electron microscopy (SEM) micrographs of the synthesized jarosite material (ACE) and the biological culture precipitates (BDF). At lower magnification (AB; scale bars = 10 μm), material generated by both processes appear generally similar. Increasing the magnification (CD; scale bars = 5 μm) begin observed morphological differences and rod shaped bacterium. In the biogenic sample, under higher magnification (F; scale bar = 1 μm) bacterial cells are clearly visible (white arrow) as is the needle-like acicular texture of the jarosites. In contrast, the synthetic sample (E, scale bar = 1 μm) exhibits a distinctly different morphology with smooth crystal surfaces, forming relatively massive rosettes.

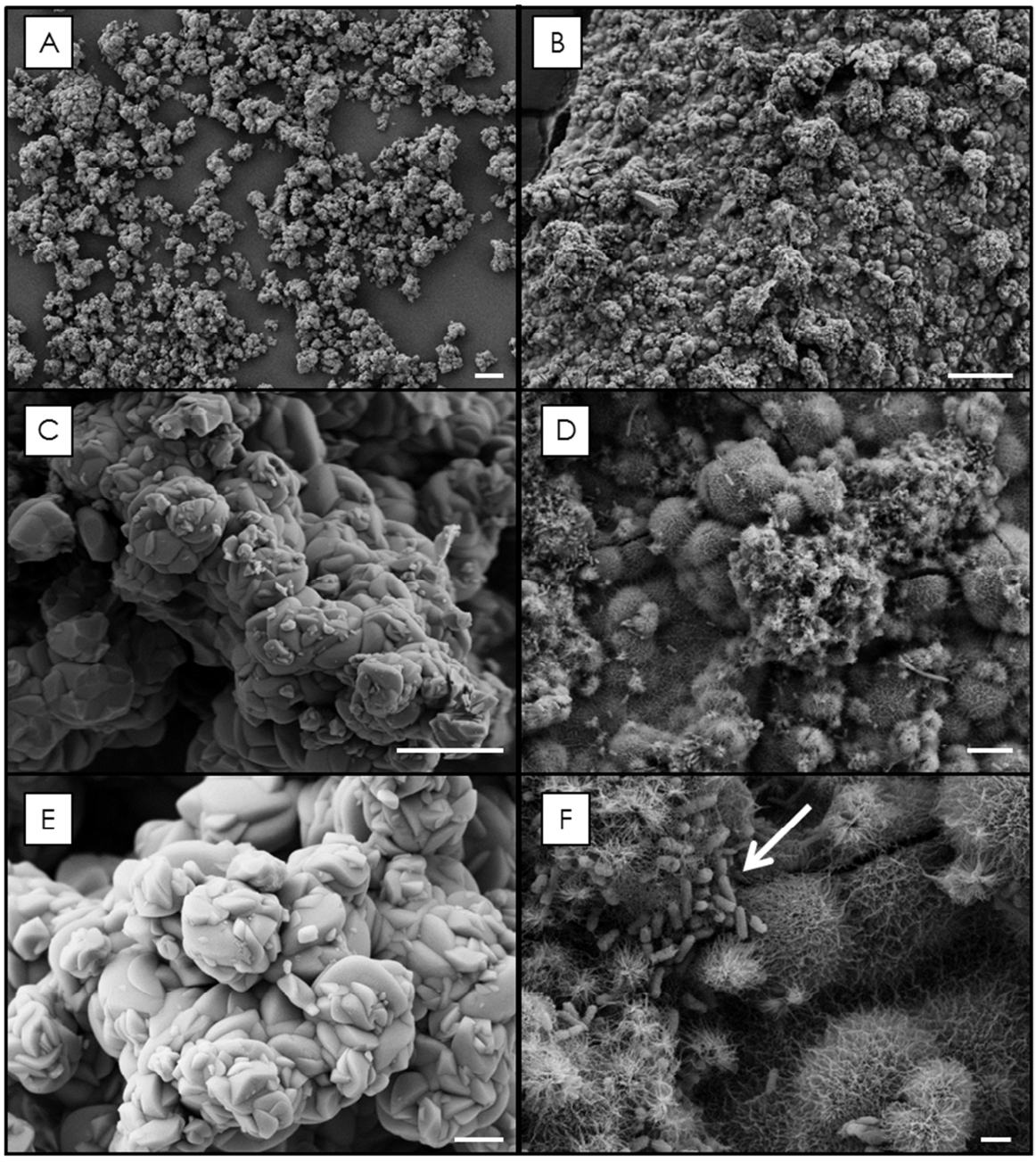
A
B
C
D
E
F

mineralogical textures and morphologies resembling blocky rosettes; this texture has not been previously reported in the literature (e.g., Barron et al., 2006; Bigham et al., 2010; Desborough et al., 2010; Dutrizac and Jambor, 2000). However, aggregates of "lumpy popcorn" textures are commonly observed in other studies (e.g., Sasaki et al., 2006) which might possibly represent blocky rosettes exposed to significant amounts of coating during SEM sample preparation, resulting in the overall loss of fine scale mineralogical textural features. In cases where the crystal morphology is clearly visible in published micrographs, cubic aggregates and platey rosettes (much flatter and less bulky than the synthetic material herein) morphologies are typically seen in synthetic preparations.

In contrast, biogenic jarosite mineralogical aggregates appear as spherical crystal aggregates of sharp, euhedral, acicular, radially oriented, filamentous needle-like grains (Figure 2.7.D). Several studies have characterized biogenic jarosite mineral precipitates using SEM analyses (Coggon et al. 2012; Lazaroff et al., 1982; Sasaki et al., 2006; Tuovinen and Carlson, 1979.; Wang et al., 2006), though none have noted a morphology like that observed in this study. Some have attributed this "hedge-hog" like morphology to the mineral schwertmannite (e.g. Wang et al., 2006). However, the biogenic material generated in this study was compared to the only known schwertmannite XRD pattern, which consists of 8 broad amorphous peaks, and the ICDD card (Bigham et al., 1994) did not match any of the peaks generated by the biogenic material (data not shown). Sasaki et al. (2006) noted that mineralogical samples generated from cultures with higher cell counts (i.e., number of cells) exhibited better defined, sharp, euhedral crystal morphologies than those with lower populations.

Microbial cells were clearly visible in high magnification SEM micrographs (Figure 2.7.D, 2.7.F, and 2.8.A) as well as other biological material such as EPS (Figure

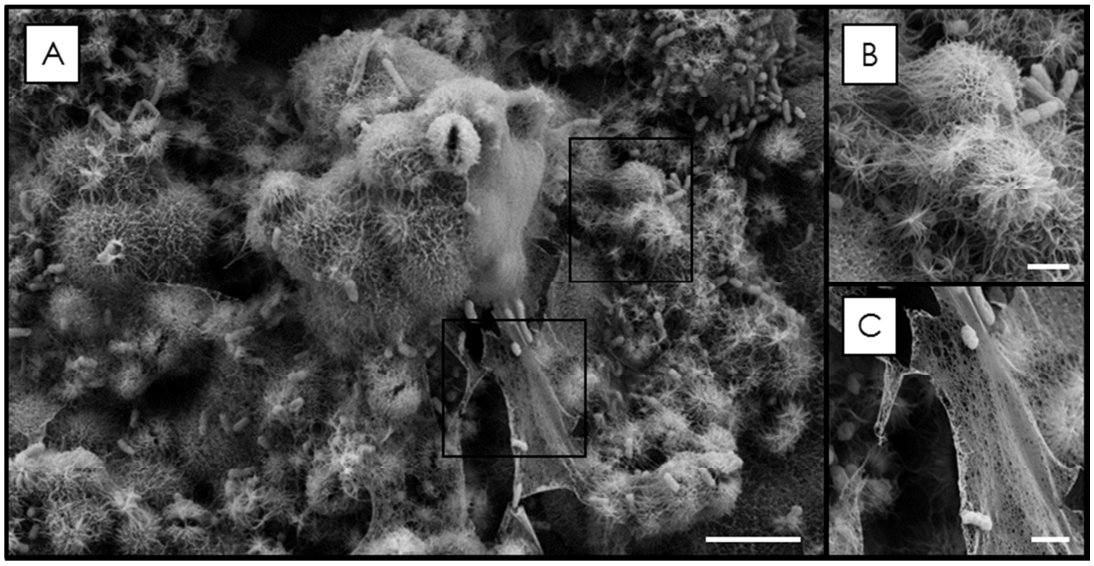

Figure 2.8. High-resolution scanning electron microscopy (SEM) micrographs of the biological culture precipitates (A), which contain rod shaped bacteria (iron oxidizers, e.g., *Acidithiobacillus ferrooxidans*) and other biological constituents, like EPS and capsule (C) as well as round, mineralogical aggregates of needle-like, acicular jarosite grains (B) that are covered with extracellular organic material. Scale bars A (5 μm), BC (1 μm).

2.8.C) and in some instances as thin films of organics coating some mineralogical aggregates (Figure 2.8.B). Previous investigations characterizing the mineralogical textural properties of biogenic jarosites have documented very poorly organized, poorly crystalline lumpy aggregates without poorly discernible morphologies (again, probably resulting from an artifact of sample preparation protocols).

Initially it was thought that the radially oriented filamentous crystal aggregates were using microbial cells to act as mineralogical templates or as nucleation sites for mineralization. TEM analyses of the biogenic jarosite material (Figure 2.9.) demonstrated that the needle-like assemblages exhibited dense mineralogical centers. Upon closer examination at higher magnifications it was very clear that the filamentous aggregates were entirely made up of mineralogical phase material (i.e., dense and dark material). There is no evidence of biomineralization of cellular materials or surfaces, as the observed lighter portions of the micrographs correspond to void spaces in the embedding plastic (visible in Figure 2.9.A and 2.9.C) resulting from the mineralogical material falling out of the embedding plastic when the material was cut into ultra-thin sections, and are not indicative of bacterial cells.

Similar textures were also observed by other studies of biogenic precipitates generated in similar environments and examined with TEM (Bigham et al., 1996; Ferris et al., 1989). Preston et al., (2011) examined enrichment cultures derived from samples from the Tharsis mine along the Rio Tinto system and observed comparable mineralization products with filamentous bacteria, thought to be similar to *Leptothrix sp.*, in TEM ultra-thin sections. Enrichment cultures in this study were dominated by a rod shaped bacterium thought to be *Acidithiobacillus ferrooxidans* and no filamentous microorganisms were observed in any of the SEM micrographs obtained of the biogenic

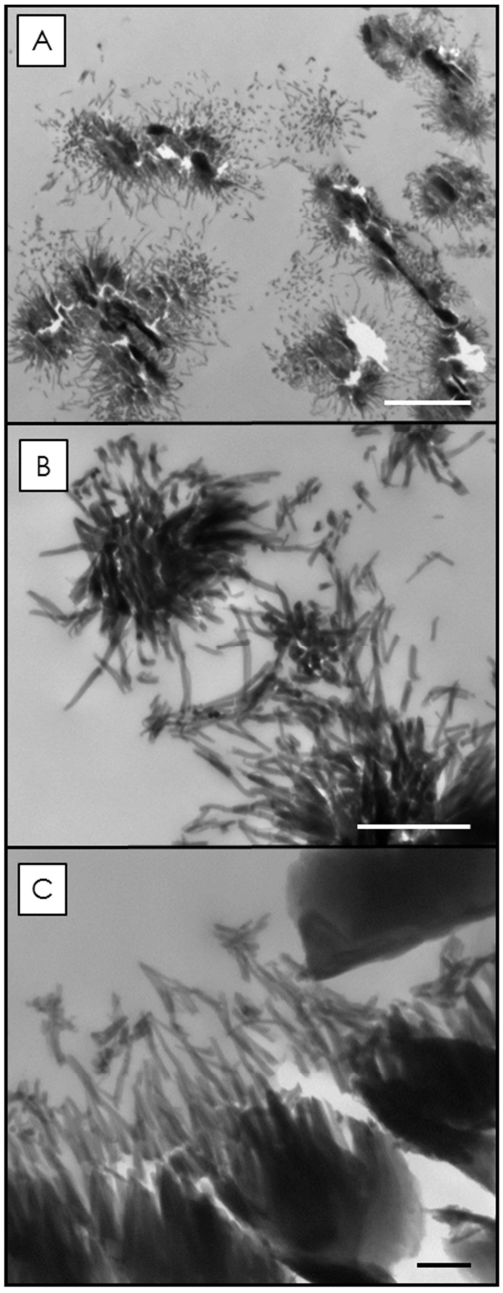

Figure 2.9. Ultrathin section TEM micrographs of biological culture material. The needle-like, acicular jarosite assemblages in ultra-thin cross section is noticeably absent of any evidence of biomineralized bacterial cells. B: The jarosite aggregates have solid, mineralogical centers and do not appear to nucleate on or use cells as mineralogical templates for precipitation. C: Needles appear to grow and radiate from a central point. (Scale bars: A = 2 μm; B = 500 nm; C = 200 nm).

material. Enders et al. (2006) documented *Acidithiobacillus ferrooxidans* populations within mineralized biofilms from the Morenci Porphyry Copper Deposit in Arizona. They observed that although the bacterial populations existed in an intensively mineralizing (jarosite) environment, the bacteria themselves were not coated with iron oxyhydroxides, and may reflect why there is no preservation of cellular material within jarosite mineralogical matrices.

Synthetic and biotic jarosite samples possess clearly different and distinct morphologies (although not necessarily at the sub-atomic or unit cell level), suggesting that biogenic jarosite is a 'good biomarker'. However, a long-term abiotic experiment testing this hypothesis revealed that when sterile culture media was left on the lab bench to chemically oxidize over 2 years under the same experimental conditions, jarosite precipitates were also generated by the control system (Figure 2.4.). Furthermore, the abiogenic 'control system' precipitates (Figure 2.9.) exhibit similar mineral morphologies as those generated in the biological systems (Figures 2.4.DF, 2.8.A and 2.10.), less the biotic material (i.e., cells, EPS, organic coatings). These abiogenic precipitates exhibit ragged elongated crystal filaments which are more poorly organized than the biogenic material as the needle-like grains appear to occur in massive aggregates with random orientations, whereas the biological aggregates consistently appeared as perfect spheres with radially oriented grains in all directions. Additionally, at high magnifications rare instances of cubic minerals occur (Figure 2.10.D), which are indicative of abiotic jarosites and do not occur in the biogenic samples. Since the abiotic 'control system' generates mineralogical precipitates with the same composition and exhibits a similar general

Figure 2.10. SEM micrographs of precipitates generated by chemical oxidation of abiotic culture media. At lower magnifications (A; scale bar = 25 μm) material appears similar to biogenic and synthetic jarosites (Figure 2.6). At higher resolution (B; scale bar = 10 μm; C; scale bar = 5 μm) ragged, more poorly crystalline acicular needles (compared to the biogenic sample) are observed. Note, the needles in this synthetic sample do not form the radiating aggregates as in the biogenic samples (Figure 2.7 and Figure 2.8). Additionally, rare instances of cubic minerals 5 μm across (D; scale bar = 2 μm) occur, which do not show up in the XRD pattern.

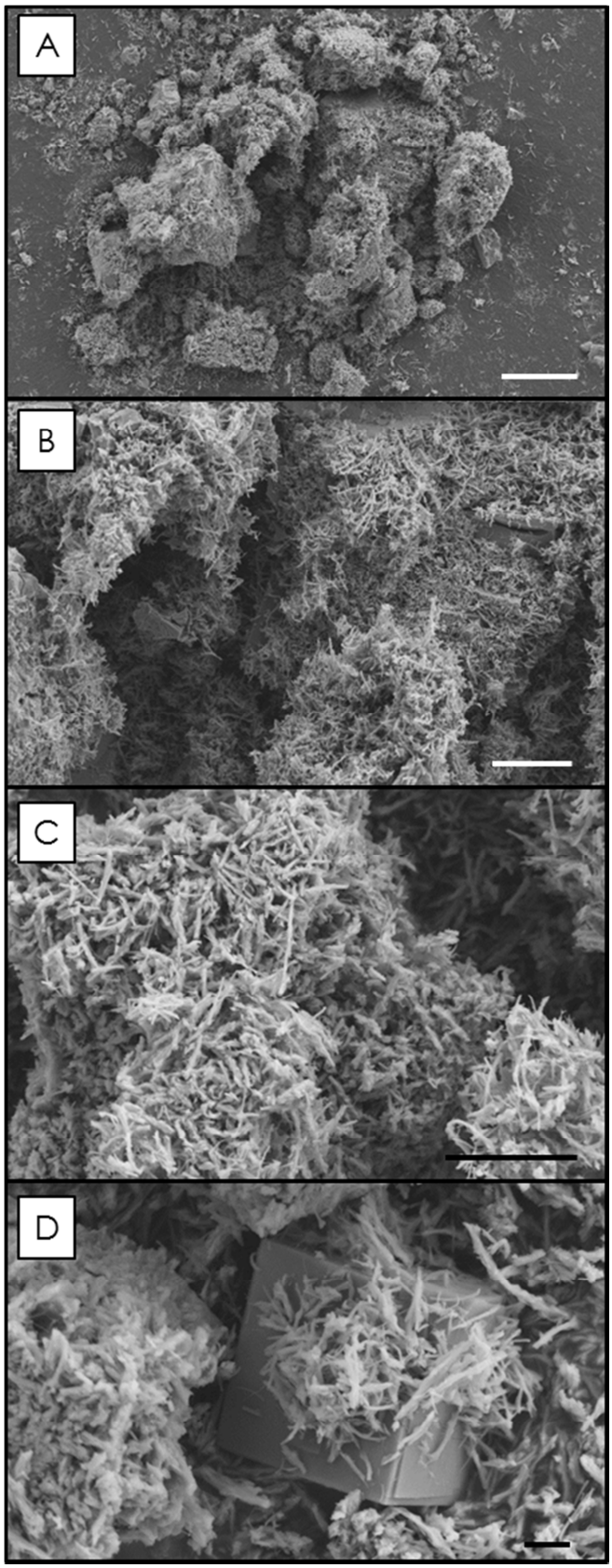
A
B
C
D

textural morphology, it can be concluded that the initial morphology of the biogenic precipitates cannot be termed a biosignature or biomarker (as it does not unambiguously indicate life). Furthermore, since the same material is generated by the biogenic and abiogenic system, as well as the lack of evidence of any biomineralization (i.e., no iron hydroxysulfate material found in association with any of the biological cell surfaces), an argument can be made that jarosite precipitation in these aqueous acid-sulfate systems is not the result of biological influence. It appears as though the biological system merely catalyzes an abiotic reaction and generates identical products (i.e., jarosite) and mineralization will precipitate in these systems regardless of the presence of biota.

2.4. Conclusions

This study demonstrates that the presence of jarosite in a system cannot immediately be attributed to biological activity and that the simple presence of the mineral is not indicative of life. Jarosite is not a mineralogical signature of biogenicity; presence of jarosite in a system does not indicate that biota was present or involved in the mineralization process. Experiments demonstrate that the mineral can form in highly acidic systems completely abiotically yielding similar crystal morphologies and textures as to those generated in systems where the deposition is catalyzed by biota. Furthermore, jarosite morphology, particularly the acicular, needle-like texture, cannot conclusively distinguish the process of formation (i.e. biogenic or abiotic), of the depositional system. Finally, this study also demonstrates the importance of conducting laboratory experimental studies and the incorporation of abiotic system control samples when examining biogenicity and searching and evaluating potential biosignatures. Future

studies in this realm should seek to examine the abiotic processes alongside materials generated as a result of biogenic processes.

References

Aguilers, A., Zettler, E., Gomez, F., Amaral-Zettler, L., Rodriguez, N., Amils, R., 2007. Distribution and seasonal variability in the benthic eukaryotic community of Rio Tinto (SW, Spain), an acidic, high metal extreme environment. System. Appl. Microbiol. 30, 531–546.

Aguilers, A., Manrubia, S.C., Gomez, F., Rodriguez, N., Amils, R., 2006. Eukaryotic community distribution and its relationship to water physicochemical parameters in an extreme acidic environment, Rio Tinto (Southwestern Spain). Appl. Environ. Microbiol. 72, 5325–5330.

Allen, J.C., 1973. The accumulation of ancient slag in the south-west of the Iberian Peninsula. Hist. Metall. Group Bull. London 7, 47–50.

Baron, D., Palmer, C.D., 1996. Solubility of jarosite at 4 - 35°C. Geochim Cosmochim Ac., 60, 185 – 195.

Barron, V., Torrent, J., Greenwood, J.P., 2006. Transformation of jarosite to hematite in simulated Martian brines. Earth Planet. Sci. Lett. 251, 380–385.

Basciano, L.C., Peterson, R.C., 2007. Jarosite-hydronium jarosite solid-solution series with full iron site occupancy: Mineralogy and crystal chemistry. Am. Mineral. 92, 1464–1473.

Basciano, L.C., Peterson, R.C., 2008. Crystal chemistry of the natrojarosite-jarosite and natrojarosite-hydronium jarosite solid-solution series: A synthetic study with full Fe site occupancy. Am. Mineral. 93, 853 – 862.

Battler, M.M., Osinski, G.R., Lim, D.S.S., Davila, A.F., Michel, F.A., Craig, M.A., Izawa, M.R.M., Leoni, L., Slater, G.F., Fairen, A.G., Preston, L.J., Banerjee, N.R., 2012. Characterization of the acidic cold seep emplaced jarositic Golden Deposits, NWT, Canada, as an analogue for jarosite deposition on Mars. Icarus (in press) http://dx.doi.org/10.1016/j.icarus.2012.05.015

Bigham, J.M., Jones, F.S., Ozkaya, B., Sahinkaya, E., Puhakka, J.A., Tuovinen, O.H., 2010. Characterization of jarosites produced by chemical synthesis over a temperature gradient from 2 to 40°C. Inter. J. Mineral Process. 94, 121–128.

Bigham, J.M., Schwertmann, U., Pfab, G., 1996. Influence of pH on mineral speciation in a bioreactor simulating acid mine drainage. Appl. Geochem. 11, 845–849.

Bigham, J.M., Carlson, L., Murad. E., 1994. Schwertmannite, a new iron oxyhydroxy-sulphate from Pyhasalmi, Findland, and other localities. Mineral. Mag. 58, 641–648.

Bonaccorsi, R., Stoker, C.R., 2008. Science results from a Mars drilling simulation (Rio Tinto, Spain) and ground truth for remote science observations. Astrobiology 8, 967–985.

BrukerAXS, 2005. DIFFRACplus Evaluation Package release 2005. Bruker AXS, Karlsruhe, Germany.

Christensen, P.R., Wyatt, M.B., Glotch, T.D., Rogers, A.D., Anwar, S., Arvidson, R.E., BAndfield, J.L., Blaney, D.L., Budney, C., Calvin, W.M., Fallacaro, A.,

Fergason, R.L., Gorelick, N., Graff, T.G., Hamilton, V.E., Hayes, A.G., Johnson, J.R., Knudson, A.T., McSween, H.Y., Mehall, G.L., Mehall, L.K., Moersch, J.E., Morris, R.V., Smith, M.D., Squyres, S.W., Ruff, S.W., Wolf, M.J., 2004. Mineralogy at Meridiani Planum from the Mini-TES experiment on the Opportunity rover. Science 306, 1733–1739.

Colmer, A.R., Temple, K.L., Hinkle, H.E., 1950. An iron-oxidising bacterium from the acid drainage of some bituminous coal mines. J. Bacteriol. 59, 317–328.

Colmer, A.R., Hinkle, M.F., 1947. The role of microorganisms in acid mine drainage: A preliminary report. Science 106, 253–256.

Coggon, M., Becerra, C.A., Nusslein, K., Miller, K., Yuretich, R., Ergas, S.J., 2012. Bioavailability of jarosite for stimulating acid mine drainage attenuation. Geochim. Cosmochim. Ac. 78, 65–76.

Davis, R.A., Welty, A.T., Borrego, J., Morales, J.A., Pendon, J.G., Ryan, J.G., 2000. Rio Tinto estuary (Spain): 5000 years of pollution. Environ. Geol. 39, 1107–1116.

Desborough, G.A., Smith, K.S., Lowers, H.A., Swayze, G.A., Hammarstrom, J.M., Diehl, S.F., Leinz, R.W., Driscoll, R.L., 2010. Mineralogical and chemical characteristics of some natural jarosites. Geochim. Cosmochim. Ac. 74, 1041–1056.

Drouet, C., Navrotsky, A., 2003. Synthesis, characterization, and thermochemistry of K-Na-H_3O jarosites. Geochim. Cosmochim. Ac. 67, 2063-2076.

Dutrizac, J.E., Kaiman, S., 1976. Synthesis and properties of jarosite-type compounds. Can. Mineral. 14, 151-158.

Dutrizac, J.E., Jambor, J.L., 2000. Jarosites and their application in hydrometallurgy. *In*: C.N., Alpers, J.L., Jambor, D.K., Nordstrom, Eds., Sulfate Minerals – Crystallography, Geochemistry, and Environmental Significance, vol. 40, p. 405–452. Reviews in Mineralogy and Geochemistry, Mineralogical Society of America, Chantilly, Virgina.

Dutrizac, D.E., Jambor, J.L., O'Reilly, J.B., 1983. Man's first use of jarosite: the pre-Roman mining-metallurgical operations at Rio Tinto, Spain. CIM Bull. 76, 78–82.

Edwards, H.G.M., Vandenabeele, P., Jorge-Villar, S.E.J., Carter, E.A., Perez, F.R., Hargreaves, M.D., 2007. Th Rio Tinto Mars Analogue site: An extremophilic Raman spectroscopic study. Spectrochim. Acta A 68, 1133–1137.

Edwards, K.J., Bond, T.M., Gihring, T.M., Banfield, J.F., 2000. An archaeal iron-oxidizing extreme acidophile important in acidic mine drainage. Science 287, 1796–1798.

Emerson, D., Revsbech, N.P., 1994a. Investigation of an iron-oxidizing microbial mat community located near Aarhus, Denmark: Field studies. Appl. Environ. Microbiol. 60, 4032–4038.

Emerson, D., Revsbech, N.P., 1994b. Investigation of an iron-oxidizing microbial mat community located near Aarhus, Denmark: Laboratory studies. Appl. Environ. Microbiol. 60, 4022–4031.

Enders, M.S., Knickerbocker, C., Titley, S.R., Southam, G., 2006. The role of bacteria in the supergene envrironment of the Morenci Porphyry Copper Deposit, Greenlee County, Arizona. Econ. Geol. 101, 59–70.

Farmer, J.D., Des Marais, D.J., 1999. Exploring for a record of ancient Martian life. J. Geophys. Res. 104, 26977–26995.

Fernandez-Remolar, D.C., Knoll, A.H., 2008. Fossilization potential of iron-bearing minerals in acidic environments of Rio Tinto, Spain: Implications for Mars exploration. Icarus 194, 72–85.

Fernandez-Remolar, D.C., Morris, R.V., Gruener, J.E., Amils, R., Knoll, A.H., 2005. The Rio Tinto Basin, Spain: mineralogy, sedimentary geobiology, and implications for interpretation of outcrop rocks at Meridiani Planum, Mars. Earth Planet. Sci. Lett. 240, 149–167.

Fernandez-Remolar, D., Gomez-Elvira, J., Gomez, F., Sebastian, E., Martiin, J., Manfredi, J.A., Torres, J., Kesler, C.G., Amils, R., 2004. The Tinto River, an extreme acidic environment under control of iron, as an analog of the *Terra Meridiani* hematite site of Mars. Planet. Space Sci. 52, 239–248.

Fernandez-Remolar, D.C., Rodriguez, N., Gomez, F., 2003. Geological record of an acidic environment driven by iron hydrochemistry: The Tinto River system. J. Geophys. Res. 108, E7, 5080, doi:10.1029/2002JE001918.

Ferris, F.G., Tazaki, K., Fyfe, W.S., 1989. Iron oxides in acid mine drainage environments and their association with bacteria. Chem. Geol. 74, 321–330.

Foster, I.S., King, P.L., Hyde, B.C., Southam, G., 2010. Characterization of halophiles in natural $MgSO_4$ salts and laboratory enrichment samples: Astrobiological implications for Mars. Planet. Space Sci. 58, 599–615.

Frost, R.L., Wain, D., Martens, W.N., Locke, A.C., Mertinez-Frias, J., Rull, F., 2007a. Thermal decomposition and X-ray diffraction of sulphate efflorescent minerals from El Jaroso Ravine, Sierra Almagrera, Spain. Thermochim. Acta 460, 9–14.

Frost, R.L., Weier, M., Martinez-Frias, J., Rull, F., Reddy, B.J., 2007b. Sulphate efflorescent minerals from El Jaroso Ravine, Sierra Almagrera – An SEM and Raman spectroscopic study. Spectrochim. Acta A 66, 177–183.

Giaveno, A., Lavalle, L., Guibal, E., Donati, E., 2008. Biological ferrous sulfate oxidation by A. ferrooxidans immobilized on chitosan beads. J. Micrbiol. Meth. 72, 227–234.

Gleeson, D.F., Pappalardo, R.T., Grasby, S.E., Anderson, M.S., Beauchamp, B., Castano, R., Chein, S.A., Doggett, T., Mandrake, L., Wagstaff, K.L., 2010. Characterization of a sulfur-rich Arctic spring site and field analog to Europa using hyperspectral data. Remote Sensing Envir. 114, 1297–1311.

Gonzalez-Toril, E., Gomez, F., Rodriguez, N., Fernandez-Remolar, D., Zuluaga, J., Marin, I., Amils, R., 2003a. Geomicrobiology of the Tinto River, a model of interest for biohydrometallurgy. Hydrometallurgy 71, 301–309.

Gonzalez-Toril, E., Llobet-Brossa, E., Casamayor, E.O., Amann, R., Amils, R., 2003b. Microbial ecology of an extreme acidic environment, the Tinto River. Appl. Environ. Microbiol. 69, 4853–4865.

Gramp, J.P., Wang, H., Bigham, J.M., Jones, F.S., Tuovinen,O.H., 2009. Biogenic synthesis and reduction of Fe(III)-hydroxysulfates. Geomicrobio. J 26, 275–280.

Grishin, S.I., Bigham, J.M., Tuovinen, O.H., 1988. Characterization of jarosite formed upon bacterial oxidation of ferrous sulfate in a packed-bed reactor. Appl. Envrion. Microbiol. 54, 3101–3106.

Kato, T., Miura, Y., 1977. The crystal structures of jarosite and synbergite. Mineral. J. 8, 419–430.

Klingelhofer, G., Morris, R.V., Bernhardt, B., Schroder, C., Rodionov, D., de Souza, P.A.J., Yen, A.S., Gellert, R., Evlanov, E.N., Zubkov, B., Foh, J., Bonnes, U., Kankeleit, E., Gulich, P., Ming, D.W., Renz, F., Wdowiak, T.J., Squyres, S.W., Arvidson, R.E., 2004. Jarosite and hematite at Meridiani Planum from Opportunity's Mössbauer spectrometer. Science 306, 1740–1745.

Konhauser, K.O., 2007. Introduction to Geomicrobiology. Blackwell Publishing, Oxford, UK, p. 145.

Lacelle, D., Léveillé, R., 2012. Acid drainage generation and associated Ca-$FeSO_4$ minerals in a periglacial environment, Eagle Plains, Northern Yukon, Canada: A potential analogue for low-temperature sulfate formation on Mars. Planet. Space Sci. 58, 509–521.

Lazaroff, N., Sigal, W., Wasserman, A., 1982. Iron oxidation and precipitation of ferric hydroxysulfates by resting Thiobacillus ferrooxidans cells. Appl. Environ. Microb. 43, 924–938.

Leblanc, M., Morales, J.A., Borrego, J., Elbaz-Poulichet, F., 2000. 4,500-year-old mining pollution in southwestern Spain: long-term implications for modern mining pollution. Econ. Geol. 95, 655–662.

Lees, H., Kwok, S.C., Suzuki, I., 1969. The thermodynamics of iron oxidation by the ferrobacilli. Can. J. Microbiol. 15, 43–46.

Liu, J.S., Li, B.M., Zhong, D.Y., Xia, L.X., Qiu, G.Z., 2007. Preparation of jarosite by Acidithiobacillus ferrooxidans oxidation. J. Cent. South Univ. Technol. 5, 623–628.

Lopez-Archilla, A.I., Marin, I., Amils, R., 2001. Microbially community composition and ecology of an acidic aquatic environment: The Tinto River, Spain. Microb. Ecol.41, 20–35.

Lopez-Archilla, A.I., Marin, I., Amils, R., 1993. Bioleaching and interrelated acidophilic microorganisms from Rio Tinto, Spain. Geomicrobiol. J. 11, 223–233.

McKay, D.S., Gibson Jr., E.K., Thomas-Keptra, K.L., Vali, H., Romanek, C.S., Clemett, S.J., Chillier, X.D.F., Maechling, C.R., Zare, R.N., 1996. Search for past life on Mars : possible relic biogenic activity in Martian meteorite ALH 84001. Science 273, 924–930.

Michel, F.A., van Everdingen, R.O., 1987. Formation of a jarosite deposit on Cretaceous shales in the Fort Norman area, Northwest Territories. Can. Mineral. 25, 221–226.

Navrotsky, A., Forray, F.L., Drouet, C., 2005. Jarosite stability on Mars. Icarus 176, 250–253.

Parro, V., Rodriguez-Manifredi, J.A., Briones, C., Compositizo, C., Herrero, P.L., Vez, E., Sebastianm E., Moreno-Paz, M., Garcia-Villadangos, M., Fernandez-Calvo, P., Gonzalez-Toril, E., Perez-Mercader, J., Fernandez-Remolar, D., Gomez-Elvira, J., 2005. Instrument development to search for biomarkers on Mars: terrestrial aidophile, iron-powered chemolithoautotrophic communities as model systems. Planet. Space Sci. 53, 729–737.

Preston, L.J., Shuster, J., Fernández-Remolar, D., Banerjee, N.R., Osinski, G.R., Southam, G., 2011. The preservation and degradation of filamentous bacteria and biomolecules within iron oxide deposits at Rio Tinto, Spain. Geobiology 9, 233 – 249.

Pullan, D., Westall, F., Hofmann, B.A., Parnell, J., Cockell, C.S., Edwards, H.G.M., Villar, E.J., Schroder, C., Cressey, G., Marinangeli, L., Richter, L., Klingelhofer, G., 2008. Identification of morphological biosignature in Martian analogue field specimens using *in situ* planetary instrumentation. Astrobiology 8, 119–156.

Roach, L.H., Mustard, J., Gendrin, A., Fernandez-Remolar, D., Amils, R., Amaral-Zettler, L., 2006. Finding mineralogically interesting targets for exploration from spatially coarse visible and near IR spectra. Earth Planet. Sci. Lett. 252, 201–214.

Roca, A., Vinals, J., Arranz, M., Calero, J., 1999. Characterization and alkaline decomposition/cyanidation of beudanite-jarosite materials from Rio Tinto gossan ores. Can. Metall. Quart. 38, 93–103.

Sasaki, K., Sakimoto, T., Endo, M., Konno, H., 2006. FE-SEM study of microbially formed jarosites by Acidithiobacillus ferrooxidans. Material. Trans. 47, 1155–1162.

Smith, A.M.L., Hudson-Edwards, K.A., Dubbin, W.E., Wright, K., 2006. Dissolution of jarosite [$KFe_3(SO_4)_2(OH)_6$] at pH 2 and 8: Insights from batch experiments and computational modelling. Geochim. Cosmochim. Ac. 70, 608–621.

Sobron, P., Sanz, A., Acosta, T., Rull, F., 2009. A Raman spectral study of stream waters and efflorescent salts in Rio Tinto, Spain. Spectrochim. Acta A 71, 1678–1682.

Souza-Egipsy, V., Aguilera, A., Mateo-Marti, E., Martin-Gago, J.A., Amils, R., 2010. Fossilization of acidophilic microorganisms. Geomicrobiol. J. 27, 692–706.

Squyres, S.W., Grotzinger, J.P., Arvidson, R.E., Bell III, J.F., Calvin, W., Christensen, P.R., Clark, B.C., Crisp, J.A., Farrand, W.H., Herkenhoff, K.E., Johnson, J.R., Klingelhofer, G., Knoll, A.H., McLennan, S.M., McSween, H.Y., Morris, R.V., Rice, J.W., Rieder, R., Soderblom, L.A., 2004. In situ evidence for an ancient aqueous environment at Meridiani Planum, Mars. Science 306, 1709–1714.

Stoker, C.R, Cannon, H.N., Dunagan, S.E., Lemke, L.G., Glass, B.J., Miller, D., Gomez-Elvira, J., Davis, K., Zavaleta, J., Winterholler, A., Roman, M., Rodrigue-Manifredi, J.A., Bonaccorsi, R., Bell, M.S., Brown, A., Battler, M., Chen, B., Cooper, G., Davidson, M., Fernandez-Remolar, D., Gonzales-Pastor, E., Heldmann, J.L., Martinez-Frias, J., Parro, V., Prieto-Ballesteros, O., Sutter, B., Schuerger, A.C., Schutt, J., Rull, F., 2008. The 2005 MARTE Robotic Drilling Experiment in Rio Tinto, Spain: Objectives, approach, and results of a simulated mission to search for life in the Martian subsurface. Astrobiology 8, 921–945.

Summons, R.E., Amend, J.P., Bish, D., Buick, R., Cody, G.D., Des Marais, D.J., Dromart, G., Eigenbrode, J.L., Knoll, A.H., Sumner, D.Y., 2011. Preservation of Martian organic and environmental records: final report of the Mars Biosignature Working Group. Astrobiology 11, 157–181.

Summons, R.E., Albercht, P., McDonald, G., Moldowan, J.M., 2008. Molecular biosignatures. Space Sci. Rev. 135, 133–159.

Sutter, B., Brown, A.J., Stoker, C.R., 2008. Visible-near infrared point spectrometry of drill core samples from Rio Tinto, Spain: Results from the 2005 Mars Astrobiology Research and Technology Experiment (MARTE) Drilling Exercise. Astrobiology 8, 1049–1060.

Tuovinen, O.H., Carlson, L., 1979. Jarosite in cultures of iron-oxidizing thiobacilli. Geomicrobiol. J. 1, 205 – 210. (check that there is IR data in this paper)

van Geen, A., Adkins, J.F., Boyle, E.A., Nelson, C.H, Palenques, A., 1997. A 120-year record of widespread contamination from mining of the Iberian Pyrite Belt. Geology 25, 291–294.

Walsh, M.M., Westall, F., 2009. Disentangling the microbial fossil record in the Barberton Greenstone belt: a cautionary tale. *In*: Seckbach, J., Walsh, M., (eds.) From fossils to astrobiology, Springer Science, Business Media B.V., pp. 25 – 37.

Wang, H., Bigham, J.M., Tuovinen, O.H., 2006. Formation of schwertmannite and its transformation to jarosite in the presence of acidophilic iron-oxidizing microorganisms. Mater. Sci. Eng. C 26, 588–592.

Westall, F., 2008. Morphological biosignatures in early terrestrial and extraterrestrial materials. Space. Sci. Rev. 135, 95–114.

Chapter 3.

Detecting biogenicity: A comparison of biogenic and synthetic jarosite samples using mass spectrometry and spectral analyses

3.1. Introduction

3.1.1. Background

Jarosites are well studied because of their association with acid mine drainage environments possessing diverse microbial life (Aguilera et al., 2007; 2005), as well as their occurrence in hydrometallurgic processes, which can sometimes be economically beneficial (Dutrizac et al., 1983). As a result of several decades of characterization and investigation, the spectral and mineralogical properties of the jarosite mineral are well known and thoroughly established (Adler and Kerr, 1965; Bishop and Murad, 2005; Clark et al., 1990; Cloutis et al., 2006; Crowley et al., 2003; Dutrizac and Kaiman, 1976; Hunt et al., 1971; Kubisz, 1972, 1971; Powers et al., 1975; Ross, 1974; Serna et al., 1986). Alunite-group minerals, including jarosites, have been identified and mapped remotely in acidic mine wastes using satellite-based reflectance spectroscopic techniques to analyze the surface of the Earth (Clark et al., 2003; King et al., 1995; Swayze et al., 2000). These remote sensing applications are a particularly useful for exploring inaccessible targets such as terrestrial planetary surfaces, [e.g., Mercury (Sprague et al., 1994; Vilas, 1998; Warell et al., 2006), Venus (Mayer et al., 1958; Taylor et al., 1980), Mars (Bibring et al., 2006; Murchie et al., 2009; 1993), Earth (Swayze et al., 2000) and the Moon (Lucey et al., 1995)], which have all been mapped using telescopic spectroscopy. Remote sensing telescopic observations of a planetary surface's geomorphology and occasionally surficial

composition and mineralogy (where possible) are often the precursor studies to determining landing sites for *in situ* missions.

The Martian planetary surface has been extensively mapped using telescopic data. In particular, the Mars Reconnaissance Orbiter (MRO) and Mars Express have been effective in discerning and understanding the surface mineralogical and compositional mapping of the Martian planet. The Compact Reconnaissance Imaging Spectrometer for Mars (CHRISM) on the MRO and the Observatoire pour la Mineralogie, l'Eau, les Glaces, et l'Activité (OMEGA) on Mars Express orbiters have both extensively mapped the surface mineralogy of the planet's surface (Bibring et al., 2005; Christensen et al., 2001; Murchie et al., 2009; 2007) using reflectance spectroscopy. Sulfate minerals have been identified on the Martian surface using spectral measurements from both remote sensing (i.e., telescopic and orbital) and *in situ* (i.e., landed rover missions) investigations. Ferrand et al. (2009) analysed visible and near infrared reflectance data from the MRO-CRISM hyperspectral imager and determined that an ovoid-shaped landform near the outflow of a channel at Mawrth Vallis has spectral features which are consistent with a potassic bearing ferric sulfate mineral, which they interpreted to be jarosite. Currently, sulfate mineral assemblages are thought to occur at Valles Marineris (Gendrin et al., 2005), Mawrth Vallis (Ferrand et al., 2009; Michalski and Niles, 2011), Aram Chaos at Terra Meridiani and Columbus crater at Terra Sirenum (Murchie et al., 2009).

The occurrence of sulfate at the Martian surface has subsequently been verified using landed missions. In 2004, jarosite was identified as one of the sulfate minerals in the Eagle Crater outcrop at Meridiani Planum through *in situ* analyses using the Mössbauer spectrometer on the MER rover Opportunity (Klingelhöfer et al., 2004; Squyres et al., 2004). This finding provided a ground truth and corroborating previous

telescopic mineralogical observations and finally resolved several predictions about the surficial composition of the planet (Burns, 1988; 1987; Burns and Fisher, 1990).

The association of diverse microbial species, supported by autotrophic iron oxidising bacteria, with jarosites on Earth combined with the general preservation of biological materials in Earth materials, e.g., banded iron formations (Barghoorn and Tyler, 1965), sulfides (Angiboust et al., 2012), gypsum (Foster et al., 2010), and in particular, jarosites (Preston et al., 2011), makes targeting them on Mars particularly important in the search for evidence of life on the planet (second origin).

One of the main goals of astrobiology is the search for life on other planets, the focus of several exobiology missions developed by NASA and ESA. When examining geological materials in the search for evidence of extant or extinct life, it is important to ground truth and test instrumentation (equipment and technologies) using analogue sites (Léveillé, 2009). In the examination of putative biomarkers it is also important to examine the null hypothesis of astrobiology. One very significant problem in assigning a biogenic origin to any signature observed in extraterrestrial material is that abiogenic processes can often create similar signatures. The possibility that these abiotic signatures may be misinterpreted as biological, and taken as signs of biogenicity, is underestimated as few exobiological studies set out to thoroughly characterize this possibility in geological materials and substrates currently targeted in rover missions.

3.1.2. Study context and aims

This chapter builds on the preliminary work completed in the previous chapter by studying the biogenic and synthetic jarosite samples using analytical techniques which are currently utilized to study the Martian surface in mineralogical investigation

telescopically [i.e., orbital or flyby; IR and VNIR; (Bibring et al., 2006; 2005; Christensen et al., 2000; Murchie et al. 2009; 2007] as well as *in situ* [i.e., landed and rover missions; reflectance spectroscopy, Mössbauer and LIBS; Christensen et al., 2004a; 2004b; Klingelhofer et al., 2004]. Additionally, samples were characterized using Time of Flight-Secondary Ion Mass Spectrometry (ToF SIMS) and Raman spectroscopy since they are instruments currently receiving significant consideration for inclusion on future landed missions (e.g., Raman on ExoMars 2018; Courrges-Lacoste et al., 2007) and are currently used to assess organic molecules in *in situ* planetary science investigations (Balsiger et al., 2007; 1998; 1987). The overall goal of this study is to ascertain if there are any quantifiably observable signatures, markers or differences in the obtained spectra of these two powder jarosite samples which can unequivocally authenticate the biogenicity of the known sample generated during bacterial culture conditions while characterizing the generation of any potential false biosignatures resulting from abiotic chemical processes in these sample substrates and systems.

3.2. Material and Methods

3.2.1 Biogenic and synthetic jarosite samples

A biogenic mineralogical sample was generated as a result of the metabolic processes of a microbial enrichment culture grown at room temperature (RT) from a sediment sample collected from the riverbed of the Rio Tinto River in Spain. The biogenic precipitate was identified as single-phase jarosite, and a synthetic single-phase jarosite compound was subsequently precipitated from solution under elevated temperature conditions using a modified method outlined in Dutrizac and Kaiman (1976; details of these processes can be found in Chapter 2 and a detailed explanation of the

selection process of a synthetic sample is found in Appendix A). The mineralogical compositions of the starting materials of this study (i.e., biogenic and synthetic samples) were confirmed by X-ray diffraction (XRD) analyses at ambient pressure and temperature. No impurities were observed within the crystal structure of either precipitate and both materials were confirmed as single-phase mineral samples. All of the peaks exhibited in both patterns corresponded to the d-spacings of jarosite (BrukerAXS, 2005) and compared well to previously published jarosite XRD patterns (Baron and Palmer, 1996; Basciano and Peterson, 2008; 2007; Drouet and Navrotsky, 2003; Dutrizac and Kaiman, 1976). Although the diffraction patterns of both jarosites were indistinguishable from one another, the pair exhibited distinctly different phenotypic crystal morphologies when examined using high resolution microscopy (Figure 3.1).

3.2.2. Raman spectroscopy (Raman)

Mineralogical characterization of the jarosite samples using Raman spectroscopy was completed at the University of Western Ontario. An argon ion laser was used as the excitation source and generated 514 nm monochromatic light. Laser output power was controlled to less than 50 mW. The scattered light was detected by a laser Raman spectrometer (JASCO NRS 2000), calibrated using neon and silicon emission spectra with a precision of measured frequency of ± 2 cm^{-1}. Collection times in the lattice mode and O-H vibrational regions were 60 sec with three total accumulations. Spectra were obtained from 200 to 3650 cm^{-1} and data were fitted to a combination of Lorentzian and Gaussian modes using PeakFit and IGOR software suites.

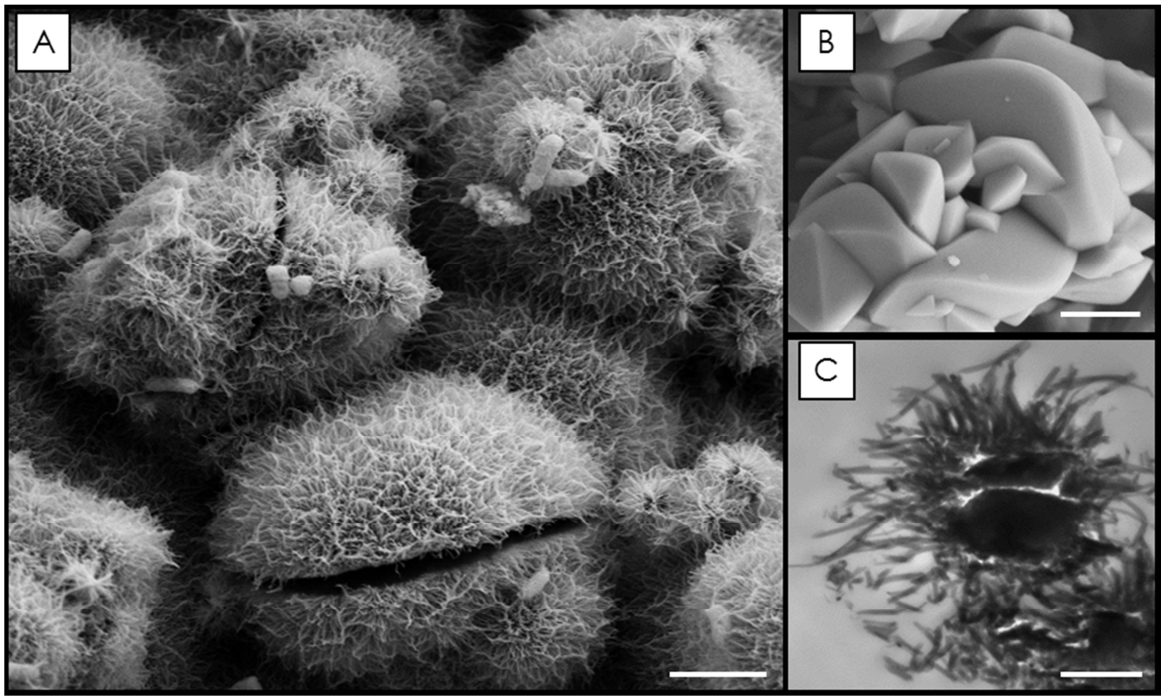

Figure 3.1. SEM and TEM micrographs of jarosite samples used in this study. SEM micrograph of microbial culture precipitate (A, scale bar = 2 μm), herein termed biogenic jarosite, shows the radiating aggregates of acicular needle-like precipitates (described in Chapter 2), in addition to the presence of rod shaped bacteria and accompanying extracellular organic materials. In contrast, the SEM micrograph of synthetic jarosite (B; scale bar = 1 μm) demonstrates a dissimilar morphology, with aggregates of blocky rosettes which has an identical XRD pattern to the material in A (see Figure 2.3.). C: TEM ultra-thin section micrograph of biological jarosite material (A) that is not hollow in the center, i.e., bacterial cells do not appear to act as nucleation sites.

3.2.3. Infrared spectroscopy (IR)

Diffuse reflectance infrared Fourier transform spectroscopy (DRIFTS) was completed on undiluted jarosite samples and analyzed in reflectance mode, over a range of scan times using a Pike AutoDIFF accessory attached to a Nicolet Nexus 670 FTIR with Globar source, KBr beamsplitter, and DTGS detector at the University of New Mexico. Prior to analysis, the entire system was purged with dry air, for a minimum of 45 min, in order to decrease the occurrence of spectral features related to absorptions pertaining to the atmosphere (i.e., CO_2) versus features from the sulfate minerals and/or any of the biological or organic constituents within the target material. For analysis, a small amount of the powdered jarosite was carefully placed into the AutoDIFF sample cup, while avoiding preferential grain alignment, pitting and/or clumping. Before acquiring any experimental data, background spectra were collected from the polished aluminum dish which was used as the reference standard for these analyses. Each sample was analyzed for 500 scans, with spectral resolution of 4 cm^{-1}, over a range of 400 – 4000 cm^{-1}. Band centers were determined using the OMNIC software package (Thermo Nicolet).

3.2.4. Visible-near infrared reflectance spectroscopy (VNIR)

VNIR absolute reflectance spectra were collected with the Analytical Spectral Devices (ASD) FieldSpec Pro High Resolution (HR) spectrometer at the University of Winnipeg Planetary Spectroscopy Facility (PSF). Spectra were acquired in absolute reflectance mode from 0.35 to 2.5 μm, and measured at 30° phase angle (i = 30°, e = 0°) using a 50 watt quartz-tungsten-halogen (QTH) collimated light source. Spectral resolution varies between 2 and 7 nm and spectral sampling was completed in 1.4 nm

steps. Data were internally resampled to output data at 1 nm intervals. Spectra were acquired relative to a Spectralon® (Labsphere, North Sutton, NH) standard and corrected for known minor irregularities in Spectralon's absolute reflectance in the 2.0 to 2.5 μm range. Spectral averaging of the 200 individual collected spectra increased the signal to noise ratio of the generated spectra. Periodic measurements of a holmium oxide-doped Spectralon® disk were acquired to ensure wavelength calibrations. Band centres were evaluated using the OMNIC software package (Thermo Nicolet) and assignments made based on previously published results.

3.2.5. Mössbauer spectroscopy (Mössbauer)

Approximately 10-20 mg of synthetic and natural jarosite samples were gently crushed under acetone then mixed with sugar and acetone to thin samples for analysis. Samples were mounted in a holder confined by Kapton® tape. Mössbauer spectra were acquired at 295K using a source of ~40 mCi ^{57}Co in Rh on a WEB Research Co. model WT302 spectrometer (Mount Holyoke College). Spectra were collected over a ± 4 mm/s velocity range in 2048 channels and corrected for nonlinearity via interpolation to a linear velocity scale, which is defined by the spectrum of the 25 μm Fe foil used for calibration. The WMOSS algorithm fits a straight line to the points defined by the published values of the Fe metal peak positions (*y* values) and the observed positions in channels (*x* values). Data were then folded before fitting, using the WMOSS Auto-fold procedure which folded the spectrum about the channel value which produces the minimum least squares sum difference between the first half of the spectrum and the reflected second half of the spectrum.

All data were corrected to remove the fraction of the baseline due to the Compton scattering of 122 keV gamma rays by electrons inside the detector. Spectra were collected for 3 to 24 hours depending on the Fe contents of each sample, in 2048 channels and corrected for nonlinearity. Data were modeled using an in-house program from the University of Ghent, in Belgium called DIST_3E (an implementation of software described in Wivel and Mørup, 1981), which uses model-independent quadrupole splitting distributions for which the subspectra are constituted by Lorentzian shaped lines and does not presume any particular shape of the distribution.

Isomer shift (δ), and quadrupole splitting (ΔE_Q) of the doublets were allowed to vary, while widths of both peaks in each doublet were coupled to vary in unison (*i.e.,* one width for each doublet, but every doublet independent). Errors are appropriately ±0.02 mm/s for center shift and quadrupole splitting, with errors of ±1-3% absolute on areas for these spectra. Error bars for Mössbauer measurements are discussed at length by Dyar (1984) and Dyar et al. (2008). All Mössbauer data were posted online for public use as part of the Mount Holyoke College database.

3.2.6. Laser induced breakdown spectroscopy (LIBS)

Laser induced breakdown spectra (LIBS) analyses of the suite of jarosite samples was completed with an Ocean Optics LIBS2000, a compact spectrometer over the wide spectral range of 200 to 970 nm with 0.1 nm resolution across the entire range. This set up is similar to that of the ChemCam instrument on the Mars Science Laboratory (MSL) Curiosity rover and other portable field instruments currently used to identify geological samples. During sample analysis all experimental parameters (i.e., pulse energy,

spectrometer spectral range, focusing distance and size of collecting optics) were selected to be similar to those expected to be used with the ChemCam instrument. A 20 mJ Q-switch Nd-YAG laser beam pulse (Spectra Physics LPY150) was focused onto the sample surface in ambient air with a 7.5 cm focal-distance lens, producing a 300 μm diameter spot size. The pulse energy was 20 mL and the repetition rate was 1 Hz. The emission from the plasma created was collected with a 4 mm-aperture, 7 mm-focus fused-silica collimator placed at a distance of ~3 cm from the sample, and then focused into an optical fiber (600 μm core diameter) which was coupled to the entrance of the spectrometer. Emission from the plasma created collimated with the same lens and collected to a compact CCD spectrometer (Ocean Optics LIBS 2000).

In addition to the biogenic and synthetic jarosite pair, two additional samples of the biogenic material were analyzed in order to investigate the effects of sample preparation on the spectra generated and any changes in and of the spectral features. Two additional biogenic samples were analyzed, an 'aged' biogenic sample prepared identically to the biogenic material, but harvested after 20 weeks incubation at RT and a 'wet' biogenic samples which was again prepared in the same manner as the biogenic sample, but this sample was analysed immediately after harvesting and not placed into an oven to dry. For each of the four samples (synthetic, biogenic, aged and wet), six spectra were acquired and then compared to that of the spectra of a glass slide in order to ensure that the spectra obtained were that of the target and not the sample holder. The spectra were normalized to overcome spectral fluctuations using the oxygen line or iron line.

3.2.7. Time-of-flight secondary ion mass spectroscopy (ToF SIMS)

An Ion-ToF (GMBH) ToF SIMS IV equipped with a Bi cluster liquid metal ion source at the Surface Science Western facility at the University of Western Ontario was used to complete all ToF SIMS analyses. A 25 keV Bi_3^+ cluster primary ion beam pulsed at 10 kHz was used to bombard the sample surface to generate secondary ions. A Cs ion beam was used to ion clean the powder samples providing a fresh surface for analysis while a pulsed, low energy electron flood was used to neutralize sample charging. Secondary ions (positive or negative) were extracted from the sample surface, mass separated and detected via a reflection-type of time-of-flight analyser, allowing parallel detection of ion fragments having a mass to charge ratio up to 900 amu within each cycle (100 μs). Ion mass spectra were collected at 128 x 128 pixels over the scanned area of 500 μm x 500 μm (100 scans with 1 shot per pixel), for the positive and negative spectrum respectively. Collected spectra were analyzed using the Ion-Spec™ and Ion-Image™ software suite (Ion-ToF, GMBH). To account for variability in individual spectra ion yields, data collected were normalized for total ion count (normalized value = ions counted/total ions x 100,000) and plotted as corrected intensities (CI).

3.3. Results

3.3.1. Raman spectroscopy (Raman)

Raman spectra of biogenic and synthetic jarosites from 200 to 1550 cm^{-1} (in two parts) and from 3150 to 3650 cm^{-1} are shown in Figures 3.2 (A-C) and are listed in Table 3.1. All acquired spectra are similar and match well to the previously reported Raman spectra of jarosite minerals. Spectral feature assignments are based on previously published values from well-established studies that have characterized the spectra of

Wavenumber(cm^{-1})		Assignment
Biogenic	*Synthetic*	
Raman	Raman	
3428b	3423b	ν_{OH}
1154	1161	$\nu_3(SO_4^{2-})$
1095	1107sp	$\nu_3(SO_4^{2-})$
	1047sh	$\nu_1(NO_3)$
1007	1013	$\nu_1(SO_4^{2-})$
712w		
622sp	628	$\nu_4(SO_4^{2-})$
565	578	γ(OH)
454sh	459sh	$\nu_2(SO_4^{2-})$
426	439sp	Fe-O
353w	361w	Fe-O
308	308	Fe-O
220sp	229s	Fe-O

Table 3.1. Raman spectral assignments of peaks collected from 200 to 3650 cm^{-} and shown in Figure 3.2., (s: strong; w: weak; sh: shoulder; b: broad; sp: sharp). Assignments based on published values found in Chio et al. (2010), Frost et al. (2005), Sasaki et al. (1998) and Serna et al. (1986).

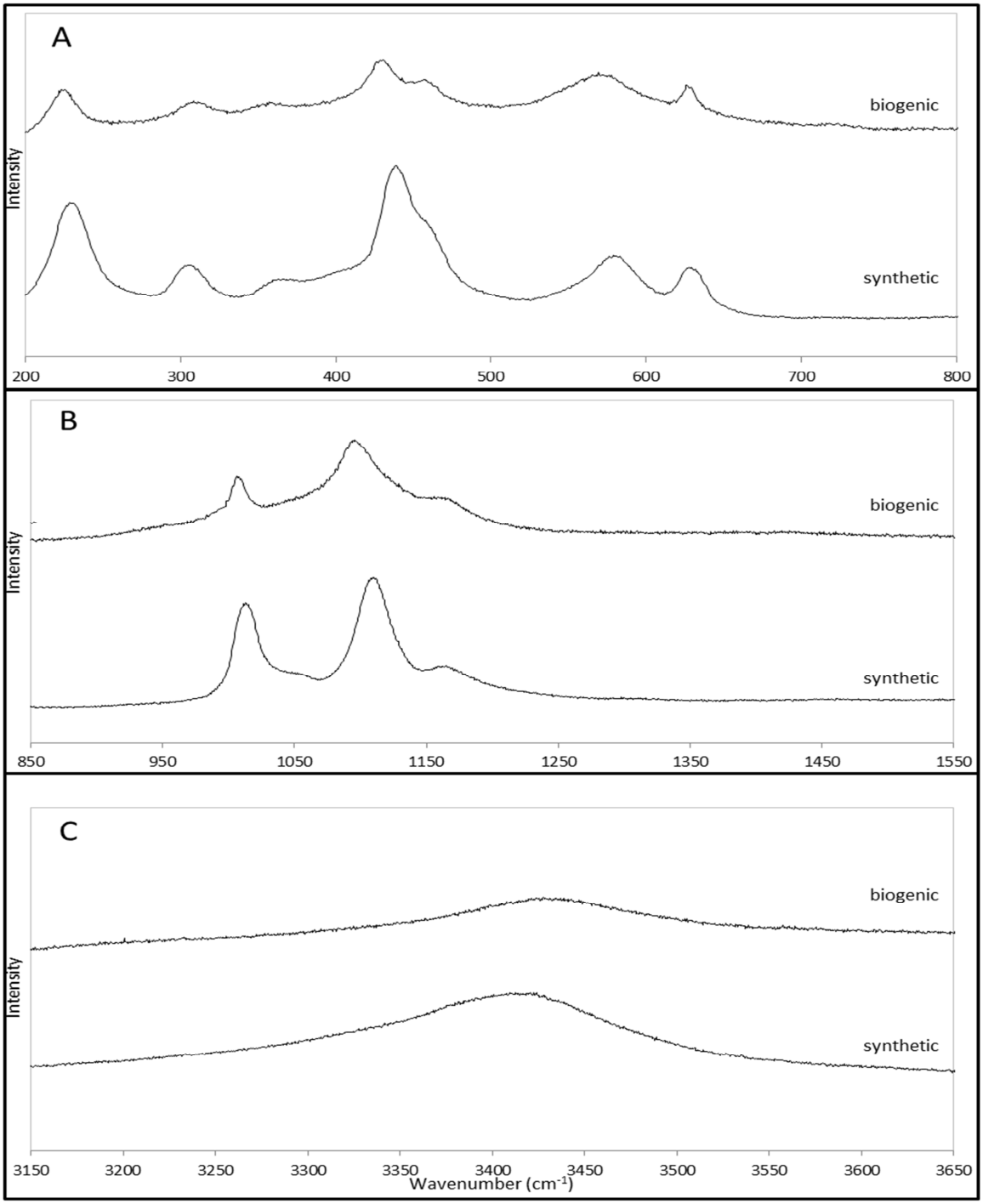

Figure 3.2. Raman spectra between 200 and 800 cm^{-1} (A), 850 and 1550 cm^{-1}(B), and 3150 and 3650 cm^{-1} (C) of synthetic and biogenic jarosites. The spectral plots are of normalized intensity (arbitrary) versus wavenumber with a spectral precision of $\pm$ 2cm^{-1}. Spectra are stacked in order to facilitate comparisons. Peak positions and assignments are listed in Table 3.1.

natural and synthetic jarosite minerals (Chio et al., 2010; Frost et al., 2005; Sasaki et al., 1998; Serna et al., 1986). No peaks were observed from 1550 to 3150 cm^{-1} in any of the spectra collected and this range was omitted from the figures.

All of the features of the Raman spectra for biogenic and synthetic jarosite samples are very similar. As shown in Figure 3.2A there is a shoulder band assigned to the sulfate ion symmetrical bending vibrational mode ($v_2(SO_4^{2-})$) around 454-459 cm^{-1}, as well as a sharp band near 622-628 cm^{-1} corresponding to the asymmetrical bending mode ($v_4(SO_4^{2-})$). There are four peaks at wavenumbers smaller than 440 cm^{-1} including a wide band at ~353-361cm^{-1} and sharper bands at 426-439 cm^{-1}, ~308 cm^{-1}, and 220-229 cm^{-1} all assigned to the vibrational modes of Fe-O bonding of jarosite group compounds. From 850 to 1550 cm^{-1} (Figure 3.2B), a pair of sharp bands sharp band occurs at 1007-1013 cm^{-1} and 1095-1107 cm^{-1} which correspond to assigned to the symmetrical ($v_1(SO_4^{2-})$) and asymmetrical stretching ($v_3(SO_4^{2-})$) vibrational modes, respectively. Additionally, a weak band occurs at 1154-1161 cm^{-1} which is assigned to the vibrational mode of $v_3(SO_4^{2-})$. A very weak Raman peak is observed at 1047 cm^{-1}, in the synthetic spectrum which does not occur in the biogenic spectra. As reported in previous studies (e.g., Frost et al., 2005), this peak may correspond to the total symmetric stretching mode of the nitrate ion. Potassium nitrate was used in the synthesis of jarosite and it is plausible that there would still be some of this molecule in the synthetic precipitate. Furthermore, Chio et al. (2010) characterized all of the starting products of their synthesis of jarosite in one of their Raman spectral investigations and they noted that the $v_1(NO_3)$ of crystalline KNO_3, one of the reagents used during synthesis, occurred at 1051 cm^{-1}. Vibrational

modes pertaining to hydroxyl occur around 565-578 cm^{-1} (γ(OH)) as well as a broad band near 3423-3428 cm^{-1} in both samples (Fig. 3.2C).

3.3.2. Infrared spectroscopy (IR)

The IR spectra of both biogenic and synthetic samples are shown in Figure 3.3. and the absorption feature assignments are listed in Table 3.2. As expected, due to the fine grained nature of powders analysed in this study, the spectral features generated in this study exhibited weaker mid-IR spectral features than spectra derived from naturally occurring jarosite deposits in the field (Bishop and Murad, 2005). Alunite group minerals exhibit spectral features due to the vibrations of hydroxyl groups, lattice vibrations, metal-oxygen bonds and sulfate groups, all of which were detected in both jarosite spectra.

Spectra obtained from synthetic jarosite samples contained no evidence of organic molecules, and possessed absorption features related to the vibrations of the sulfate ion at 680, 980, 1012, 1053, 1136, 1245, and again from 1968 – 2460 cm^{-1}. The spectral feature at 1245 cm^{-1} may also be the Christiansen feature, which typically occurs at 1250 cm^{-1} in jarosites (Cloutis et al., 2006). Features at 594, 1634, 3405, 3835, and 3956 cm^{-1} are related to the vibrational modes of hydroxyl and water while the absorption feature at 485 cm^{-1} is caused by an metal-oxygen bending vibration. The feature at 1445 cm^{-1} has been assigned to the vibration of the S=O bond in the sulfate ion. Two absorption features (1301 and 1401 cm^{-1}) which occur in the spectrum remain unassigned, although they have been observed in other synthetic jarosite spectral studies (Hyde et al., 2011).

The biogenic spectra exhibits less spectral absorbance features than the synthetic

Wavenumber(cm^{-1})		Assignment
Biogenic	*Synthetic*	
	3956	3 $\nu(SO_4^{2-}$, νOH
	3835	3 $\nu(SO_4^{2-})$, νOH
3406	3405	νOH, νH_2O
	2460	2 $\nu(SO_4^{2-})$, 2δ(OH)
	2322	2 $\nu(SO_4^{2-})$, 2δ(OH)
2163	2175	2 $\nu(SO_4^{2-})$, 2δ(OH)
2069	2075	2 $\nu(SO_4^{2-})$, 2δ(OH)
2025	2031	2 $\nu(SO_4^{2-})$, 2δ(OH)
1945	1968	2 $\nu(SO_4^{2-})$, 2δ(OH)
1639	1634	$\delta(H_2O)$
1426	1445	ν S=O
	1401	
	1301	
	1245	$\nu_3(SO_4^{2-})$, Christansen feature
1187	1136	$\nu_3(SO_4^{2-})$
1058	1053	$\nu_3(SO_4^{2-})$
	1012	$\nu_3(SO_4^{2-})$
974	980	$\nu_1(SO_4^{2-})$
733	680	$\nu_4(SO_4^{2-})$
556	594	γ(OH)
510		Fe-O
461	485	Fe-O, $\nu_2(SO_4^{2-})$
428		Fe-O
410		Fe-O

Figure 3.3. Infrared peak positions and assignments of spectra in Figure 3.3. collected from 400 to 4000 cm^{-1}. Assignments were made based on values published in Bishop and Murad (2005), Cloutis et al. (2006), Powers et al. (1974), as well as Sasaki et al. (1998).

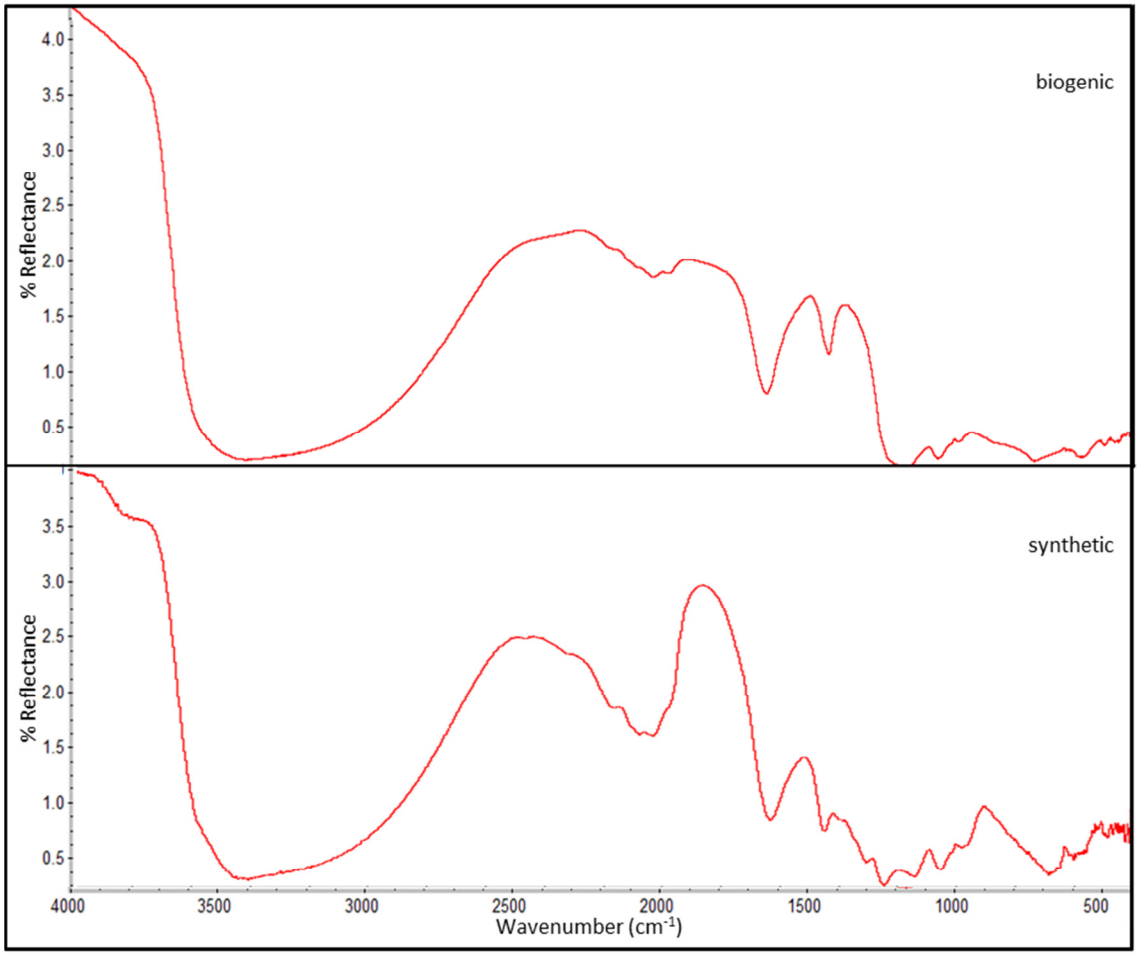

Figure 3.3. Infrared spectra of biogenic and synthetic jarosite samples collected from 400 to 4000 cm^{-1}. Peak positions and assignments are listed in Table 3.2. Plots are of percent reflectance versus wavenumber. The spectra are stacked in order to facilitate comparisons with a spectral resolution of 4 cm^{-1}.

material, yet both spectra are very similar. Absorption features related to the vibrational modes of the sulfate ion in the biogenic material were observed at 974, 733, 1058, 1187, and several between 1945–2163 cm^{-1}. Four Fe–O bending vibrational mode contributions are observed in this spectrum at 410, 428, 461, and 510 cm^{-1}. An absorbance feature due to the vibrational mode of S=O is observed at 1426 cm^{-1}, while spectral contributions related to OH and H_2O groups occur at 556, 1639, and 3406 cm^{-1}. Unlike the synthetic spectra, all of the absorption features that occur in the biogenic spectrum are assigned. Furthermore, all of the assignments can be explained by molecular vibrations of the jarosite mineral and no organic molecules were detected.

3.3.3. Visible – near infrared reflectance spectroscopy (VNIR)

The reflectance spectra of both jarosite samples collected from 300 to 2500 nm (VNIR) generally correlate but are not an identical match (Figure 3.4.) and there are absorbance features in each spectrum that do not appear in the other (Table 3.3.) Both spectra, albeit slightly different, match well to published jarosite spectra of natural (Cloutis et al., 2008; 2006; Crowley et al., 2003; Hunt and Ashley, 1979) and synthetic specimens (Bishop and Murad, 2005). Absorption bands characteristic of crystal field transitions in ferric iron occur at 437 and 905 nm, with a weak shoulder centred at 602 nm. Absorption bands related to the vibrational modes of hydroxyl (or adsorbed water) occur at 1470, 1848, and 1969 nm. The absorption doublet feature at 2264 nm is related to the Fe-O-H vibrational mode and after this feature there is a well-defined decrease in reflectance.

The biogenic jarosite sample spectrum is similar when compared to the synthetic spectrum, but it exhibits fewer absorbance features as was observed in the mid-IR

Band location (nm)		Assignment
Biogenic	*Synthetic*	
	437	Fe^{3+} crystal field transition
506[a]	602[a]	Fe^{3+} crystal field transition
902	905	Fe^{3+} crystal field transition
1427	1470	OH overtones
	1848	Combinations of OH- or H_2O- bending, stretching, and rotational fundamentals
1941	1969	Combinations of OH- or H_2O- bending, stretching, and rotational fundamentals
2230[a]	2033[a]	$\nu OH/H_2O + \gamma/\delta\ OH/H_2O$
	2263	Fe –O–H combination
2319[a]		$3\nu_3$S-O or OH/H_2O combination and overtone
2351[a]		$3\nu_3$S-O or OH/H_2O combination and overtone

Table 3.3 Reflectance spectroscopy band locations and assignments of synthetic and biogenic jarosite in Figure 3.4. Spectra was collected continuously from 300 to 2500 nm Band assignments are based on previously established values from Bishop and Murad (2005), Cloutis et al. (2008 ; 2006), Crowley et al. (2003), Dyar et al. (2006), Hunt et al. (1971). [a] denotes a weak absorption band.

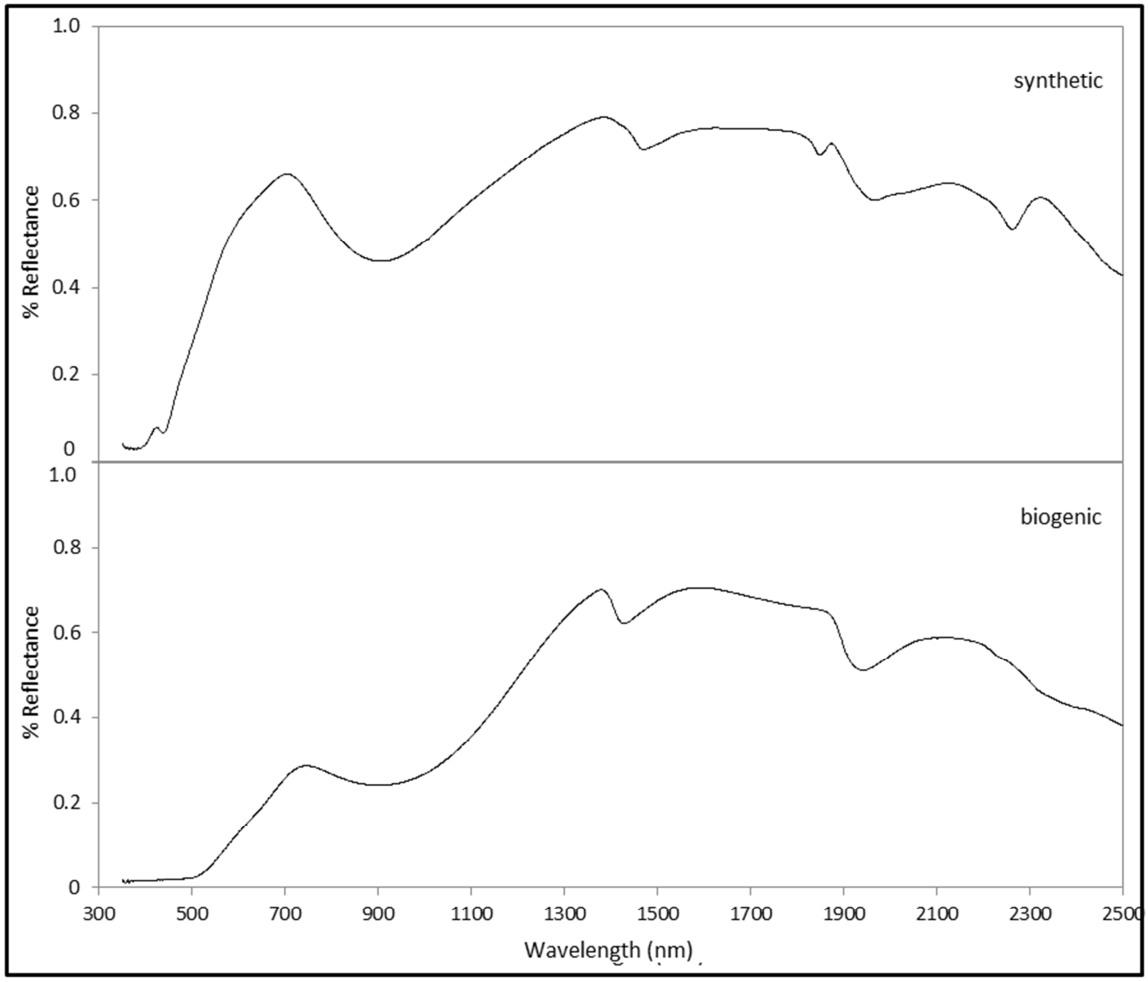

Figure 3.4. VNIR reflectance spectra (i = 30°, e = 0°; 0.35-2.5 μm) of synthetic and biological jarosite minerals obtained from 300 to 2500 nm. Band centers and peak assignments are listed in Table 3.3. Plots are of absolute reflectance versus wavelength with variable resolutions across the spectral range (2 to 7 nm). Sample spectra are stacked in order to facilitate comparisons.

reflectance spectroscopic analyses. The biogenic sample exhibits Fe^{3+} crystal field transitions at 902 nm with a broad shoulder at 506 nm, however, the feature at ~430 nm is not observed in the biogenic spectrum. It is documented that this crystal field transition at ~430 nm can be unobservable in reflectance spectra due to a masking effect which occurs when large quantities of iron oxides are present and mask the ferric contribution of the jarosite (Hunt and Ashley, 1979). A series of weak absorption features which occur in the biogenic spectrum at 2319 and 2351 nm are due to S-O bend overtones or hydroxyl/water combinations and overtones. The absorption at 2230 nm, albeit weak, is related to the $\nu OH/H_2O$ fundamental. Hydroxyl overtones are present at 1427 and 1941 nm.

Both spectra obtained in this study, although not identical, match well published jarosite spectra, particularly of Cloutis et al. (2006) where samples of several sulfate minerals were analyzed using reflectance spectroscopy and the spectra herein match very well to two of the spectra obtained for natural jarosites from Greece and New Mexico. No absorbance features were observed that were not assigned within the expected fundamentals and overtones of all vibrational modes for jarosite, indicating that both samples were pure single phased jarosite and that no organic molecules were detected from the biological material within the biogenic samples.

3.3.4. Mössbauer spectroscopy (Mössbauer)

Mössbauer spectra of biogenic and synthetic jarosite samples measured at RT are found in Figure 3.5 (fit parameters listed in Table 3.4). Both spectra exhibit the characteristic ferric doublet of all jarosites, with no evidence of a sextet, whose fit lines

	Biogenic	*Synthetic*
Fit 1: Single Curve		
δ (mm/s)	0.37	0.38
ΔE_Q (mm/s)	0.65	1.23
Γ (mm/s)	0.33	0.27
A (%)	1.00	1.00
Fit 2: Double Curve		
Fe^{3+}		
δ (mm/s)	0.37	0.37
ΔE_Q (mm/s)	0.61	1.28
Γ (mm/s)	0.34	0.23
A (%)	0.77	0.47
Fe^{3+}		
δ (mm/s)	0.39	0.39
ΔE_Q (mm/s)	0.96	1.04
Γ (mm/s)	0.36	0.38
A (%)	0.23	0.53

Table 3.4. Mössbauer parameters for octahedrally coordinated Fe in the jarosites at 295 K. δ is the isomer shift, ΔE_Q is the quadrupole splitting, Γ is the line width, and A is the spectral area. Mössbauer spectra of these jarosite samples fit with a single curve are plotted in Figure 3.5.

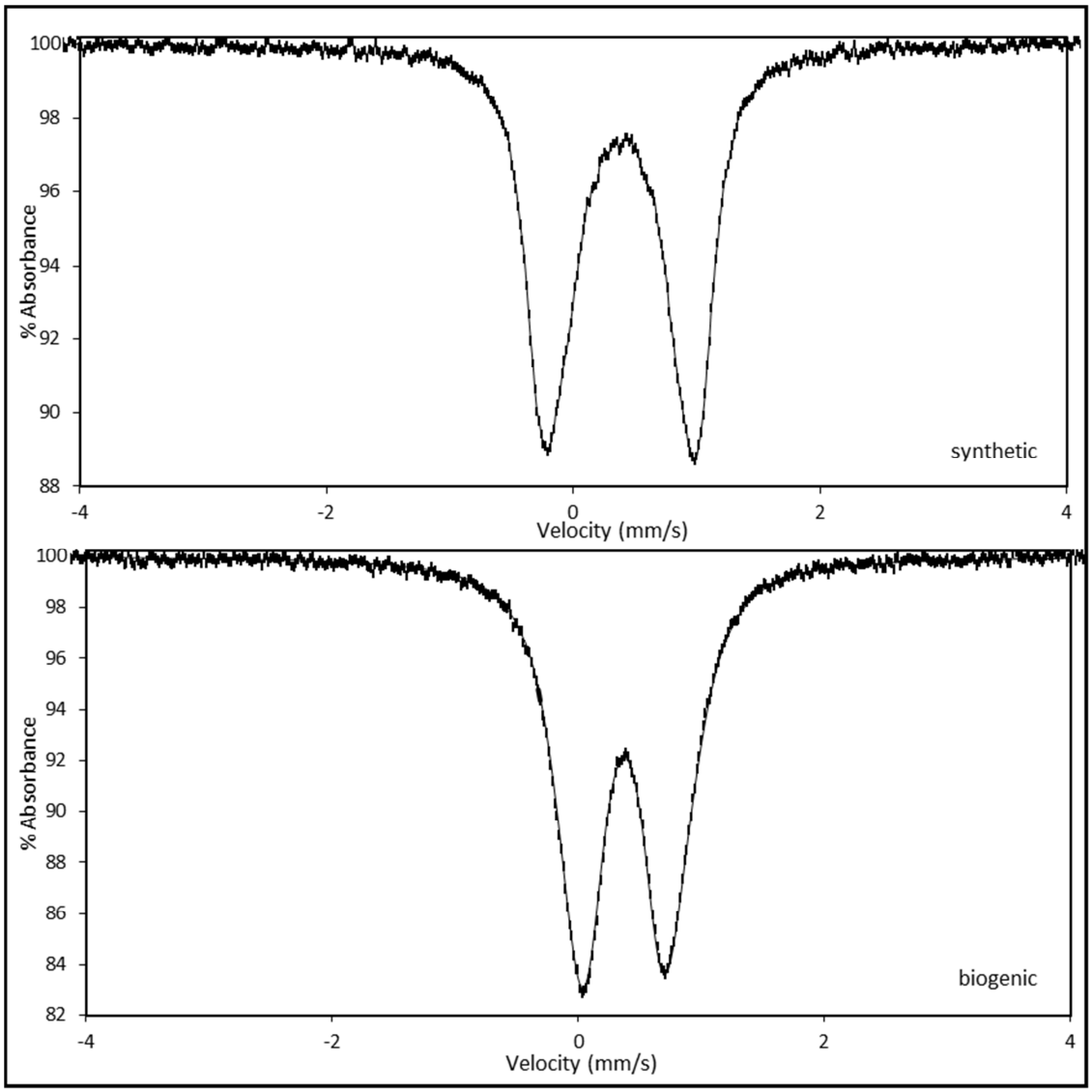

Figure 3.5. Mössbauer spectra of synthetic and biogenic jarosite samples collected over a $\pm$4 mm/s velocity range. Plots are of absolute absorbance versus velocity with acceptable range errors ($\pm$0.02 mm/s). Each plot shown is fit with a single curve and fit parameters are listed in Table 3.4.

depart slightly from a Laurentian curve typical of jarosite-type compounds. Spectral parameters of the doublet correspond to ferric ions occupying only one octahedral site in the minerals. Spectra were fit with single line and curve parameters are recorded in Table 3.4. No ferrous iron is observed in either fine grained powder samples. Synthetic and biogenic samples exhibited similar isomer shift (δ) values (0.38 and 0.37 mm/s respectively) but distinctly different quadrupole splitting (ΔE_Q) values (1.23 mm/s and 0.65mm/s in turn). The synthetic jarosite exhibited the characteristic high quadrupole splitting value (ΔE_Q = 1.23 mm/s) expected for jarosite minerals (Majzlan et al., 2011), while the biogenic (ΔE_Q = 0.65mm/s) falls outside of the range of values anticipated for alunite group minerals (Dyar et al., 2006; Bishop and Murad, 1999;).

3.3.5. Laser induced breakdown spectroscopy (LIBS)

LIBS spectral databases are limited. To our knowledge, this is one of the first instances of a pure single phase jarosite LIBS spectrum. LIBS spectra of synthetic and biogenic jarosite samples are shown in Figure 3.6. as well as the spectra of 'dry' and 'wet' biogenic samples used to investigate the effects of sample preparation conditions on the generated LIBS spectra. A qualitative approach was taken to analyze and compare these four spectra.

The LIBS spectra of the four jarosite samples (1 synthetic and 3 biogenic preparations) studied in this investigation were divided into the three spectral ranges ultraviolet (240–340 nm; A), blue (380–470 nm; B), and visible/near-infrared (490 –900 nm; C). All samples analyzed generated spectra that were different from those of the sample holder (i.e., glass slide; data not shown) indicating that spectra acquired were only

	λ (nm) of brightest lines		
	UV (239.15–339.66 nm)	*VIS (383.82–471.44 nm)*	*VNIR (490.61– 928.02nm)*
H		434	656.46
Li		460.42	610.52, 670.97, 812.88
C	247.93, 283.75	426.82	589.14, 657.99
N			500.65
O			777.41, 777.63, 844.36
Na	312.53,	589.16, 589.76	818.55, 819.71
Mg	279.63, 279.88, 280.53, 285.29, 292.9 , 293.7	448.24	517.41, 518.51
Al	308.31, 309.36	394.56, 396.21	704.40, 705.85
P			537.97, 550.87, 558.48
S	330.33	402.99	468.26, 639.91, 639.97
Cl		310.53, 414.5, 426.7,	507.97, 521.94, 545.4 , 547.4 , 551.0 , 556.5 560.0 , 771.97, 837.82
Ar			750.59, 795.04
K		404.7, 418.74	693.6, 766.49, 769.90
Ca	315.98, 318.02	393.48, 396.96, 422.79	559.60, 616.30
Mn	289.04, 294.01, 295.01	423.63, 446.32	537.91, 601.51
Fe	275.01, 275.65, 278	404.69, 427.23, 432.70, 438.48	516.89, 521.77, 522.86, 561.6
Ar			750.59, 795.04

Table 3.5 Compiled list of LIBS brightness (emission) lines from published studies conducted on geological materials (Cousins et al., 2011; Dyar et al., 2012b; Ollila et al. 2012) used in this study to ascertain the presence of elements in the LIBS spectra generated in Figure 3.6.

Figure 3.6. Laser induced breakdown spectroscopy (LIBS) spectra from ultraviolet (240 to 340 nm; A), blue (380 to 470 nm; B) and visible/near-infrared (490 to 940 nm; C) ranges of the four jarosite samples analyzed in this study: synthetic, biogenic, dry, and wet. Samples plots are vertically offset to facilitate comparison and analysis and are of intensity (arbitrary) versus wavelength. All spectra were normalized using the oxygen emission line at 777 nm. Spectra were collected continuously over the wide range and have a 0.1nm resolution and are vertically offset to facilitate qualitative comparisons.

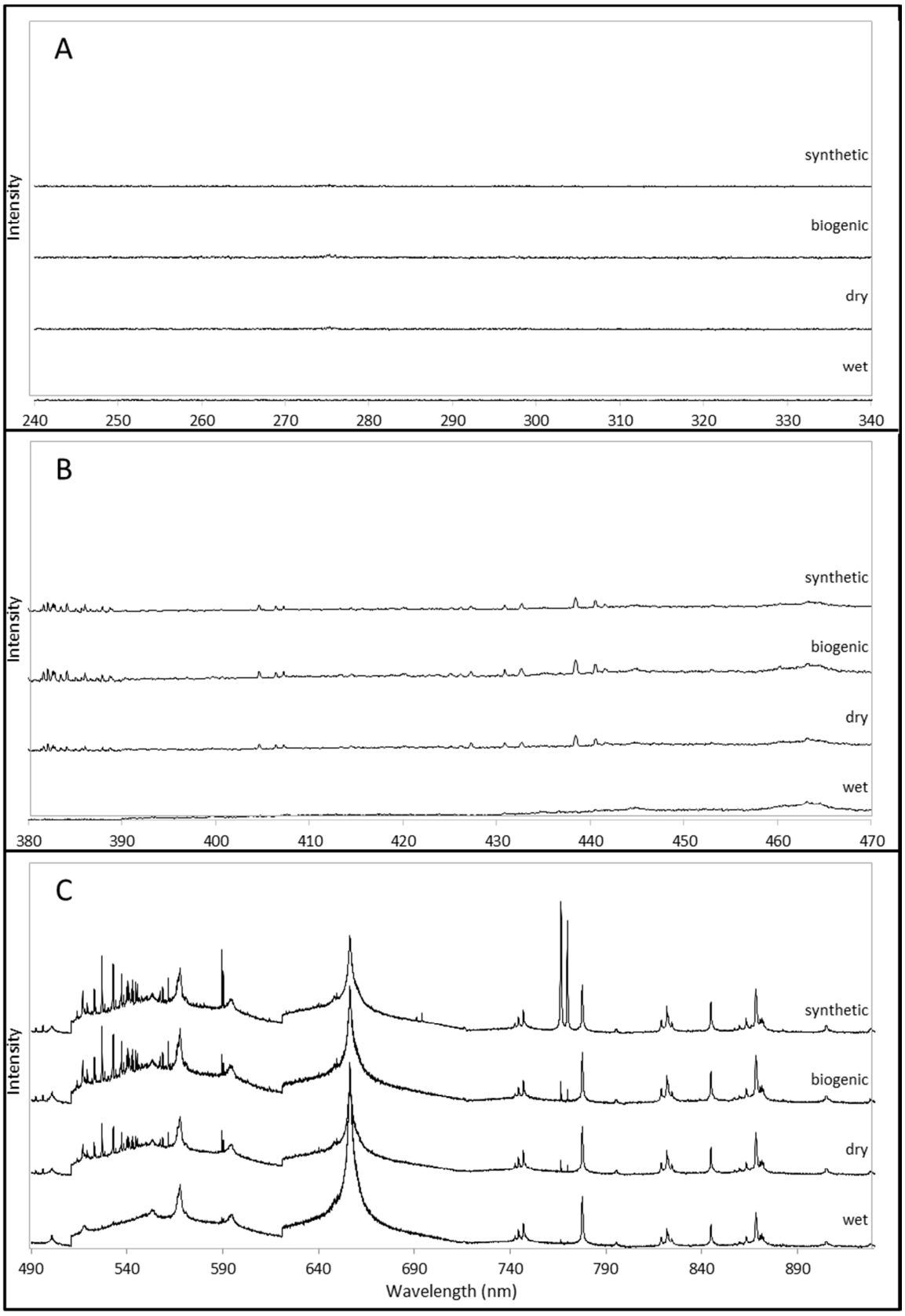
A
synthetic
biogenic
dry
wet
Intensity
240 250 260 270 280 290 300 310 320 330 340
B
synthetic
biogenic
dry
wet
Intensity
380 390 400 410 420 430 440 450 460 470
C
synthetic
biogenic
dry
wet
Intensity
490 540 590 640 690 740 790 840 890
Wavelength (nm)

generated by the target material being probed and that the laser had not ablated away all of the fine grained jarosite powders (data not shown). It was expected that these jarosite powders would generate spectral signatures of the elements K, Fe, S, O, and H as well as the possibility of minor contributions from Al, Mg, N, Na, and P in these jarosite powders based on the salts included in the microbial culture media (see CH 2 microbial culturing for more details, pg.27) Note, samples analyzed in this study did not have uniform surfaces, which resulted in spectral fluctuations as a result of heterogeneous laser focus across the spectra collected. In order to compensate for this physical matrix effect (Sorbon et al., 2012), all spectra were normalized with respect to the 777 nm oxygen line for this sample suite.

Qualitative comparison of sample spectra and comparisons of the presence or absence of spectral lines are herein described. Spectral lines were assigned based on values from established reports which are compiled in Table 3.5. Unassigned lines occur in the spectra at 742, 744, 824, 867, 870, and 871 nm in the ultraviolet range (Figure 3.6.C). Hydrogen (H), oxygen (O), nitrogen (N), sodium (Na), phosphorous (P), potassium (K), and iron (Fe) were detected in all samples by exhibiting all of theoretically expected emission lines. Additionally, samples contained spectral evidence of argon (Ar; 795.04 nm) and chlorine (Cl; 545.4 and 414.4 nm) as some of their emission lines were detected in all four spectra. Calcium may potentially also occur as in addition to the strong emission line at 866.214 nm, weaker response at 370.6, 373.7, 616.30 and 396.96 nm may also occur, but they are difficult to resolve without further spectra fitting or refinement. For these three elements, Ar, Cl and Ca, the remainder of the brightness lines expected were either not present or very difficult to differentiate from the background. Brightness lines corresponding to lithium (Li) only appeared in the dry sample spectra,

but appear to be interference from other, stronger emission lines in all cases. Spectral contributions pertaining to aluminium (Al), manganese (Mn) and sulfur (S) were not observed in any of the spectra.

Generally, the spectra of all four samples spectra were very similar. The synthetic sample, generally, exhibits the highest overall intensity of all four spectra (Figure 3.6.). The emission lines at 589 (Na) and 765 (K) and 769 (K) are the most intense emission lines in this spectra, and are significantly more intense than the corresponding emissions from the three biogenic samples. Additionally, brightness lines at 691 (K) and 693 (K) nm are only observed in the synthetic spectra and are likely visible as the contribution of the potassium emission lines to the overall synthetic spectra is very large. Apart from alkali line intensities, the synthetic spectrum is very similar to both of the dry biogenic samples. The 'wet' jarosite sample analyzed generates a general spectrum that is similar to the other samples, however it exhibits a significantly more intense 656 (H) nm emission line than any of the dried samples analyzed and is missing several iron emission lines in the blue range (380 to 470 nm) especially when compared to the dried samples. The observed increased intensity of H emission lines in the wet sample is likely due to the increased presence of adsorbed H_2O molecules to the precipitate surface when the sample is analyzed while still wet – and that the spectrum are normalized using the O 777 nm line, so the expected associated increase in O intensity is not as easily observed. Additionally, the plasma generated from a wet sample will be cooler, and this might be why we do not observe as many Fe emission lines as the dried samples. The energy levels of Fe are higher than those of Na and K, thus if the plasma temperature slightly decreases, not as much high level energy is imparted into the sample to excite the higher

energy levels, and they are ultimately not emitted. Distinct, biological (organic) material was not detected using LIBS.

3.3.6. Time-of-flight secondary ion mass spectroscopy (ToF SIMS)

ToF SIMS spectra for positive and negative ions from 0 to 900 amu (in four parts) are shown in Figures 3.7AB, 3.8CD, 3.9EF and 3.10GH. ToF SIMS databases are also limited. Previous geological studies using ToF SIMS pertain to the identification of molecules in oil. To our knowledge, this is the first instance of a jarosite ToF SIMS spectrum for either a natural or synthetic jarosite material. The experimental setup only allowed for a crude fit of the spectra. Qualitative analyses of normalized spectra with known values from a literature review are included here.

The ToF SIMS spectra of negative ions (Figure 3.9 and Figure 3.10) for both jarosite samples are very similar across the entire 900 amu spectral range generating large numbers of ions with repetitive cluster peaks, particularly above 250 amu (Figure 3.9F, 3.10GH). Synthetic spectra are slightly higher in intensity in comparison to the biogenic spectra until ~810 amu where the ion intensity suddenly decreases, whereas the positive ions generated from the biogenic material generates ions until a sudden decrease at ~825 amu (Figure 3.10.H).

The ToF SIMS spectra of the positive ions generated from both materials (Figure 3.7.and Figure 3.8) are similar, but can be easily differentiated from one another as the biogenic sample generates an overall spectrum with higher intensity than the synthetic material. At masses greater than 350 amu, the synthetic material generates spectral peaks which are an entire order of magnitude lower in intensity counts than the biogenic sample (Figure 3.7.B, Figure 3.8 C–D).

Figure 3.7. ToF SIMS positive spectrum of secondary ions of biogenic and synthetic powdered jarosite samples from 0 to 250 amu (A) and 250 to 450 amu (B). Spectra are stacked to facilitate comparison. Plots are of normalized intensity (arbitrary) versus atomic mass unit.

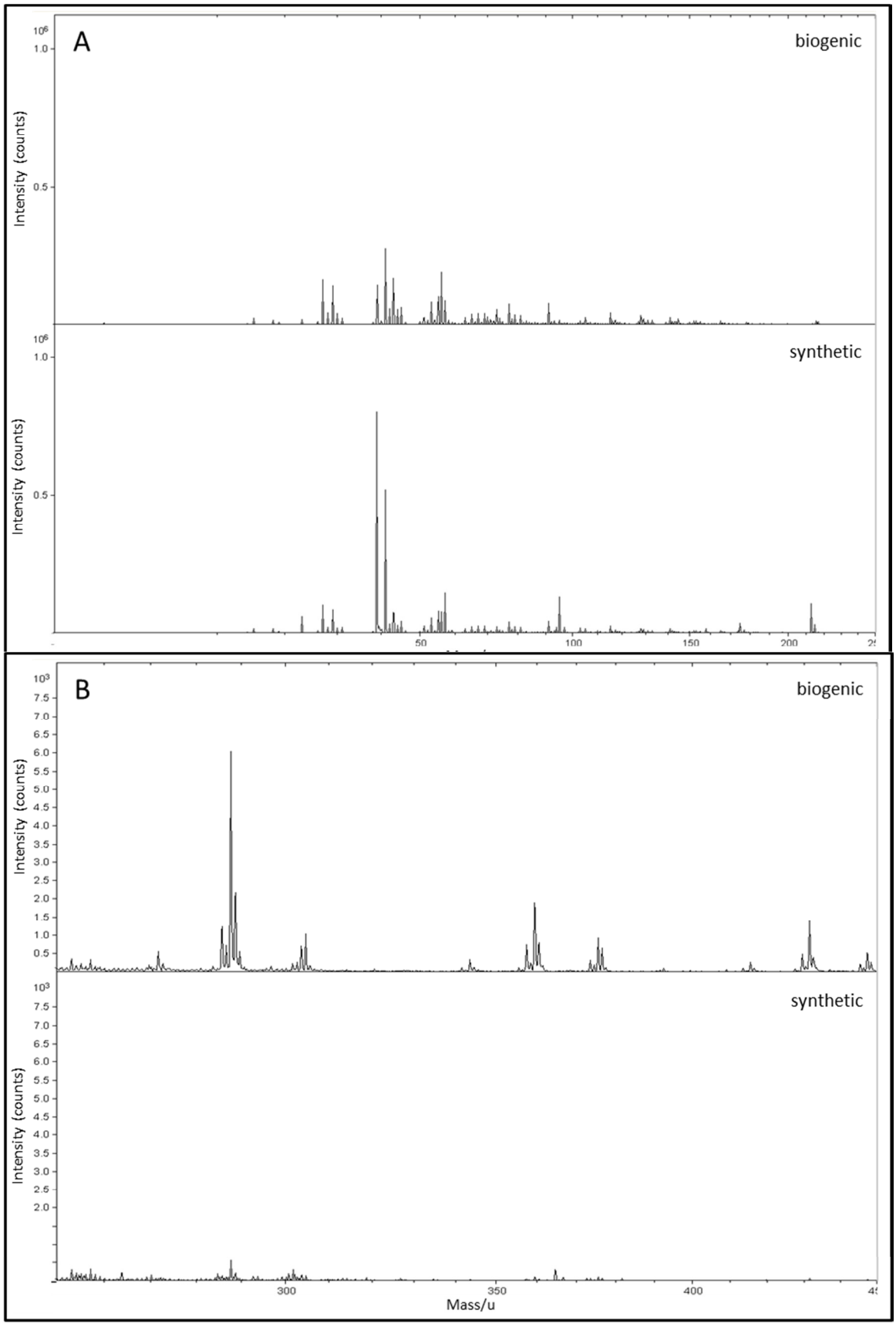
A
biogenic
synthetic
Intensity (counts)
B
biogenic
synthetic
Intensity (counts)
Mass/u

Figure 3.8. ToF SIMS positive spectrum of secondary ions of biogenic and synthetic powdered jarosite samples from 450 to 650 amu (C) and 650 to 900 amu (D). Spectra are stacked to facilitate comparison. Plots are of normalized intensity (arbitrary) versus atomic mass unit.

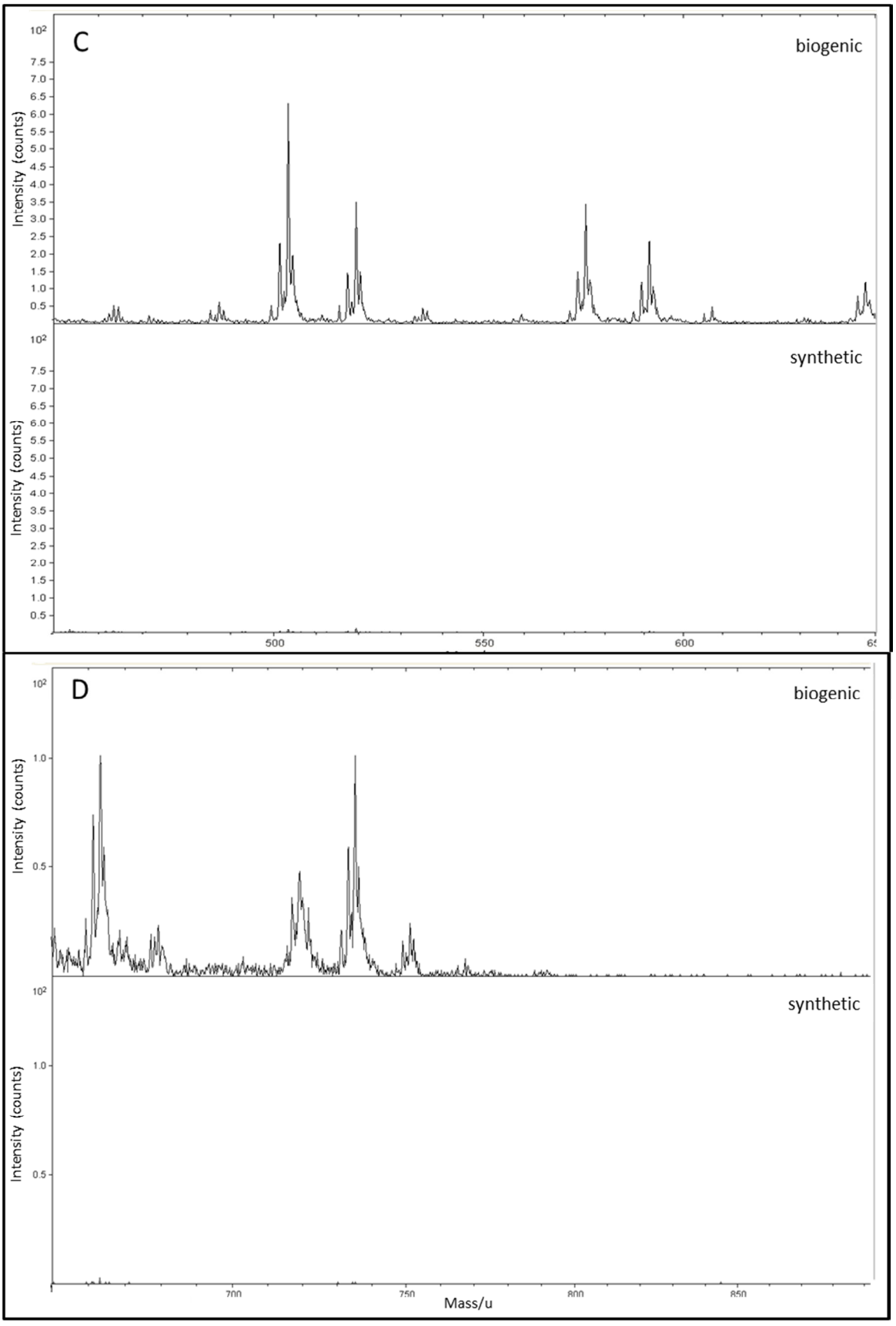
C
biogenic
synthetic
Intensity (counts)
D
biogenic
synthetic
Intensity (counts)
Mass/u

Figure 3.9. ToF SIMS negative spectrum of secondary ions of biogenic and synthetic powdered jarosite samples from 0 to 250 amu (E) and 250 to 450 amu (F). Spectra are stacked to facilitate comparison. Plots are of normalized intensity (arbitrary) versus atomic mass unit.

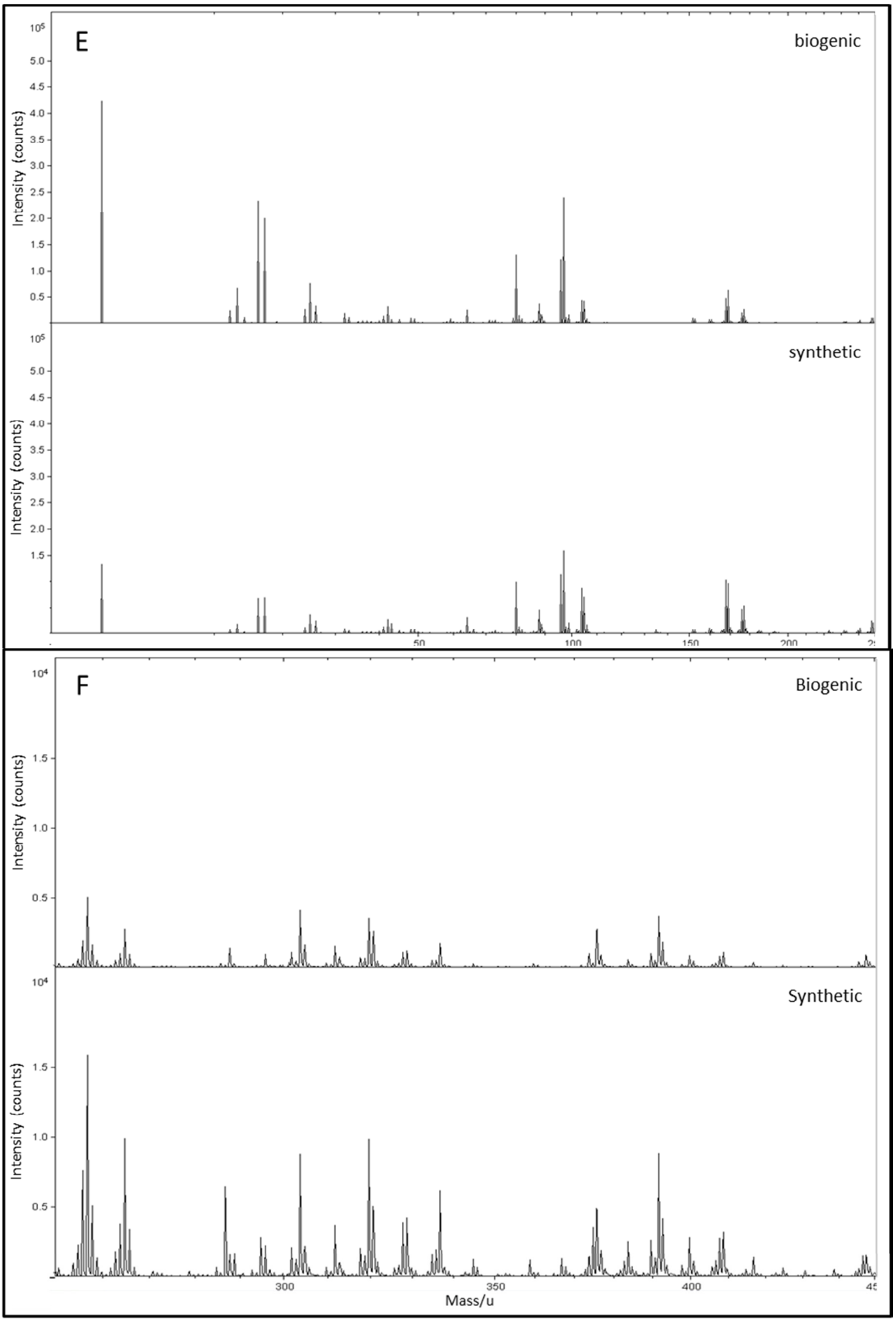
E
biogenic
synthetic
Intensity (counts)
F
Biogenic
Synthetic
Mass/u

Figure 3.10. ToF SIMS negative spectrum of secondary ions of biogenic and synthetic powdered jarosite samples from 450 to 650 amu (G) and 650 to 900 amu (H). Spectra are stacked to facilitate comparison. Plots are of normalized intensity (arbitrary) versus atomic mass unit.

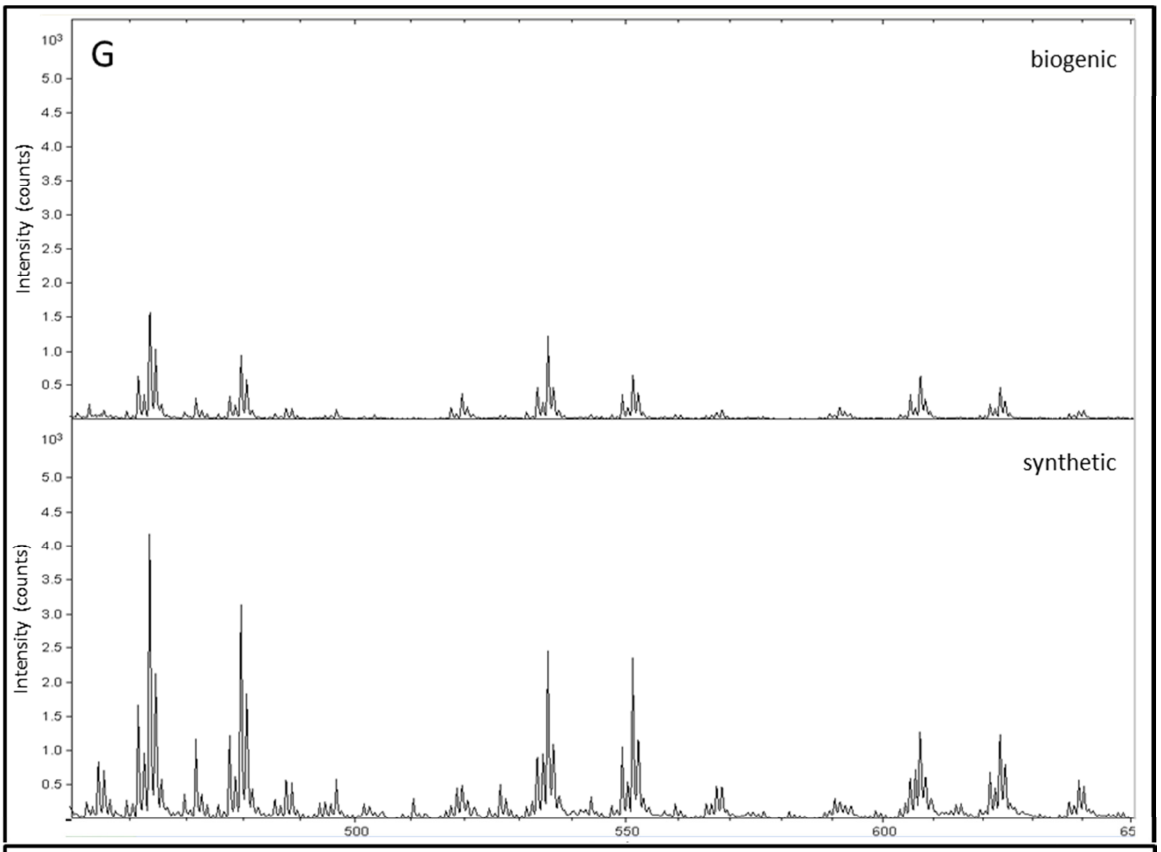
G
biogenic
synthetic
Intensity (counts)
10³
5.0
4.5
4.0
3.5
3.0
2.5
2.0
1.5
1.0
0.5
500
550
600
65

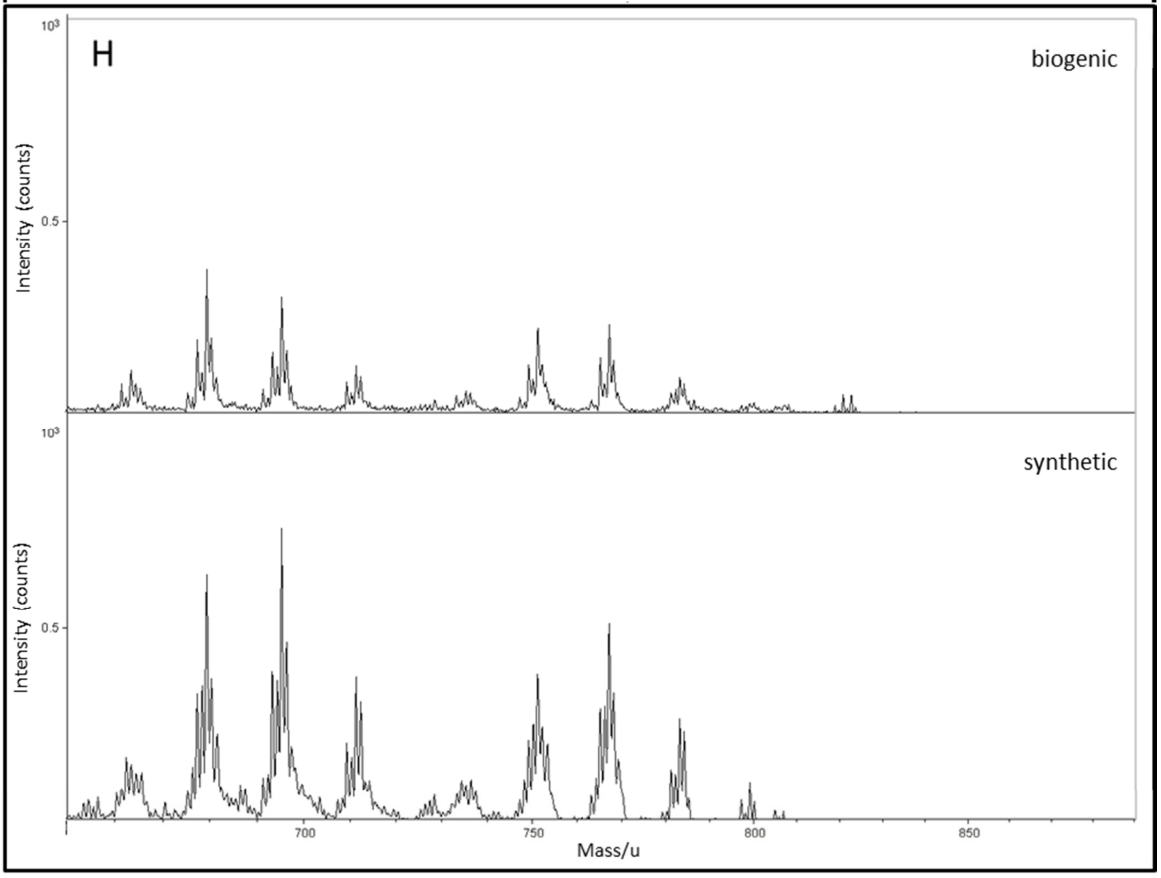
H
biogenic
synthetic
Intensity (counts)
10³
0.5
700
750
800
850
Mass/u

Generally, both spectra demonstrate the same repetitive clusters of peaks but at different intensities; here, the spectra are presented as normalized corrected intensities. That said it would be very difficult to determine the biogenicity of an unknown jarosite sample with similar spectra if the plot was in absolute intensity, given the similarity of the patterns. Intensity is a function of the number of secondary ions generated from the target sample during analysis – and it is not enough to make a distinction based solely on differences in intensity.

The most intense peaks in the synthetic material correspond to potassium ($^{39}K^{+}$ and $^{41}K^{+}$; Figure 3.7.A), but elsewhere, all intensities are weaker in the synthetic jarosite spectra at comparable mass/u. Spectral intensities generally, decrease as mass/u increase over the entire spectrum range. The overall intensity of synthetic jarosite decreases significantly relative to the biogenic matter (by orders of magnitude) at similar mass/u, and is barely visible after 350 amu. Note, the experimental setup only allowed for a crude fit of the spectra. Qualitative analyses of normalized spectra with known values from a literature review are included here. To our knowledge, this is the first occurrence of a ToF SIMS jarosite spectrum obtained using a ToF SIMS and the software suite did not have any reference material in its database.

3.4. Discussion

3.4.1. Missing organic responses in ToF SIMS, Raman and reflectance spectroscopy

Laboratory spectroscopy (Raman, IR and VNIR) completed during this study did not detect the presence of any organic functional groups diagnostic of biomolecules within the suite of jarosite samples studied. Raman and mid-IR spectroscopy can be used

to differentiate the jarosite group compounds (Sasaki et al. 1998), particularly when attempting to characterize the ion in the alkali spot of the mineral, and they are useful tools to identify specific jarosite-group minerals in geochemical samples. Biomolecules such as carbohydrates, nucleic acids, proteins, fatty acids, pigments, phospholipids, glycoproteins, amine, amides, and DNA could serve as unambiguous signs of extant life; however these molecules are not preserved well over geological time, especially when exposed to acidic environments. Biominearlized products are also subjected to degradation (e.g., chemical weathering, diagenesis, metamorphism, etc.) however, they are more durable and remain more stable for extended periods of time relative to organic markers (Farmer and Des Marais, 1999).

Organic macromolecules are relatively large compared to the unit cell mass of most minerals and when exposed to a ToF SIMS beam they can produce a wide range of molecular fragments from a few to several amu (light to heavy). An array of several peaks above 100 amu is indicative of organics and organic macromolecule fragments (Theil and Sjovall, 2011). Inorganic compounds are typically made up of small molecules, when compared to organics, and when these inorganic compounds fragment they do so in a more predictable manner that generates peaks at specific predictable mass numbers. However, we did not observe this even though there are bacterial cells and organics (Figure 3.1.) associated with the biogenic material. It possible that the ToF SIMS spectra generated were from samples with a low proportion of biological material or that only the mineralogical phase was sampled as this technique is spot sensitive on a relatively small scale, and not a bulk sample analysis. As with the Raman and reflectance spectroscopies, the detection of organic macromolecules is directly proportional to the

concentration of molecular bonds within the sample. This may also have been a factor as to why the Raman and reflectance spectroscopies did not detect any organic material in any of the biogenic jarosite spectra of this study, as previous work on Martian analogous sediments have yielded more positive results.

Previous studies have been able to detect organics within geological materials; Gleeson et al. (2010) were able to detect absorption features pertaining to proteins and fatty acids within sulfur deposits from an Arctic-spring deposit analogous to the Europa surface using reflectance spectroscopy, while Foster et al., (2011) also had success in observing organic molecular vibrations corresponding to biogenically derived vibrations in a suite of natural gypsum samples with haliophic endolithic communities within them.

Furthermore, laboratory studies have been able to identify and classify bacterial species using IR spectroscopy (Booth et al., 1966; Helm et al., 1991). In comparison to these studies, the biogenic sample used in this study is much darker and very opaque in comparison to the material used in these other studies (e.g. gypsum). Geological matrices with poor transmission can be difficult to study using this technique, even in a controlled laboratory with high resolution instrumentation (Izawa et al., 2011).

Finally, one of the largest difficulties in detecting organic signals, particularly in mid-infrared reflectance spectroscopy, is that absorptions caused by the sulfate anion vibrations (and in some instances hydroxyl) can in fact mask the biogenic signal, which would be proportionally much weaker, or be misinterpreted as a biogenic molecular vibration. For example, the absorbance bands at 1634 and 1639 cm^{-1} (Table 3.3.) were assigned to the bending H_2O vibrational mode, but absorbance pertaining to the C=C bond of alkene and the amide I vibration mode of protein also occur in this narrow region

(Preston et al., 2011). Additionally, the vibration observed in the synthetic sample at 1245 cm^{-1} was assigned to the Christansen feature associated with the sulfate in the samples of this study, but absorbances resulting from molecular vibrations of phosphate anions derived from nucleic acids and proteins also occur (Foster et al. 2011). Biomacromolecules including amino acids, amines, amides, glycoproteins and protein all have absorbance features from 630 to 670 cm^{-1} and this region of the spectra generated in this study are devoid of any spectral features. Mineral absorption features will most often be more prominent than those associated with biogenic materials and processes. It is important to see if we can detect any organic molecular bonds within an abiotic or synthetic sample to establish a base line and compare that to a known biogenic sample to see if there are any observable differences, as organics can be imparted into geological material by completely abiotic process.

3.4.2. Elemental detection of organics in LIBS spectra?

This is the first time, to our knowledge, that this instrumentation has characterized a biologically influenced material and, additionally, attempted to ascertain the technique's ability to ascertain and detect biogenicity of a geological material. Previous investigations using geological materials have been successful in discerning carbonate types (Lanza et al., 2010), accurately characterizing competing types of weathering reactions in paleosols (Dyar et al., 2012a) as well as deriving the elemental concentrations and the degrees of hydration of Ca- and Mg-sulfates (Sobron et al., 2012). Jarosites have been sparsely analysed using LIBS; typically natural samples that occur as minor secondary phases within igneous hosts or mixtures are characterized (Ollila et al., 2012).

LIBS has rapidly becoming part of the geochemists toolkit for planetary missions and exploration and will be used by the MSL rover Curiosity to conduct chemical analyses of the Martian surface (Dyar et al., 2012). The spectra obtained in this study are not directly comparable to those spectra collected *in situ* with ChemCam as it is well known and understood that the Martian atmosphere actively interacts with the plasma generation and generates different spectra there than under Earth atmospheric conditions (Cousin et al., 2011). These differences are well understood and include a higher signal to noise ratio under Martian conditions as well as narrower peak widths in the generated spectra and no self-absorption, all of which have been experimentally scrutinized and understood prior to the launch of MSL. For this reason, our spectra are not directly or quantitatively comparable to any spectra obtained from the ChemCam instrument, however qualitative comparisons may be possible.

LIBS spectra of synthetic and biogenic jarosite samples are shown in Figure.3.6. as well as the spectra of 'dry' and 'wet' biogenic samples used to investigate the effects of sample preparation conditions on the generated LIBS spectra. A qualitative approach was undertaken to compare the four different samples relative to one another. Organics, (i.e., carbon) could, and may have been detected in the spectra at 426, 589, and 656 nm. However, it is difficult to tell whether these contributions are generated by C in the samples or by the coupling carbon from the breakdown of atmospheric CO_2, particularly without aid of elemental calibration standards. Additionally, these emission lines correspond to the brightest emission lines of chlorine (426 nm), sodium (589 nm) and hydrogen (656 nm) respectively. It is also very difficult to distinguish between contributions from carbon in the target sample and emission lines from carbon dioxide in

the atmosphere; any C emission lines detected in spectra collected under Earth's atmospheric conditions are questionable. This is an ongoing topic of study and concern in the LIBS community as there are serious implications for Martian surficial compositional mapping as the LIBS instrument will not be able to be used to detect organics unambiguously.

This problem, unlike the other concerns with LIBS analyses in a Martian atmosphere (e.g., higher signal to noise ratio and better resolved peaks) will become more amplified on the Martian surface as the CO_2 concentration is higher there, and it will be nearly impossible to differentiate any organic contributions from Martian surface organics from the carbon dioxide in the atmosphere with any certainty. This is a large limit in terms of exobiological investigations searching for organics on the Martian surface. Furthermore, LIBS spectral analyses limitations make it highly improbable that this tool will contribute to the identification of organic markers, molecules and signatures. Although the Martian atmosphere will provide higher resolution data, interactions with the Martian atmosphere, specifically interactions with carbon dioxide molecules, will make analysis and detection of C lines very difficult.

Sulfur is not detected in any of the LIBS spectra in this study even though it is one of the main elements in jarosite. Sulfur lines were not expected since data collected under Earth atmospheric conditions generates plasma which interacts with O_2, generating a lower signal to noise ratio for S brightness lines in the 400 to 600nm spectral region; several Fe brightness lines occur in the same region that are noticeably stronger and overprint the S lines (Dudragne et al., 1998). Thus quantification of S lines are subject to large uncertainties and thought by some (Sobron et al., 2012) to not be possible in Earth's

atmosphere; however, plasma S will interact to a lesser extent with the less readily available O_2 generated by the CO_2 rich Martian atmosphere, so both S and Fe brightness lines are expected when sampling material on the Martian surface (Knight et al., 2000). The first LIBS instrument for extraterrestrial applications is part of the ChemCham instrument of the NASA MSL rover Curiosity. Any data collected pertaining to elemental C identification (i.e. organics) with the LIBS instrument on ChemCam will be questionable, especially in mineral assemblages not known to have carbon (e.g., not at carbonate). Additional lines of evidence will be required to putatively suggest organic molecules on Mars.

3.4.3. Mössbauer spectroscopy- potential biosignature or false biosignature

Most minerals exhibit a range of Mössbauer parameters as a function of temperature as well as cation substitution. For jarosite sub-group minerals, ΔE_Q values increase in order of K>Na>H_3O (Hurynkiewicz 1965; Klingelhofer et al., 2004). Silicates are known to have narrower ranges and more suited to this technique than oxides and sulfides which tend to have broader parameter ranges. In this study, both samples yielded identical isomer shift values while they diverged in quadrupole splitting values with the synthetic jarosite value (ΔE_Q = 1.23 mm/s) correlating well to previous values obtained from natural and synthetic jarosite studies (Hyde et al., 2011). The biogenic value (ΔE_Q =0.65 mm/s) is significantly lower than expected values for jarosite materials, and it may possibly represent a value that can be used to differentiate the biogenicity of these two jarosite samples.

The Mössbauer parameters of the spectrum generated by the jarosite minerals utilized in this study are shockingly similar to the values obtained *in situ* with the MER Opportunity. The trend of the biologically mediated material having a larger ΔE_Q value when compared to an identical unidentified ferric hydroxide chemical precipitate was also observed by Lees et al. (1969), who used similar bacteria as this study. Mössbauer spectroscopy is not ideally suited for mineral identification and it is typically not used for this purpose (e.g. rock forming minerals such as amphibole, mica and pyroxene have nearly indistinguishable parameters; Dyar et al., 2006), although it has been maneuvered into such service in extraterrestrial applications.

Klingelhofer et al. (2004) discovered an anhydrous sulfate with parameters most consistent with a potassium-sodium jarosite with some aluminum substitution in the B site (δ = 0.39 mm/s, ΔE_Q = 1.22 mm/s) at the Eagle Crater outcrop in Meridiani Planum. Additionally, they characterized a secondary, non-mineral specific, octahedrally coordinated, ferric doublet with an identical isomer shift but with a lower quadrupole splitting value (δ = 0.39 mm/s, ΔE_Q = 0.64 mm/s), attributed to akaganerite, ferryhydrite, supermagnetic hematite and goethite, lepidocrocite, some phyllosilicates, and schwertmannite (Bishop and Murad, 1996; Morris et al., 1989; 2000; Murad and Wanger, 1994; Sherman and Vero, 1988). The isomer shift values of the biogenic jarosite are identical as hematite and goethite yet diverge significantly in quadrupole splitting values (ΔE_Q = -0.20 and -0.26, respectively; Dyar et al., 2006). Schwertmannite, on the other hand, is a perfect match for both values (Bigham et al. 1990; 1994; 1996; Bishop and Murad, 1996; Dyar et al., 2006). Abiogenic and biogenic schwertmannite minerals demonstrate radially oriented filamentous crystals, termed “hedge-hog” morphology

(Schwertmann and Cornell, 1991), which is very similar to the crystal morphology observed in the biogenic jarosite material. Thus, the differences in the ΔE_Q values observed in this study may be a reflection of the distinct morphologies exhibited by the jarosite samples and particularly a reflection of the hedge-hog like aggregate crystal morphologies (Bigham et al., 1990, 1994, 1996; Schwertmann and Cornell, 1991) observed in the biogenic material.

Although the Mössbauer spectra appear to be able to discern the biogenicity of the jarosites studied in this study, this technique and this data are not able to unambiguously differentiate the biogenic jarosite samples from any other mineral which have similar morphologies (e.g., abiotic long term chemical oxidation product of this study, biogenic jarosite, abiotic and biotic schwertmannite).

3.5. Conclusions

No biological signatures were observed with any of the techniques used in this study for either of the jarosites characterized. No organics were observed in Raman or reflectance spectra. Mössbauer analyses were able to differentiate the biogenic material from the synthetic sample; however, this signature is not unambiguous and represents a false biosignature as abiotic and biotic schwertmannite generate similar Mössbauer parameters. LIBS was unable to conclusively detect any organics, and will not conclusively detect organics on the Martian surface. It is important that we understand the limits of resolution of the techniques employed to geochemically and mineralogically explore other planetary bodies and that they are used appropriately to obtain meaningful data during astrobiological investigations on Mars. This study highlights how difficult it

is to search organics and/or biosignatures in geological materials by demonstrating that even when samples are known to have life (and organics) in them; it is not always possible to detect it using spectral and mass spectrometry techniques. This represents a critical limitation of the search for life on other planetary bodies using remote sensing and *in situ* instruments targeting organic materials.

References:

Adler, H.H., Kerr, P.F., 1965. Variations in infrared spectra, molecular symmetry and site symmetry of sulfate minerals. Am. Mineral. 50, 132–147.

Aguilera, A., Zettler, E., Gomez, F., Amaral-Zettler, L., Rodriguez, N., Amils, R., 2007. Distribution and seasonal variability in the benthic eukaryotic community of Rio Tinto (SW, Spain), an acidic, high metal extreme environment. Syst. Appl. Microbiol. 30, 531–546.

Aguilera, A., Manrubia, S.C., Gomez, F., Rodriguez, N., Amils, R., 2006. Eukaryotic community distribution and its relationship to water physicochemical parameters in an extreme acidic environment, Rio Tinto (Southwestern Spain). Appl. Environ. Microbiol. 72, 532 –5330.

Angiboust, S., Fayek, M., Power, I.M., Camacho, A., Calas, G., Southam, G., 2012. Structural and biological control of the Cenozoic epithermal uranium concentrations from the Sierra Peña Blanca, Mexico. Mineralium Deposita. DOI 10.1007/s00126-012-0408-5.

Balsiger, H., Altwegg, K., Bochsler, P., Eberhardt, P., Fisher, J, Graf, S., Jackel, A., Kopp, E., Langer, U., Mildner, M., Muller, J., Riesen, T., Rubin, M., Scherer, S., Wurz, P., Wuthrich, S., Arijs, E., Delanoye, S., De Keyser, J., Neefs, E., Nevejans, D., Reme, H., Aoustine, C., Mazelle, C., Medale, J.L., Sauvaud, A., Berthelier, J.J., Bertaux, J.L., Duvet, L., Illiano, J.M., Fuselier, S.A., Ghielmetti, A.G., Magoncelli, T., Shelley, E.G., Korth, A., Heerlein, K., Lauche, H., Livi, S., Loose, A., Mall, U., Wilken, B., Gliem, F., Fiethe, B., Gombosi, T.I., Block, B., Carignan, G.R., Fisk, L.A., Waite, J.H., Young, D.T., Wollnik, H., 2007. Rosins – Rosetta Orbiter Spectrometer for Ion Neutral Analysis. Space Sci. Rev. 128, 745–801.

Balsiger, H., Atwegg, K., Arijs, E., Bertaux, J.L., Berthelier, J.J., Boshsler, P., Carignan, G.R., Eberhardt, P., Fisk, L.A., Fuselier, S.A., Ghielmetti, A.G., Gliem, F., Gombosi, T.I., Kopp, E., Korth, a., Livi, S., Mazelle, C., Reme, H., Sauvaud, J.A., Shelley, EG., Waite, J.H., Wilken, B., Woch, J., Wolnki, H., Wurz, P., Young, D.T., 1998. Rosetta orbiter spectrometer for ion and neutral analysis – ROSINIA. Adv. Space Rev. 21, 1527–1535.

Balsiger, H., Altwegg, K., Benson, J., Buhler, F., Fisher, J., Geiss, J., Goldstein, B.E., Goldstein, R., Hemmerich, P., Kulzer, G., Lazarus, A.J., Meier, A., Neugebauer, M., Rettenmund, U., Rosenbauer, H., Sager, K., Sanders, T., Schwenn, R., Shelley, E.G., Simpson, D., Young, D.T., 1987. The ion mass spectrometer on Giotto. J Phys. E Sci Instrum. 20, 759–767.

Barghoorn, E.S., Tyler, S.A., 1965. Microorganisms from the Gunflint Chert. Science 147, 563–577.

Baron, D., Palmer, C.D., 1996. Solubility of jarosite at 4 - 35°C. Geochim Cosmochim Ac, 60, 185 – 195.

Basciano, L.C., Peterson, R.C., 2008. Crystal chemistry of the natrojarosite-jarosite and natrojarosite-hydronium jarosite solid-solution series: A synthetic study with full Fe site occupancy. Am. Mineral. 93, 853 – 862.

Basciano, L.C., Peterson, R.C., 2007. The crystal structure of ammoniojarosite, $(NH_4)Fe_3(SO_4)_2(OH)_6$ and the crystal chemistry of the ammoniojarosite-hydronium jarosite solid-solution series. Mineral. Mag. 71, 427 – 441.

Bibring, J.P., Langevin, Y., Mustard, J.F., Poulet, F., Arvidson, R., Gendrin, A., Gondet, B., Mangold, N., Pinet, P., Forget, F., the OMEGA team, 2006. Global mineralogical and aqueous Mars history derived from OMEGA/Mars Express Data. Science 312, 400– 404.

Bibring, J.P., Langevin, Y., Gendrin, a., gondet, b., Poulet, F., Berthe, M., Soufflot, A., Arvidson, R., Mangold, N., Mustard, J., Drossart, P., 2005. Mars surface diversity as revealed by the OMEGA/Mars Express observations. Science 307, 1576–1581.

Bigham, J.M., Schwertmann, U., Carlson, L., Murad, E., 1990. A poorly crystallized oxyhydroxysulfate of iron formed by bacterial oxidation of Fe(II) in acid mine waters. Geochim. Cosmochim. Act. 54, 2743–2758.

Bigham, J.M., Carlson, L., Murad, E., 1994. Schwertmannite, a new iron oxyhydroxysulfate from Pyhasalmi, Finland, and other localities. Miner. Mag. 58, 641–648.

Bigham, J.M., Schwertmann, U., Traina, S.J., Winland, R.L., Wolf, M., 1996. Schwertmannite and the chemical modeling of iron in acid sulfate waters. Geochim. Cosmochim. Act. 60, 2111–2121.

Bishop, J.L., Murad, E., 2005. The visible and infrared spectral properties of jarosite and alunite. Am. Mineral. 90, 1100–1107.

Bishop, J.L., Murad, E., 1996. Schwertmannite on Mars? Spectroscopic analyses of schwertmannite, its relationship to other ferric minerals, and its possible presence in the surface material on Mars. In *Mineral Spectroscopy: A Tribute to Roger G. Burns*. Eds. Dyar, M.D., McCammon, C., Schaefer, M.W.. Huston: *The Geochemical Society*, Special Publication No. 5, pp. 337–358.

Booth, G.H., Miller, J.D.A., Paisley, H.M., Saleh, A.M., 1966. Infrared spectra of some sulfate-reducing bacteria. J. Gen. Microbiol. 44, 83–87.

Bruker AXS, 2005. DIFFRACplus Evaluation Package release 2005. Bruker AXS, Karlsruhe, Germany.

Burns, R.G., 1987. Ferric sulfates on Mars. J. Geophys. Res. 92, E570-E574.

Burns, R.G., 1988. Gossans on Mars. Proceedings 18th Lunar and Planet. Sci. Conf., LPI, Huston, 713–721.

Burns, R.G., Fisher, D.S., 1990. Iron-sulfur mineralogy of Mars: Magmatic evolution and chemical weathering products. J Geophys. Res. 95, 14415–14421.

Chio, C.H., Sharma, S.K., Ming, L.C., Muenow, D.W., 2010. Raman spectroscopic investigation on jarosite-yavapaiite stability. Spectrochim. Acta A 75, 162–171.

Christensen, P.R., Ruff, S.W., Fergason, R.L., Knudson, A.T., Arvidson, R.E., Bandfield, J.L., Blaney, D.L., Budney, C., Calvin, W.M., Glotch, T.D., Golombek, M.P., Graff, T.G., Hamilton, V.E., Hayes, A., Johnson, J.R., McSween, H.Y., Mehall, G.L., Mehall, G.L., Moersch, J.E., Morris, R.V., Rogers, A.D., Smith, M.D., Squyres, S.W., Wolff, M.J., Wyatt, M.B., 2004a. Initial results from the Mini-TES experiment in Gusev crater from the Spirit Rover, Science 305, 837–842.

Christensen, P.R., Wyatt, M.B., Glotch, T.D., Rogers, A.D., Anwar, S., Arvidson, R.E., BAndfield, J.L., Blaney, D.L., Budney, C., Calvin, W.M., Fallacaro, A., Fergason, R.L., Gorelick, N., Graff, T.G., Hamilton, V.E., Hayes, A.G., Johnson, J.R., Knudson, A.T., McSween, H.Y., Mehall, G.L., Mehall, L.K., Moersch, J.E., Morris, R.V., Smith, M.D., Squyres, S.W., Ruff, S.W., Wolf, M.J., 2004b. Mineralogy at Meridiani Planum from the Mini-TES experiment on the Opportunity rover. Science 306, 1733–1739.

Christensen, P.R., Bandfield, J.L., Hamilton, V.E., Ruff, S.W., Kieffer, H.H., Titus, T.N., Malin, M.C., Morris, R.V., Lane, M.D., Clark, R.L., Jakosky, B.M., Mellon, M.T., Pearl, J.C., Conrath, B.J., Smith, M.D., Clancy, R.T., Kuzmin, R.O., Roush, T., Mehall, G.L., Gorelick, N., Bender, K., Murray, K., Dason, S., Greene, E., Silverman, S., Greenfield, M., 2001. Mars Global Surveyor Thermal Emission Spectrometer experiment: Investigation description and surface science results. J. Geophys. Res. 106, E10, 23823–23871.

Christensen, P.R., Bandfield, J.L., Smith, M.D., Hamilton, V.E., Clark, R.N., 2000. Identification of a basaltic component on the Martian surface from Thermal Emission Spectrometer data. J. Geophys. Res. 105, 9609–9622.

Clark, R.N., Swayze, G.A., Livo, K.E., Kokalyy, R.F., Sutley, S.J., Dalton, J.B., McDougal, R.R., Gent, C.A., 2003. Imaging spectroscopy: Earth and planetary remote sensing with the USGS Tetracorder and experst systems. J. Geophys. Res. 108, 5131, doi:10.1029/2002JE001847.

Clark, R.N., King, T.V.V., Klejwa, M., Swayze, G.A., Vergo, N., 1990. High spectral resolution reflectance spectroscopy of minerals. J. Geophys. Res. 95, 12653–12680.

Cloutis, E. A., Craig, M.A., Kruzelecky, R.V., Jamroz, W.R., Scott, A., Hawthorne, F.C., Mertzman, S.A., 2008. Spectral reflectance properties of minerals exposed to simulated Mars surface conditions. Icarus 195, 140–168.

Cloutis, E.A., Hawthorne, F.C., Mertzman, S.A., Krenn, K., Craig, M.A., Marcion, D., Methot, M., Strong, J., Mustard, J.F., Blaney, D.L., Bell III, J.F., Vilas, F., 2006. Detection and discrimination of sulfate minerals using reflectance spectroscopy. Icarus 184, 121–157.

Cousin, A., Forni, O., Maurice, S., Gasnault, O., Fabre, C., Sautter, V., Wiens, R.C., Mazoyer, J., 2011. Laser induced breakdown spectroscopy library for the Martian environment. Spectrochim. Acta B 66, 805–814.

Crowley, J.K., Williams, D.E., Hammarstrom, J.M., Piatak, N., Chou, I.M., Mars, J.C., 2003. Spectral reflectance properties (0.4–2.5μm) of secondary Fe-oxide, Fe-hydroxide, and Fe-sulfate-hydrate minerals associated with sulphide-bearing mine wastes. Geochem – Explor Env A 3, 219–228.

Courrges-Lacoste, G.B., Ahlers, B., Perez, F.R., 2007. Combined Raman spectrometer/laser-induced breakdown spectrometer for the next ESA mission to Mars. Spectrochim. Acta A 68, 1023–1028.

Drouet C., Navrotsky, A., 2003. Synthesis, characterization, and thermochemistry of K-Na-H_3O jarosites. Geochim Cosmochim Ac. 67, 2063–2076.

Dudragne, L., Adam, P., Amouroux, J., 1998 Time-resolved laser-induced breakdown spectroscopy : application for qualitative and quantitiative detection of fluorine, chloring, sulfur, and carbon in air. Appl. Spectrosc. 52, 1321–1327.

Dutrizac, J.E., Kaiman, S., 1976. Synthesis and properties of jarosite-type compounds. Can. Mineral. 14, 151-158.

Dutrizac, J.E., Jambor, J.L., O'Reilly, J.B., 1983. Man's first use of jarosite: The pre-Roman mining-metallurgical operations at Rio Tinto, Spain. CIM Bull. 76, 78–82.

Dyar, M.D., 1984. Precision and interlaboratory reproducibility of measurements of the Mössbauer effect in minerals. Amer. Mineral. 69, 1127-1144.

Dyar, M.D., Carmosino, M.L., Tucker, J.M., Brown, E.A., Clegg, S.M., Wiens, R.C., Barefield, J.E., Delaney, J.S., Ashley, G.M., Driese, S.G., 2012a. Remote laser-induced breakdown spectroscopy analysis of East African Rift sedimentary samples under Mars conditions. Chem. Geol. 295, 135–151.

Dyar, M.D., Carmosino, M.L., Breves, E.A., Ozanne, M.V., Clegg, S.M., Wiens, R.C., 2012b. Comparison of partial least squares and lasso regression techniques as applied to laser-induced breakdown spectroscopy of geological samples. Spectrochim. Acta B 70, 51–67.

Dyar, M.D., Agresti, D.G., Schaefer, M., Grant, C.A., Sklute, C., 2006. Mössbauer spectroscopy of Earth and Planetary materials. Annu. Rev. Earth Planet. Sci. 34, 83–125.

Dyar, M.D., Schaefer, M.W., Sklute, E.C., and Bishop, J.L., 2008. Mössbauer spectroscopy of phyllosilicates: Effects of fitting models on recoil-free fractions and redox ratios. Clay Mins. 43, 3-33.

Farmer, J.D., Des Marais, D.J., 1999. Exploring for a record of ancient Martian life. J.Geophys. Res. 104, 26977–26995.

Fernández-Remolar, D.C., Rodriguez, N., Gómez, F., Amils, R., 2003. Geological record of an acidic environment driven by iron hydrochemistry: the Tinto River system. J. Geophys. Res. 108, E75080, doi:10.1029/2002JE001918.

Ferrand, W.H., Glotch, T.D., Rice, J.W., Hurowitz, J.A., Swayze, G.A., 2009. Discovery of jarosite within the Mawrth Vallis region of Mars: Implications for the geologic history of the region. Icarus 204, 478–488.

Frost, R.L., Willis, R.A., Weier, M.L., Martens, W., 2005. Comparison of the Raman spectra of natural and synthetic K- and Na-jarosites at 298 and 77 K. J Raman Spectrosc. 36, 435–444.

Foster, I.S., King, P.L., Hyde, B.C., Southam, G., 2010. Characterization of halophiles in natural $MgSO_4$ salts and laboratory enrichment samples: Astrobiological implications for Mars. Planet. Space Sci. 58, 599–615.

Gendrin, A., Mangold, N., Bibring, J.P., Langevin, Y., Gondet, B., Poulet, F., Bonello, G., Quantin, C., Mustard, J., Arvidson, R., LeMouelic, S., 2005. Sulfates in Martian layered terrains: the OMEGA/Mars Express View. Science 1587–1591.

Gleeson, D.F., Pappalardo, R.T., Grasby, S.E., Anderson, M.S., Beauchamp, B., Castano, R., Chwin, S.A., Doggett, T., Mandrake, L., Wagstaff, K.L., 2010. Characterization of a sulfur-rich Arctic spring site and field analog to Europa using hyperspectral data. Remote Sensing of Envir. 114, 1297–1311.

Helm, D., Labischinski, H., Schallehn, G., Naumann, D., 1991. Classification and identification of bacteria by Fourier-transform infrared spectroscopy. J. Gen. Microbiol. 137, 69–79.

Hunt, G.R., Ashley, R.P., 1979. Spectra of altered rocks in the visible and near infrared. Econ. Geol. 74, 1613–1629.

Hunt, G.R., Salisbury, J.W., Lenhoff, C.J., 1971. Visible and near-infrared spectra of minerals and rocks: IV Sulphides and sulphates. Modern Geology 3, 1–14.

Hrynkiewicz, A.Z., Kubiz, J., Kulgawczuk, D.S., 1965. Quadrupole splitting of the 14.4 keV gamma line of ^{57}Fe in iron sulfates of the jarosite group. J. Inorg. Nucl. Chem. 27, 2513–2517.

Hyde, B.C., King, P.L., Dyar, M.D., Spilde, M.N., Ali, A.M.S., 2011. Methods to analyze metastable and microparticulate hydrated and hydrous iron sulfate minerals. Am. Mineral. 96, 1856–1869.

Izawa, M.R.M., Flemming, R.L., King, P.L., Peterson, R.C., McCausland, P.J.A., 2010. Mineralogical and spectroscopic investigation of the Tagish Lake carbonaceous chondrite by X-ray diffraction and infrared reflectance spectroscopy. Meteor. Plant. Sci. 45, 675–698.

Knight, A.K., Sherbarth, N.L., Cremers, D.A., Ferris, M.J., 2000. Characterization of laser-induced breakdown spectroscopy (LIBS) for application to space exploration. Appl. Spectrosc. 54, 331–340.

King, T.V.V., Clark, R.N., Ager, C., Swayze, G.A., 1995. Remote minerals mapping using AVIRIS data at Summitville, Colorado and the adjacent San Juan Mountains. In Posey, H.H., Pendelton, J.A., Van Zyl, D., Eds., Proceedings:

Summitville Forum ’95, Colorado Geological Survey Special Publication 38, pp. 59–63.

Klingelhofer, G., Morris, R.V., Bernhardt, B., Schroder, C., Rodionov, D., de Souza, P.A.J., Yen, A.S., Gellert, R., Evlanov, E.N., Zubkov, B., Foh, J., Bonnes, U., Kankeleit, E., Gulich, P., Ming, D.W., Renz, F., Wdowiak, T.J., Squyres, S.W., Arvidson, R.E., 2004. Jarosite and hematite at Meridiani Planum from Opportunity’s Mössbauer spectrometer. Science 306, 1740–1745.

Kubisz, J., 1971. Studies on synthetic alkali-hydronium jarosites. II. Thermal investigations. Mineral. Polonica 2, 51–59.

Kubisz, J., 1972. Studies on synthetic alkali-hydronium jarosites. III. Infrared absorption study. Mineral. Polonica. 3, 23–35.

Lanza, N.L., Wiens, R.C., Clegg, S.M., Ollila, A.M., Humphries, S.D., Newsom, H.E., Barefield, J.E., ChemCam Team, 2010. Calibrating the ChemCam laser-induced breakdown spectroscopy instrument for carbonate minerals on Mars. App. Optics 49, C211–C217.

Lees, H., Kwok, S.C., Suzuki, I., 1969. The thermodynamics of iron oxidation by the ferrobacilli. Can. J. Microbiol. 15, 43–46.

Léveillé, R., 2009. Validation of astrobiology technologies and instrument operations in terrestrial analogue environments. C. R. Palevol 8, 637–648.

Lucey, P.G., Taylor, G.J., Malaret, E., 1995. Abundance and distribution of iron on the moon. Science 268, 1150–1153.

Majzlan, J., Alpers, C.N., Koch, C.B., McCleskey, R.B., Myneni, S.C.B., Neil, J.M., 2011. Vibrational, X-ray absorption, and Mössbauer spectra of sulfate minerals form the weathered massive sulfide deposit at Iron Mountain, California. Chem. Geol. 284, 296–305.

Michalski, J.R., Niles, P.B., 2011. Formation of jarosite in the Mawrth Vallis region of Mars by weathering within paleo-ice deposits. Proceedings 42nd Lunar and Planetary Science Conference, abstract # 1926, LPI, Huston,

Murchie, S.L., Mustard, J.F., Ehlmann, B.L., Milliken, R.E., Bishop, J.L., McKeown, N.K., Dobrea, E.Z.N., Seelos, P., Buczkowski, D.L., Wiserman, S.M., Arvidson, R.E., Wray, J.J., Swayze, G., Clark, R.N., Des Marais, D.J., McEwen, A.S., Bibring, J.P., 2009. A synthesis of Martian aqueous mineralogy after 1 Mars year of observations from the Mars Reconnaissance Orbiter. J. Geophys. Res. 114, E00D06, doi:10.1029/2009JE003342.

Murchie, S., Arvidson, R., Bedini, P., Beisser, K., Bibring, J.P., Bishop, J., Boldt, J., Cavender, P., Choo, T., Clancy, R.T., Darlington, E.H., Des Marais, D., Espiritu, R., Fort, D., Green, R., Guinness, E., Hayes, J., Hash, C., Heffernan, K., Hemmler, J., Heyler, G., Humm, D., Hutcheson, J., Izenberg, N., Lee, R., Lees, J., Lohr, D., Malaret, E., Martin, T., McGovern, J.A., McGuire, P., Morris, R., Mustard, J., Pelkey, S., Rhodes, E., Robinson, M., Toush, T., Schaefer, E.,

Seagrve, G., Seelos, F., Silverglate, P., Slaveny, S., Smith, M, Shyong, W.J., Strohbehn, Taylor, H., Thompson, P., Tossman, B., Wirzburger, M., Wolff, M., 2007. Compact Reconnaissance Imaging Spectrometer for Mars (CRISM) on Mars Reconnaissance Orbiter (MRO). J. Geophys. Res. 112, E05S03, doi:10.1029/2006JE002682.

Murchie, S., Mustard, J., Bishop, J.L., Head, J., Pieters, C., Erard, S., 1993. Spatial variations in the spectral properties of bright regions on Mars. Icarus 105, 454–468.

Ollila, A.M., Lasue, J., Newsom, H.E., Multari, R.A., Wiens, R.C., Clegg, S.M., 2012. Comparison of two partial least squares-discriminant analysis algorithms for identifying geological samples with the ChemCam laser-induce breakdown spectroscopy instrument. Appl. Optics 51, B130–B142.

Powers, D.A., Rossman, G.R., Shugar, H.J., Gray, H.B., 1975. Magnetic behavior and infrared spectra of jarosite, basic iron sulfate and their chromate analogs. J. Sol. Stat. Chem. 13, 1–13.

Preston, L.J., Shuster, J., Fernández-Remolar, D., Banerjee, N.R., Osinski, G.R., Southam, G., 2011. The preservation and degradation of filamentous bacteria and biomolecules within iron oxide deposits at Rio Tinto, Spain. Geobiology 9, 233–249.

Ross, S.D., 1974. Sulphates and other oxy-anions of group VI, In: The infrared spectra of minerals. V.C. Farmern, London, Mineralogical Society, pp. 423–444.

Sasaki, K., Tanakie, O., Konno, H. 1998. Distinction of jarosite-group compounds by Raman spectroscopy. Can. Mineral. 36, 1225-1235.

Serna, C.J., Parada Cortina, C., Garcia Ramos, J.V., 1986. Infrared and Raman study of alunite-jarosite compounds. Spectrochim. Acta 42A, 729 – 734.

Sprague, A.L., Kozlowski, R.W.H., Witteborn, F.C., Cruikshank, D.P., Wooden,D.H., 1994. Mercury: Evidence for anorthosite and basalt from mid-infrared 7.3-13.5 um spectroscopy. Icarus 109, 156–167.

Sobron, P., Wang, A., Sobron, F., 2012. Extraction of compositional and hydration information of sulfates from laser-induced plasma spectra recorded under Mars atmospheric conditions – Implications for ChemCam investigations on Curiosity rover. Spectrochim. Acta B 68, 1–16.

Squyres, S.W., Grotzinger, J.P., Arvidson, R.E., Bell III, J.F., Calvin, W., Christensen, P.R., Clark, B.C., Crisp, J.A., Farrand, W.H., Herkenhoff, K.E., Johnson, J.R., Klingelhofer, G., Knoll, A.H., McLennan, S.M., McSween, H.Y., Morris, R.V., Rice, J.W., Rieder, R., Soderblom, L.A., 2004. In situ evidence for an ancient aqueous environment at Meridiani Planum, Mars. Science 306, 1709–1714.

Swayze, G.A., Smith, K.S., Clark, R.N., Sutley, S.J., Pearson, R.M., Vance, J.S., Hageman, P.L., Briggs, P.H., Meier, A.L., Singleton, M.J., Roth, S., 2000. Using

imaging spectroscopy to map acidic mine waste. Environ. Sci. Technol. 34, 47–54.

Taylor, F.W., Beer, R., Chahine, M.T., Diner, D.J., Elson, L.s., Haskins, R.D., McCleese, D.J., Martonchik, J.V., Reichley, P.E., Bradley, S.P., Delderfield, J., Schofield, J.T., Farmer, C.B., Froidevaux, L., Leung, J., Coffey, M.T., Gille, J.C., 1980. Structure and meterology of the middle atmosphere of Venus: Infrared remote sensing from the Pioneer orbiter. J. Geophys. Res. 85, A13, 7963–8006.

Theil, V., Sjovall, P., 2011. Using Time-of-Flight secondary ion mass spectrometry to study biomarkers. Annu. Rev. Earth Planet. Sci. 39, 125–156.

Vilas, F., 1988. Surface composition of Mercury from reflectance spectrophotometry, In: Mercury, Vilas, F., Chapman, C.R., Matthews, M.S., eds., University of Arizona Press, Tucson, pp. 59-76.

Warell, J., Sprague, A.L., Emery, J.P., Kozlowski, R.W.H., Long, A., 2006. The 0.7–5.3 μm IR spectra of Mercury and the Moon: Evidence for high-Ca clinopyroxene on Mercury. Icarus 180, 281–291.

Wivel, C. and Mørup, S., 1981. Improved computational procedure for evaluation of overlapping hyperfine parameter distributions in Mössbauer spectra. J. Phys. E. Sci. Instrum. 14, 605–610.

Chapter 4.

Conclusion

Astrobiology investigations aim to evaluate the capacity, capability, and ability of life to occur, extant or extinct, on other planetary realms and within extraterrestrial materials. A small number of these studies generate and receive a great deal of attention from both the scientific community and the general public (e.g., Fisk et al., 2006; McKay et al., 1996; Wolfe-Simon et al., 2010). These exobiological investigations particularly highlight the importance of acquiring a detailed understanding of life's interactions within the context of terrestrial environments before we can confidently recognize any clues, indicators or signatures of biogenic interactions in geological material on other planetary bodies (e.g., Mars, Enceladus, Europa, and Titan) or in extraterrestrial materials (e.g. Martian meteorites ALH84001 and Nakhla). Namely, our capacity to detect and assign biogenicity in any extraterrestrial material, regardless if we attempt to do so based on data returned by remote sensing, *in situ*, or sample return missions, is only as good as our ability to detect and discern biogenicity in terrestrial materials and is a reflection of our understanding of microbe mineral interactions in the context of the terrestrial biosphere (Farmer and Des Marais, 1999; Summons et al., 2011).

In this study, biosignatures in jarosites were investigated in the context of our ability to evaluate the biogenicity of a known geological material using analytical techniques and instrumentation currently used to characterize and examine geological materials *in situ* on the Martian surface. This study plainly demonstrates that jarosite cannot be used as a mineralogical marker for biological activity in acidic, oxidizing,

aqueous environments and that the jarosite minerals formed within these type of environments do not retain any biosignatures, biomolecules, or organic markers which can be detected using spectral or mass spectrometric techniques above the baseline of the mineralogical material itself.

The recognition of biogenicity within jarosites of known origin using spectroscopic instrumentation (i.e., Raman, IR, VNIR, Mössbauer, and LIBS) and mass spectrometry (ToF SIMS) generated slight differences between the respective spectra of the biogenic and synthetic jarosite materials. Even though the biogenically derived material contained cells, EPS, and evidence of other organic materials in SEM images, not a single technique used in this study was able to detect any sign of organics. Furthermore, it was impossible to differentiate which material was biogenic by simply looking at the data collected using these analyses, even collectively (representing a multi-instrument approach).

Electron microscopy characterizations were paramount in discerning the only observable and quantifiable difference between the jarosite specimens, their crystal morphologies on the microscopic scale. It should be noted, however, that without prior knowledge that this material was jarosite, the observed morphological differences would not have been indicative of a biogenic origin, as biogenic and abiotic schwertmannite exhibit identical mineral morphologies as that of the biological precipitates in this study (Bingham et al., 1996). Furthermore, even if the mineral composition of the sample was established as jarosite, morphology would still not be considered a biological signature as it is not an unambiguous indication of biological process, since the identical system, less biological cells (i.e., abiogenic control system), yielded similar crystal morphologies. This study demonstrates that extreme caution should be used when using mineral

morphologies to ascertain the biogenicity of a geological material. Furthermore, the structural characterization of these jarosites has demonstrated that the sheer presence of this mineral in an environment, even if it is associated with microbial populations, cannot be taken as unequivocal evidence of biomineralization (i.e., jarosite is not a mineralogical biomarker).

This study represents the first time, to our knowledge, a comparison has been attempted to evaluate biosignatures of a biologically mediated jarosite material while examining the identical abiotic 'control' process associated with the thermodynamic reactions being catalyzed by the biota and subsequent documentation of similarities or difference. Albeit the 'control system' took significantly longer periods of time to produce precipitates, future studies should aim to prioritize the evaluation of such pairings (i.e., biomineralized products in comparison to directly analogous 'control system' samples (i.e., no life)), as they represent a controlled experimental system which truly assesses biological influences in the system as well as the possibility of ascertaining unambiguous biosignatures. In all cases of mineralization, thermodynamic principles guiding the process are identical irrespective of the system (i.e., abiotic or biogenic) which induces the mineralization of precipitates (Konhauser, 2007). Here on Earth, it is often quite difficult to delineate microbial versus abiological contributions to mineral precipitation, particularly in natural environments, as the simple association of a microbe to a mineralizing environment does not mean that it was involved in the development (e.g., directly or indirectly).

Past conditions on Mars may have allowed life to develop, particularly an early liquid-water rich era, however in order to properly characterize the habitability of geological materials and environments on the Martian planet, investigations need to be conducted at the magnitude corresponding to the life forms we are searching for in order to anticipate success. Namely, the search for microscopic life will continually generate equivocal findings and outcomes [i.e. Viking lander biological experiments (Navarro-Gonzalez et al., 2006)] when utilizing the macroscopically resolved techniques which are commonly included on mission payloads. Exobiological investigations substantiating and establishing proof of life on another planetary body will ultimately require sample return.

Apart from the biological experiments conducted by the Viking lander, the investigations pertaining to exobiological interests which have led to the most persuasive and compelling evidence for the case of life on Mars, thus far, have all been the result of intensive analysis of Martian meteorites, particularly ALH84001 (Thomas-Keprta et al., 2009) and Nakhla (Gibson et al., 2001), which represent a type of sample return samples. Furthermore, the pivotal findings made pertaining to the justification of biological influence and habitability on Mars [i.e., carbonate and magnetite assemblages in ALH84001, and discovery of a network of intricate dendritic tubules, some with carbonaceous material (Fisk et al., 2006; McKay et al. 2006)] have all come from studying the Martian materials with sophisticated instruments, most requiring a vacuum. These significant findings would not have been detected using the instrument suites aboard landed and rover missions, as they lack the resolution and sensitivity of the techniques that were used to document these findings (i.e., nanoSIMS, SEM and TEM), and would have been overlooked during *in situ* analyses.

Presently our suite of sample return materials are limited to the 63 Martian meteorites discovered on Earth. Unlike the Moon and a few asteroids, no samples have been collected from Mars as the result of a planned return mission; however, plans are made to cache samples and develop sample return missions by both NASA and the ESA, yet this mission remain in the early planning stages. Future landed, rover, and sample return missions with exobiological interests should focus on searching for extinct life. This approach will be more successful than searching for extant life as the detection of fossils will provide a better unambiguous indication of biogenicity or biogenic processes (Farmer and Des Marais, 1999). Additionally, organic compounds such as amino acids and PAHs can be derived by abiotic processes while other organic molecules commonly associated with biogenic processes (i.e. DNA, RNA), are particularly unstable under acidic conditions (Tosca et al., 2008) and undoubtedly susceptible to rapid degradation upon exposure to current surface conditions on the planet which may inhibit our capacity to detect organics positively [e.g. perchlorates in soil (Navarro-Gonzalez et al., 2010)].

Astrobiological interest in jarosite lies with the *in situ* detection of jarosite on the Martian planetary surface at Meridiani Planum as the material is speculated to represent a mineralogical marker of biomineralization processes and is thought to possess the capacity to retain and preserve signatures of any *in situ* biological influence during its formation (Navrotsky et al, 2005). Given that NASA is planning sample return, in light of the results of this study, jarosite is not recommended as a target material for sample return as no evidence of biomineralization and/or fossilization of biological materials was observed in the jarosite mineralogical matrix. Although there are advantages to selecting

jarosites for sample return, including its capacity to be used in geochronological investigations, jarosites should be seen as paleo- environmental indicators of acid-sulfate aqueous conditions and not as substrates that will hold unambiguous biogenetic information pertaining to life on Mars.

The analysis of Mars analogue environments on Earth are of paramount importance for the interpretation of data from previous, current and future orbital and landed missions as well as when planning future robotic and human sample return missions. Future investigations pertaining to jarosite should focus on 1) characterizing the substrates ability to retain evidence of biological process and biogenic imprints; 2) finding evidence which is suggested to be in the Martian jarosite deposits in terrestrially analogous materials; and 3) using only the techniques which will be used on the mission, before targeting the mineral for a future sample return or exobiological investigations *in situ*.

Finally, it is important to note that even with the targeted selection of materials and the use of human or robotic sample return missions, there are no guarantees. Extraterrestrial life will be discovered by discerning the chemical, isotopic, mineralogical, paleontological, or textural features that are generated in its surroundings as a consequence of its existence; similar approaches are used in the search for the origin of life here on Earth. Presently, even with researchers having unlimited access to the most up to date and highest resolution analytical techniques, the search for the origin of terrestrial life remains controversial and contested here on Earth (e.g. Walsh and Westall, 2009).

References

Bigham, J.M., Schwertmann, U., Pfab, G., 1996. Influence of pH on mineral speciation in a bioreactor simulating acid mine drainage. Appl. Geochem. 11, 845–849.

Farmer, J.D., Des Marais, D.J., 1999. Exploring for a record of ancient Martian life. J. Geophys. Res. 104, 26977–26995.

Fisk., M.R., Popa, R., Mason, O.U., Storrie-Lombardi, M.C., Vicenzi, E.P., 2006. Iron-magnesium silicate bioweathering on Earth (and Mars?). Astrobiology 6, 48–68.

Gibson Jr., E.K., McKay, D.S., Thomas-Keprta, K.L., Wentworth, S.J., Westall, F., Steele, A., Romanek, C.S., Bell, M.S., Toporski, J., 2001. Life on Mars: evaluation of the evidence within Martian meteorites ALH84001, Nakhla, and Shergotty. Precambrian Research 106, 15–34.

Konhauser, K.O., 2007. Introduction to Geomicrobiology. Blackwell Publishing, Oxford, UK, p. 145.

McKay, D.S., Clemett, S.J., Thomas-Keprta, K.L., Wentworth, S.J., Gibson, Jr., E.K., Robert, F., Veechovsky, A.B., Pillinger, C.T., Rice, T., VanLeer, B., 2006. Observation and analysis of *in situ* carbonaceous matter in Nakhla: Part I. Lunar and Planetary Science XXXVII, abstract no. 2251.

McKay, D.S., Gibson Jr., E.K., Thomas-Keptra, K.L., Vali, H., Romanek, C.S., Clemett, S.J., Chillier, X.D.F., Maechling, C.R., Zare, R.N., 1996. Search for past life on Mars : possible relic biogenic activity in Martian meteorite ALH 84001. Science 273, 924–930.

Navarro-Gonzalez, R., Vargas, E., de la Rosa, J., Raga, A.c., McKay, C.P., 2010. Reanalysis of the Viking results suggests perchlorate and organics at midlatitudes on Mars. J. Geophys. Res. 115, E12010, doi: 10.1029/2010JE003599.

Navarro-Gonzalez, R., Navarro, K.F., de la Rosa, J., Iniguez, E., Molina, P., Miranda, L.D., Morales, P., Cienfuegos, E., Coll, P., Raulin, F., Amils, R., McKay, C.P., 2006. The limitations on organic detection in Mars-like soils by thermal volatilization-gas chromatography-MS and their implications for the Viking results. PNAS (Proceedings of the National Academy of Sciences of the United States of America) 103, 16089–16094.

Navrotsky, A., Forray, F.L., Drouet, C., 2005. Jarosite stability on Mars. Icarus 176, 250–253

Summons, R.E., Amend, J.P., Bish, D., Buick, R., Cody, G.D., Des Marais, D.J., Dromart, G., Eigenbrode, J.L., Knoll, A.H., Sumner, D.Y., 2011. Preservation of Martian organic and environmental records: final report of the Mars Biosignature Working Group. Astrobiology 11, 157–181.

Thomas-Keprta, K.L., Clemett, S.J., McKay, D.S., Gibson, E.K., Wentworth, S.J., 2009. Origins of magnetite nanocrystals in Martian meteorite ALH84001. Geochim. Cosmochim. Ac. 73, 6631–6677.

Tosca, N.J., Knoll, A.H., McLennan, S.M., 2008. Water activity and the challenge for life of earyl Mars. Science 320, 1204–1207.

Walsh, M.M., Westall, F., 2009. Disentangling the microbial fossil record in the Barberton Greenstone belt: a cautionary tale. *In*: Seckbach, J., Walsh, M., (eds.) From fossils to astrobiology, Springer Science, Business Media B.V., pp. 25 – 37.

Wolfe-Simon, F., Blum, J.S., Kulp, T.R., Gordon, G.W., Hoeft, S.E., Pett-Ridge, J., Stolz, J.F., Web, S.M., Weber, P.K., Davies, P.C.W., Anbar, A.D., Oremland, R.S., 2010. A bacterium that can grow by using arsenic instead of phosphorus. Science 332, 1163 – 1166.

Appendix A

Experimental synthesis of alkali jarosite minerals

Introduction

This appendix summarizes the experimental procedures used to synthesize the alkali members (ammonium-, hydronium-, potassium-, and sodium) of jarosite minerals of the alunite group. Synthetic materials were synthesized as single-phased products by duplicating or modifying published methods, primarily focusing on conventional methods of precipitating constituents from aqueous solutions under elevated temperatures and/or pressure conditions. Reagent grade chemicals were used for all syntheses. Some studies (e.g., Drutizac and Kaiman, 1976, Dutrizac and Jambor, 2000) use mineral names to describe naturally occurring jarosites and chemical names to describe their synthetic products. For consistency and simplicity, mineral names are used herein to describe the products analyzed in this study.

Several attempts were made to synthesize the various alkali end members of the jarosite group of minerals and only those outlined below were found to have produced minerals (Figure A.1). All products outlined in this appendix were systematically X-rayed using a Rigaku Rotaflex, EVA software, and ICDD Powder Diffraction Files – 2005 release, in order to verify the mineralogical compositions of the synthetic precipitates (Figure A.2). Synthesized minerals whose diffraction pattern matched that of the microbial culture precipitate utilized in this study (Chapter 2, 2.2.2 Microbial culturing (pg. 27)); Figure 2.3 (pg.39) and Figure 2.4 (pg. 41), ICDD card no. 00-036-0427, (Figure A.2)) were further characterized and imaged using a scanning electron

Figure A.1. Photograph of experimental synthetic alkali jarosites mineralogical powders. Various materials were generated in search of an analogous mineral substrate to compare to the microbial culture precipitate (more details are found in Chapter 2 of this thesis), demonstrating the variety of colours generated across the suite of alkali jarosites.

microscope (SEM) in order to determine the particle morphologies resulting from the various methodologies utilized (Figure A.3). Mineralogical powders were pressed onto carbon adhesive tabs on aluminum stubs, coated with platinum or osmium and imaged using a LEO 1530 Field Emission SEM (CarlZiess SM AG, Oberkochem, Germany) at the Nanofabrication Facility, University of Western Ontario.

Methods

Jarosite, $(K)Fe_3(SO_4)_2(OH)_6$

Jarosite was prepared following the method outlined by Dutrizac and Kaiman (1976) and labelled [K^+ - D&K1976]. Briefly, 8 g of ferric sulfate ($Fe_2(SO_4)_3 \bullet XH_2O$; Alfa Aesar, Reagent Grade) and 0.01M H_2SO_4 were added to 1 L of ultrapure water (18 MΩ cm^{-1}). After the solution was filtered, 30 g of potassium nitrate was added, and then the solution was heated to 85°C in air with continuous agitation for 3 h. Precipitates were collected, generously rinsed, and dried for 48 h in a 60°C oven, removing any excess absorbed water.

The next synthesis of jarosite followed the method described by Baron and Palmer (1996) [K^+ - B&P1996] was made by dissolving 5.6 g potassium hydroxide (reagent grade; KOH) and 17.2 g ferric sulfate hydrate (reagent grade; $Fe_2(SO_4)_3 \bullet nH_2O$) into 100 mL ultrapure water (18 MΩ cm^{-1}). The solution was covered, continuously stirred and heated to 95°C for 4 h. Upon decanting the residual solution, the precipitate was rinsed thoroughly with ultrapure water and dried in an oven at 110°C for 24 h.

The final synthetic preparation of jarosite was attempted using a method adapted from the experimental protocol outlined by Dutrizac and Hardy (1997) [K^+ - D&H1997]. A 1 L solution was made up containing 0.15M $Fe_2(SO_4)_3$ and 0.2M K_2SO_4, and dispensed

into a series of sterile serum vials, capped with sterile butyl stoppers, aluminum crimped and placed into an AllAmerican© 15.5 quart aluminum pressure cooker, on top of a hot plate in a fume hood. The exhaust nozzle of the pressure cooker was partially sealed using Teflon tape and a 20 lb weight to limit the amount of water evaporation from the chamber, and to maintain a constant experimental pressure and temperature, (i.e., 111°C at 1.5 atm for 1 week). The precipitates were collected by filtration, thoroughly rinsed with ultrapure water and heated in an oven for 24 to 72 h at 110°C in order to remove any loose water particles adsorbed to the surface of the precipitates.

Natrojarosite, $(Na)Fe_3(SO_4)_2(OH)_6$

The initial attempt to synthesize natrojarosite entailed dissolving 17.2 g ferric sulfate hydrate (reagent grade; $Fe_2(SO_4)_3 \bullet nH_2O$) and 4.0 g NaOH into 100 mL ultrapure water (18 MΩ cm^{-1}) following the method of Baron and Palmer (1996). The solution was continuously stirred and brought to a slow boil, then left undisturbed for 4 hours. The resulting precipitate [Na^+ - B&P1996] was rinsed thoroughly with ultrapure water and dried in an oven at 120°C for 24 h.

The second synthesis of natrojarosite followed the method of Dutrizac and Kaiman (1976). To summarize, 35.8 g $Fe_2(SO_4)_3 \bullet XH_2O$ (Alfa Aesar, Reagent Grade) and 0.01M H_2SO_4 was added to 1 L of ultrapure water (18 MΩ cm^{-1}). Upon filtration, 64 g of $Na_2(SO_4)$ was added and the solutions was heated to 95°C and continuously stirred uncovered. After 3 h, the precipitate was allowed to settle and the supernatant solution decanted. The precipitate [Na^+ - D&K1976] was rinsed several times with ultrapure water then dried at 60°C for 48 h.

Additional attempts to synthesize natrojarosite minerals using similar solutions and modified published synthesis procedures using the pressure cooker setup were all unsuccessful.

Ammoniojarosite, $(NH_4)Fe3(SO_4)_2(OH)_6$

Ammoniojarosite was synthesized following the method outlined by Dutrizac and Kaiman (1976). In short, 53.7 g ferric sulfate ($Fe_2(SO_4)_3 \bullet XH_2O$; Alfa Aesar, Reagent Grade) and 0.01M H_2SO_4 were added to 1 L of ultrapure water (18 MΩ cm^{-1}). Ammonium sulfate (132 g) was added to the filtered solution which was then heated in open air to 95°C for 3 h and stirred continuously. The precipitate was collected by gravity and well rinsed prior to 48 h of drying in a 60°C oven. Coarse, dried precipitate aggregates were ground to a fine-grained powder using a mortar and pestle [NH_4^+ - D&K1976]. As with the natrojarosite synthesis, attempts to synthesize ammoniojarosite using a pressure cooker experimental setup were unsuccessful.

Hydronium jarosite, $(H_3O)Fe_3(SO_4)_2(OH)_6$

Attempts to synthesize hydronium jarosite were made using a modified published methods adapted from those outlined in Frost et al. (2006), Drouet and Navrotsky (2003) and that of Dutrizac and Kaiman (1976). Note that in early literature hydronium jarosite is referred to as carphosiderite (Dutrizac and Kaiman, 1976).

Initially, an attempt to synthesize hydronium jarosite was made by modifying the method of Frost et al. (2006). Briefly, 4 g of $Fe_2(SO_4)_3 \bullet XH_2O$; Alfa Aesar, Reagent Grade was dissolved into 40 mL of ultrapure water (18 MΩ cm^{-1}). The solution was placed into serum vials with 25% air headspace then capped with a butyl stopper and

sealed. Vials were then placed into a 15.5 quart pressure cooker and heated at 111°C at 1.5 atm for a week. The supernatant solution was decanted and the precipitate [H_3O^+ - Frost2006] was rinsed several times with ultrapure water and then dried at 60°C for 48 to 72 h.

The synthesis was repeated using an identical experimental setup up and modifying the initial solutions, following a protocol outlined by Drouet and Navortsky (2003). In short, 500 mg of ferric sulfate ($Fe_2(SO_4)_3 \bullet XH_2O$; Alfa Aesar, Reagent Grade) was dissolved into 5 mL of ultrapure water (18 MΩ cm^{-1}). The filtered ferric solution was dispensed into sterile serum vials, with 25% air headspace, capped and sealed and then placed into the same pressure cooker as described above. The mineralogical precipitates were collected on a filter [H_3O^+ - D&N2003], rinsed several times with several litres of ultrapure water and then dried at 60°C for 48 to 72 h.

The final preparation used a method outlined by Dutrizac and Kaiman (1976) [H_3O^+ - D&K1976]. A batch solution was made by dissolving 15 g of $Fe_2(SO_4)_3$ into 1 L of ultrapure water (18 MΩ cm^{-1}). As before, the filtered solution was dispensed into a series of sterile serum vials, capped, and sealed then placed into a 15.5 quart aluminum pressure cooker (AllAmerican®) which was heated at 111°C for a week at 1.5 atm. Collected precipitates were well rinsed prior to being dried in and oven for 48 to 72 h at 110°C, removing any loosely bound water molecules to the mineral surface.

Results and Discussion

No synthetic ammoniojarosite or natrojarosite mineral precipitates were successfully generated in this investigation when protocols used the pressure cooker experimental set up. Furthermore, ammoniojarosite and natrojarosite minerals produced

Figure A.2. Powder X-ray diffraction patterns of various synthetic alkali jarosite minerals. Patterns are vertically offset for clarity and to facilitate the comparison of microbial culture precipitate (also included) as well as mineral synthesis products. Ammoniojarosite ([NH_4^+ - D&K1976]) and natrojarosite ([Na^+ - B&P1996], [Na^+ - D&K1976]) powders did not correlate well to that of the microbial culture. Hydronium jarosites ([[H_3O^+ - D&N2003], [H_3O^+ - D&K1976]) had very high intensities with narrow, well defined peaks, as well as additional peak in the 60-80° region when compared to the culture precipitates. The jarosite group of precipitates generated ([K^+ - D&K1976], [K^+ - B&P1996], [K^+ - D&H1997]) patterns were all analogous and they were all comparable with the microbial material.

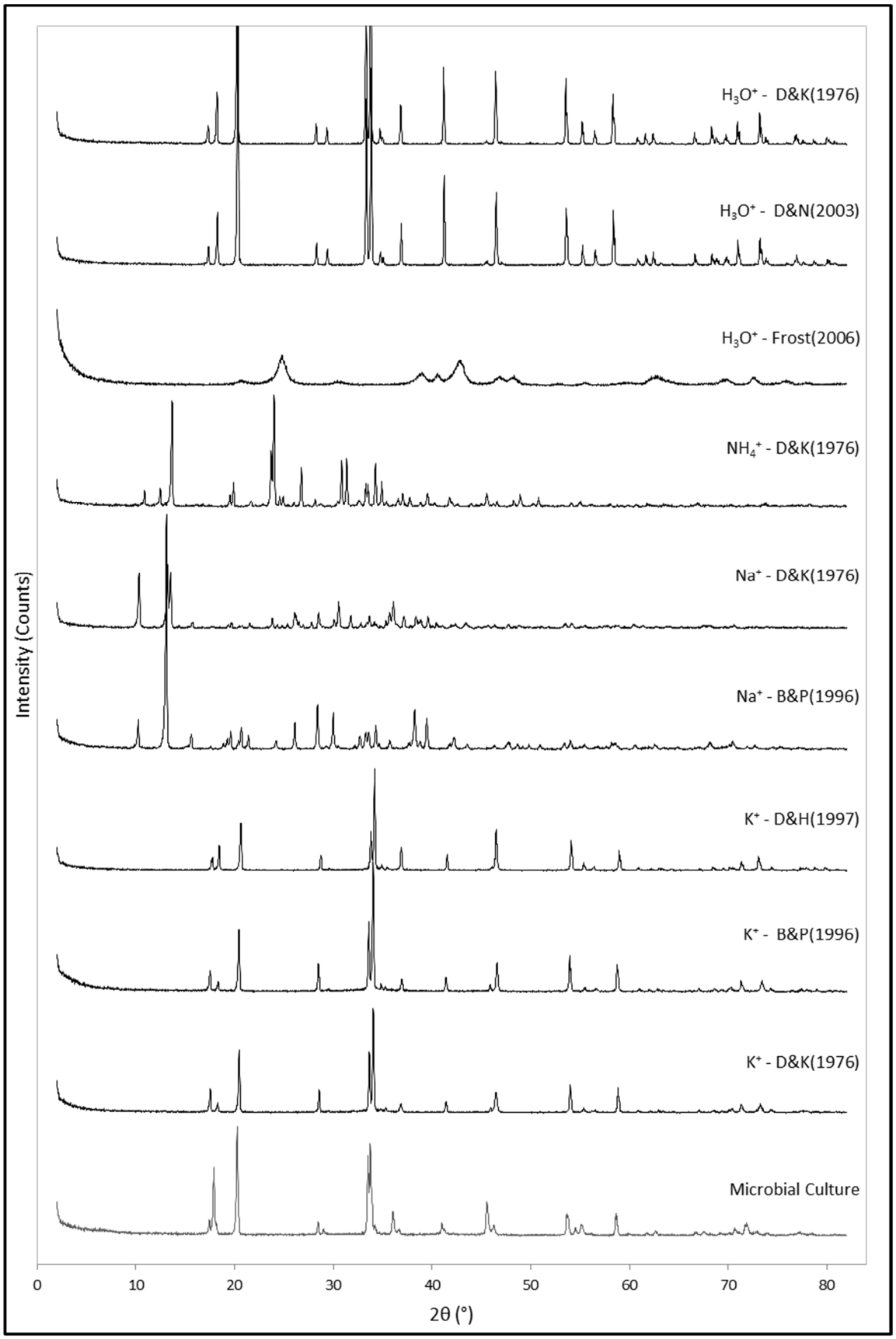
H_3O^+ - D&K(1976)
H_3O^+ - D&N(2003)
H_3O^+ - Frost(2006)
NH_4^+ - D&K(1976)
Na^+ - D&K(1976)
Na^+ - B&P(1996)
K^+ - D&H(1997)
K^+ - B&P(1996)
K^+ - D&K(1976)
Microbial Culture
Intensity (Counts)
0
10
20
30
40
50
60
70
80
2θ (°)

from open air boil methods (i.e., [Na^+ - B&P1996] , [Na^+ - D&K1976 and [NH_4^+ - D&K1976] generated XRD patterns that did not agree or resemble the diffraction pattern generated by the microbial culture (Figure A.2).

Three published methods were employed to try and generate hydronium jarosite precipitates that corresponded to a ICDD powder diffraction database, two modified protocols using the pressure cooker setup (Dutrizac and Kainman, 1976; Frost et al., 2006) and one following an established open air boil method (Dutrizac and Kaiman, 1976). The [H_3O^+ - Frost2006] sample generated a pattern with wide peaks which was different than the other two hydronium jarosite patterns and poorly correlated to the biogenic material (Figure A.2) and was immediately omitted from further consideration. The remaining hydronium jarosite samples (i.e., [H_3O^+ - D&N2003], [H_3O^+ - D&K1976]) although generated using different experimental heating methods (i.e., open air boil vs. pressure cooker setup) produced a similar XRD pattern to the biological material. Additionally, these patterns had the highest peak intensities observed for all of the synthetic samples analyzed and exhibited several peaks in the 60 to 80° region that were not observed or resolved (i.e., above background) in any of the other analyzed samples, including the biogenic material. Although synthesis protocols employed in this investigation targeted the production of single phase mineral samples, the hydronium jarosite samples generated herein are thought to be a mixed solid-solution series with jarosite as the major mineralogical phase and an undetermined minor mineralogical phase. Hydronium jarosite precipitates were difficult to generate as the protocols employed generated very small reaction recovery yields. Also, it was determined that the microbial precipitates generated were unlikely to be pure hydronium jarosite since it is

well established that hydronium jarosite can only form in solutions that are depleted in sodium and potassium ions (Basciano and Peterson, 2007 and references therein), and the microbial culture medium contains both sodium and potassium. Furthermore, hydronium jarosite is much less stable relative to ammoniojarosite or natrojarosite (Dutrizac and Jambor, 2000) and is considered to be relatively rare and quantitatively sparse in nature. Therefore, [H_3O^+ - D&N2003] and [H_3O^+ - D&K1976] were no longer considered as synthetic analogous candidate specimen.

It was generally observed that jarosites synthesized using the open-air boil method generated the highest yields of all materials synthesized. The three jarosite samples synthesized (i.e., [K^+ - D&K1976], [K^+ - B&P1996], [K^+ - D&H1997]) generated similar XRD patterns (Figure A.2), all of which resembled the microbial culture precipitate pattern. Additionally, when mineralogical phases within these three samples were identified using the ICCD database, they all matched the same card (no. 00-036-0427; jarosite, OH-rich (K, H_3O)$Fe_3(SO_4)_2(OH)_6$) and moreover, this is the same card that matches the mineralogical phases of the biogenic material. All synthetic jarosite samples derived from the protocols outlined herein also possessed similar particle morphologies when examined using a scanning electron microscopy (SEM; Figure A.3). Micrographs indicate that there are very little morphological differences between the three synthetic jarosite samples (Figure A.3) but that these materials exhibited a distinct morphology from the biogenic sample (refer to Chapter 2 for a more detailed discussion). It is also worth mentioning that none of the synthetic alkali jarosites characterized using SEM analyses matched the needle-like, acicular textures observed in the biogenic precipitates, nor did they reproduce the morphological textures that were observed in the suite of

Figure A.3. SEM micrographs of synthetic jarosite minerals. All three synthetically derived jarosites with matching XRD ICDD card patterns to the biogenic jarosite material, (A: [K^+ - D&K1976], scale bar = 1μm; B: [K^+ - B&P1996], scale bar = 2 μm; C: [K^+ - D&H1997], scale bar = 1 μm), demonstrating similar and analogous particle morphology at high resolution.

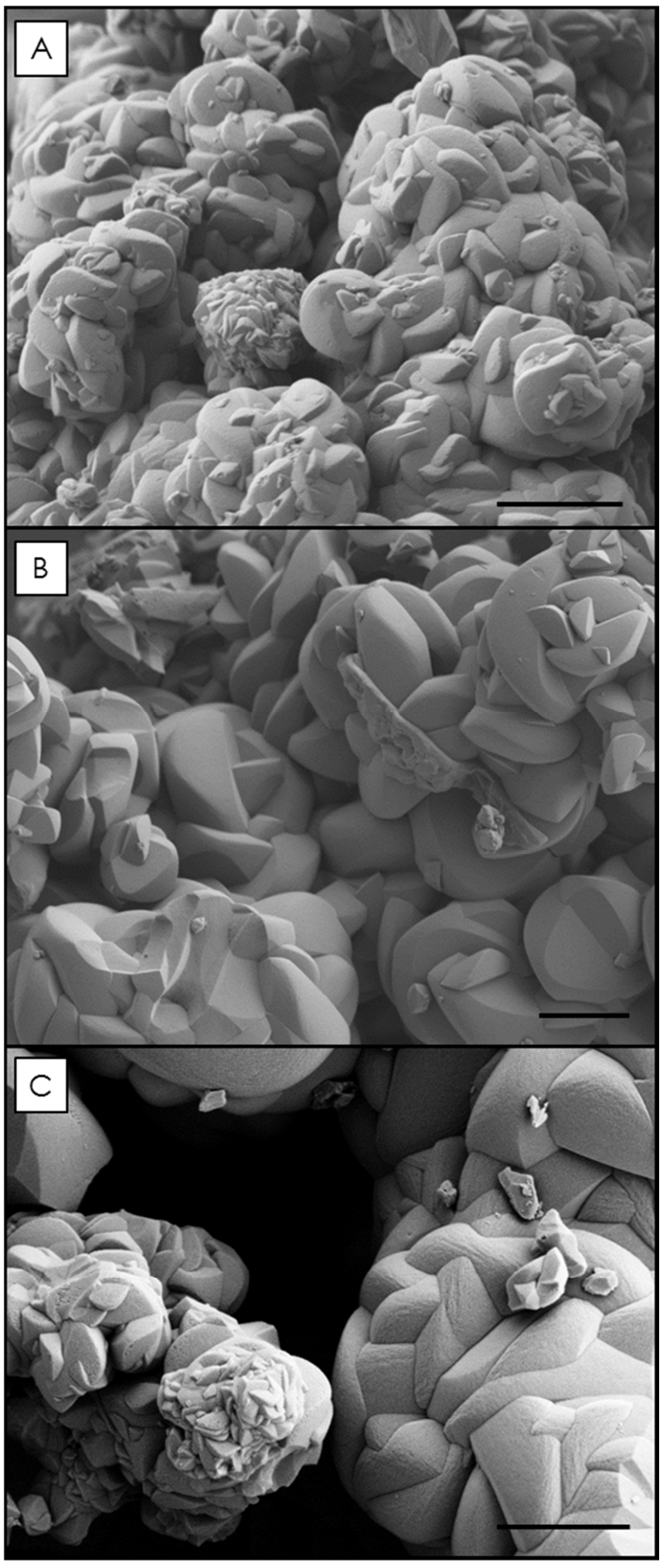
A
B
C

jarosite samples. Since all synthetic jarosites examined had similar XRD patterns and morphologies the [K^+ - D&K1976] sample was ultimately chosen to be the representative 'synthetic' sample for the additional investigations outlined in this dissertation (Chapter 2 and Chapter 3) as it had the simplest protocol with the highest reaction yield of the jarosites investigated.

Conclusion

The XRD pattern of the biogenic material was matched with a synthetic material that was chemically and mineralogically similar to the biogenic sample. XRD patterns of all the ammoniojarosite and natrojarosite did not agree with that of the biogenic material and were not considered further as potential synthetic specimen candidates. Additionally, hydronium jarosite was also removed from consideration as the XRD pattern although it was a good general match, except for overall pattern intensity and the presence of several peaks in the 60 to 80° region which were not observed in the biogenic sample. Jarosite XRD patterns matched the biogenic material, independently of the biogenic material being identified as jarosite from the ICDD mineralogical database. SEM analyses demonstrated that all of the jarosite samples synthesized generated similar particle morphologies, thus the synthetic jarosite sample was chosen based upon highest reaction yield and ease of generation. [K^+ - D&K 1976] was selected as a representative synthetic counterpart to the biogenic material and was subsequently used in the investigations outlined in this body of work.

References

Baron, D., Palmer, C.D., 1996. Solubility of jarosite at 4°-35°C. Geochim. Cosmochim. Acta 60, 185-195.

Basciano, L.C., Peterson, R.C., 2007. Jarosite-hydronium jarosite solid-solution series with full iron site occupancy: Mineralogy and crystal chemistry. Am. Mineral. 92, 1464 – 1473.

Driscoll, R., Leinz, R., 2005. Methods for synthesis of some jarosites: U.S. Geological Survey Techniques and Methods 05-D1, 6p.

Drouet, C., Navrotsky, A., 2003. Synthesis, characterization, and thermochemistry of K-Na-H_3O jarosites. Geochim. Cosmochim. Acta 67, 2063-2076.

Dutrizac, J.E., Hardy, D.J., 1997. The behaviour of thiocyanate and cyanate during jarosite precipitation. Hydrometallurgy 45, 83-95.

Dutrizac, J.E., Jambor, J.L., 2000. Jarosites and their application in hydrometallurgy. In C.N., Alpers, J.L., Jambor, D.K., Nordstrom, Eds., Sulfate Minerals – Crystallography, Geochemistry, and Environmental Significance, vol. 40, p. 405-452. Reviews in Mineralogy and Geochemistry, Mineralogical Society of America, Chantilly, Virgina.

Dutrizac, J.E., Kaiman, S., 1976. Synthesis and properties of jarosite-type compounds. Can. Mineral. 14, 151-158.

Frost, R.L., Willis, R.A., Kloprogge, J.T., Martens, W.N., 2006. Thermal decomposition of hydronium jarosite $(H_3O)Fe_3(SO_4)_2(OH)_6$. J. Therm. Anal. Calorim. 83, 213-218.

Curriculum Vitae

Name:	Liane Loiselle
Post-secondary Education and Degrees:	McMaster University, Hamilton, Ontario, Canada 2004 – 2009 B.Sc. The University of Western Ontario, London, Ontario, Canada 2009 – 2012 M.Sc.
Honours and Awards:	Canadian Astrobiology Training Program, Graduate Student Fellowship 2010 – 2012 Graduate Research Thesis Award 2011 Canadian Space Agency, Travel Grant 2011 Hodder Travel Bursary 2011 Canadian Space Agency, Learning Grant 2010
Related Work Experience:	Teaching Assistant, The University of Western Ontario London, Ontario, Canada 2009 – 2012 Research Assistant, IPBSL team, Cento Astrobiologica, Nerva, Huelva, Spain 2011 Research Affiliate, Canadian Space Agency (CSA), Saint–Hubert, Quebec, Canada 2010